Doctoral Dissertation
Doctoral Program in Management, Production and Design (33th Cycle)

Energy efficiency and circular economy implications of additive manufacturing

By

Vincenzo Lunetto
* * * * * *

Supervisors
Prof. Luca Settineri
Prof. Paolo C. Priarone

Doctoral Examination Committee:
Prof. Daniel Brissaud, Referee, INPG Grenoble (France)
Prof. Sebastian Thiede, Referee, University of Twente (Netherlands)
Prof. Alessandro Simeone, Shantou University (China)
Prof. Maurizio Galetto, Politecnico di Torino (Italy)
Prof. Michele Dassisti, Politecnico di Bari (Italy)

Politecnico di Torino

I dedicate this work to
my parents, Gioacchino and Anna

Acknowledgment

When I received my Bachelor's degree after studying in the Università degli Studi di Palermo, I decided to move to Turin to continue with my master studies. I was certainly excited about living in a multicultural context, but at the same time aware that I left behind my home.

Since my arrival at the Politecnico di Torino, I found a dynamic and enriching reality. I immediately realised how much this would have helped me and I tried to work hard to take advantage from this new life. In Prof. Luca Settineri and in Prof. Paolo C. Priarone, I found two guides who introduced me to the academic life, until they become my Supervisors for my master's thesis. I am happy to have started my PhD under their supervision. I thank them for the opportunities they gave me during my PhD, which was rich of inputs and of formative experiences.

I thank Prof. Luca Iuliano, his research group and Mr. Marchiandi for the research activities carried out together at the Integrated Additive Manufacturing (IAM) laboratory of Politecnico di Torino.

I remember my colleagues at Politecnico di Torino, for the lunches spent together that delighted the working days and for the friends that I have found.

I developed part of my PhD at the UNSW Sydney - Australia's Global University, under the supervision of Prof. Sami Kara (head of Sustainability in Manufacturing & Life Cycle Engineering Research Group @ UNSW). He did not only give me the possibility to enlarge my knowledge. Most of all, he gave me a warm welcome and made me part of his research group.

I remember the colleagues in Sydney. Since the beginning, they welcomed me and they soon became as a family in the other part of the world.

Finally, I do thank my family and my dearest friends. They gave me the ambition and the desire to always improve myself, the tenacity to work hard, the patience to overcome obstacles. I want to cite a sentence my father uses to tell me in the difficult moments: "Calati juncu ca passa la china".

Vincenzo Lunetto
Palermo, 24th of December 2020

Abstract

The study entitled “The trajectory of the Anthropocene: The Great Acceleration” [1] shows a great acceleration for socio-economic and earth system trends, starting from the post war world II. Moreover, after the 1950 there is a clear evidence that fundamental changes in the functioning of the Earth System are guided by human activities. These trends brought the research community to define a sustainable development paradigm for the Anthropocene with an integrated point of view [2,3]. The Earth’s Life Support System is seen as the higher limit that includes society, which in turn includes economy, which in turn includes the manufacturing industry. Therefore, the idea of “Absolute Sustainability” was introduced [4], as well as that of the IPAT equation to quantify the overall environmental impact of an human activity [5,6]. At the same time, the attention to the efficient use of energy and resources is grooving among the political authorities. At worldwide level, the G7 Summit Declaration of June 2015 launched the G7 Alliance on Resource Efficiency with the aim to promote Circular Economy (CE), Remanufacturing and Recycling concepts as strategic actions [7]. A report produced by Ellen MacArthur Foundation with the McKinsey Center for Business and Environment and the SUN Institute, strongly recommends the need to switch to a CE system for Europe in order to remain competitive in the manufacturing sector at global level [8]. Therefore, it is possible to notice how the CE actions are currently seen as solution to meet the requirements of our world. However, it is necessary to contextualise the CE logics with the current manufacturing paradigm. According to [9], the main characteristic of the current paradigm (i.e., the direct digital manufacturing - DDM) is that the design requirements of a product are directly created by a network of different people. The Additive Manufacturing (AM) technology is considered as one of the drivers of DDM. In fact, with AM, CAD files and open-source printer software, products can be directly manufactured close to the customer and directly derived from digital models [9,10].

This work finds its space into this panorama. More in details, it aims to answer to the following research questions:

Research Question 1 (RQ1). With a Circular Economy point of view, how to assess the remaining useful lifetime of products and how to perform a LCA study under a function-oriented analysis?

Research Question 2 (RQ2). How to evaluate the energy efficiency of a manufacturing technology at the unit process level and which can be a good methodology to achieve this goal?

The RQ1 comes from the need of LCA methodologies customised for a CE-based scenario. In fact, the available LCA methodologies applied to a linear economy scenario mainly focus on a single production of the product and do not pursue the comparison for the further lives the product may have. Moreover, the implications of the reliability property on the iterated products represent a central topic still to be addressed. The study in this work is performed considering AM processes to offer an immediate relationship with the current manufacturing paradigm [11,12], even if, the proposed methodology can be applied to other production techniques.

The RQ2 mainly comes from the need to feed the developed LCA methodologies with data that are closely related to the considered case study. In particular, the literature showed practices already available for conventional processes (e.g., machining, injection moulding). On the other hand, the study of the state-of-the-art literature regarding the AM techniques produced the need to fill different research gaps. Moreover, the boundary constrains of the current manufacturing paradigm require an investigation of the advantages and disadvantages that AM can also bring regarding the sustainability at its unit process level. For instance, AM techniques are characterised from low productivity and high energy demand, especially in comparison with bulk and subtractive techniques [13–16]. Therefore, this kind of study are particularly worth for this technology.

This thesis is articulated as follows: (a) an introduction section to better contextualise the performed work; (b) Chapter 1 for the literature review to support the RQ1 and RQ2 and to define the state-of-the-art literature gaps and the aims of this work; (c) Chapter 2 develops the LCA methodology for a CE scenario; (d) Chapter 3 investigates the energy efficiency at the unit process level of different AM technologies; finally, (e) the conclusion section summaries the results and makes considerations on the entire work.

Papers related to the PhD research activities

During the preparation of this Ph.D. thesis, some of the results have been published and presented by the Author in international journals and conferences. A chronological list of publications and technical presentations (last modified on February 26th, 2021) is given in the following.

Publications

2018 Priarone PC, Ingarao G, **Lunetto V**, Di Lorenzo R, Settineri L. *The Role of re-design for Additive Manufacturing on the Process Environmental Performance*. Proceedings of the 25th CIRP conference on Life Cycle Engineering, Copenhagen, Denmark, 30 April-2 May 2018. Procedia CIRP 69 (2018) 124-129.

2018 Priarone PC, **Lunetto V**, Atzeni E, Salmi A. *Laser powder bed fusion (L-PBF) additive manufacturing: On the correlation between design choices and process sustainability*. Proceedings of the 6th CIRP Global Web Conference, 23-25 October 2018. Procedia CIRP 78 (2018) 85-90.

2019 **Lunetto V**, Catalano AR, Priarone PC, Settineri L. *Comments about the human health risks related to additive manufacturing*. Proceeding of the 5th International Conference on Sustainable Design and Manufacturing (SDM), Gold Coast, Australia, 24-26 June 2018. Sustainable Design and Manufacturing 2018, Smart Innovation, Systems and Technologies 130, Springer Nature Switzerland AG 2019, pp. 95-104, DOI 10.1007/978-3-030-04290-5_10.

2019 Catalano AR, **Lunetto V**, Priarone PC, Settineri L. *A survey on energy efficiency in metal wire deposition processes*. Proceeding of the 6th International Conference on Sustainable Design and Manufacturing (SDM), Budapest, Hungary, 4-5 July 2019. Sustainable Design and

Manufacturing 2019, Smart Innovation, Systems and Technologies 155, Springer Science and Business Media Deutschland GmbH, pp. 311-322, DOI 10.1007/978-981-13-9271-9_26.

2020 **Lunetto V**, Galati M, Settineri L, Iuliano L. *Unit process energy consumption analysis and models for Electron Beam Melting (EBM): Effects of process and part designs*. Additive Manufacturing 33 (2020) 101115.

2020 **Lunetto V**, Priarone PC, Galati M, Minetola P. *On the correlation between process parameters and specific energy consumption in fused deposition modelling*. Journal of Manufacturing Processes 56 (2020) 1039-1049.

2020 Davis V, **Lunetto V**, Priarone PC, Centea D, Settineri L. *An appraisal on the sustainability payback of additively manufactured molds with conformal cooling*. Proceedings of the 27th CIRP conference on Life Cycle Engineering, Grenoble, France, 13-15 May 2020. Procedia CIRP 90 (2020) 516-521.

2021 **Lunetto V**, Catalano AR, Priarone PC, Salmi A, Atzeni E, Moos S, Iuliano L, Settineri L. *Additive Manufacturing for an urban vehicle prototype: Re-design and sustainability implications*. Proceedings of the 14th CIRP conference on Intelligent Computation in Manufacturing Engineering, Gulf of Naples, Italy, 15-17 July 2020. Procedia CIRP (2021) (In press).

2021 **Lunetto V**, Priarone PC, Kara S, Settineri L. *A comparative LCA method for environmentally friendly manufacturing: Additive manufacturing versus Machining case*. Proceedings of the 28th CIRP conference on Life Cycle Engineering, Jaipur, India, 10-12 March 2021. Procedia CIRP (2021) (In press).

Contents

List of Tables 4
List of Figures 6
Nomenclature of key variables 10
Introduction 13
The role of Additive Manufacturing 14
Conceptual framework of the thesis 15
Gantt chart of the activities 18
Literature review 22
1.1 The Circular Economy challenges 22
1.1.1 The Earth's Life Support System 22
1.1.2 Pillars of the Circular Economy 24
1.1.3 Additive Manufacturing and Circular Economy 28
1.2 The unit process level of AM 31
1.2.1 Fused Deposition Modelling 34
The FDM technology 34
Energy efficiency of the FDM process 35
1.2.2 Electron Beam Melting 37
The EBM technology 37
Energy efficiency of the EBM process 38
1.2.3 Continuous Filament Fabrication 40
The CFF technology 41
Energy efficiency of other processes to manufacture composites 42
1.3 Research questions and aims of the thesis 44
The Circular Economy challenges 48
2.1 Methodology 48

2.1.1 Work assumption 1: Physical lifetime and technology lifetime 51
2.1.2 Work assumption 2: Bathtub curve and failure modes 52
2.1.3 Work assumption 3: Availability, Capability and Dependability ...53
2.1.4 Work assumption 4: A Markov chain approach to model the remanufacturing process 55
2.1.5 Work assumption 5: A Markov chain approach to model the behaviours of the users 58
2.1.6 MATLAB and Excel codes 59
2.1.7 Summary of the methodology 61
2.2 Case study and Data Inventory 62
2.2.1 Materials and Technologies 64
2.2.2 Data Inventory 66
2.3 Results 70
2.4 Discussion 76
2.4.1 Effect of the remanufactured material percentage 78
2.4.2 Effect of the initial distribution of the users 79
2.4.3 Effect of the awareness campaigns for the users 81
2.4.4 Effect of the behaviours of the users 83
The unit process level of AM 85
3.1 Methodology 85
3.1.1 Fused Deposition Modelling 87
3.1.2 Electron Beam Melting 92
3.1.3 Continuous Filament Fabrication 95
3.2 Results 99
3.2.1 Fused Deposition Modelling 99
Sample characterisation 101
3.2.2 Electron Beam Melting 104
Process subphase (1): Vacuum generation 105
Process subphase (2): Build process 106
Process subphase (3): Cooling 109
3.2.3 Continuous Filament Fabrication 109
Sample characterisation 111
3.3 Discussion 114

3.3.1 Fused Deposition Modelling....115
Empirical models for energy consumption....117
Model validation....119
3.3.2 Electron Beam Melting....120
Empirical models for energy consumption....125
3.3.3 Continuous Filament Fabrication....127
Empirical models for energy consumption....129
Model validation....132
Energy prediction of 3D printed composites via CFF....133
3.3.4 Final considerations....135
Melting energy and overall energy demand: the weight of the machine subunits....136
Comparison between AM technologies: FDM, EBM and CFF....138
Sustainability and design for AM (DfAM)....139
Interdependencies with quality criteria....140
Conclusions and outlooks....141
Appendix A: MATLAB code to compute the Markovian steps of the market evolution for each life....147
Appendix B: MATLAB code to compute the Markovian steps of the remanufacturing process for each life....148
References....152

List of Tables

Table 1. Electric energy and time efficiency data available in the literature for FDM. The values marked with "*" have been computed in this work. Full build is intended for the saturation of the start plate. 36

Table 2. Electric energy and time efficiency data available in the literature for EBM applied to Ti6Al4V. The values marked with "*" have been computed in this work. Full capacity is intended for the saturation of the start plate. 40

Table 3. Summary of the methodology applied in Chapter 2. 61

Table 4. "State transition probabilities" for "M_R". 64

Table 5. "State transition probabilities" for "M_U". 64

Table 6. Data inventory for the selected case study. A ±10% range of variability is considered for the parameters marked with "*". MJ is intended for MJ (oil equivalent). 69

Table 7. "State transition probabilities" for the sensitivity analysis performed with "M_U". 81

Table 8. Main characteristics for ABS and PC-ABS materials provided from Stratasys [78]. 90

Table 9. Samples manufactured on the Stratasys F370. * Software estimations. 91

Table 10. Main characteristics for Ti6Al4V powder provided from Arcam [29]. 93

Table 11. Samples manufactured on the Arcam A2X. * Software estimations. 94

Table 12. Process parameters for the melting phase of the EBM process. 95

Table 13. Main characteristics for the materials provided from Markforged [84]. 96

Table 14. Not reinforced samples manufactured on the Markforged Mark Two. * Software estimations. 98

Table 15. Reinforced samples manufactured on the Markforged Mark Two. * Software estimations. 98

Table 16 Time and energy demand for phases (1), (2), (3) and (5) for the Stratasys F370. 101

Table 17. Printing phase: energy, time and mass results for samples manufactured on the Stratasys F370. 102
Table 18. Process time and energy demand results for the vacuum generation process of the Arcam A2X. 105
Table 19. Process time and energy consumption of the subphases (2.1) and (2.2) of the Arcam A2X. 106
Table 20. Process time and energy demand results for the printing phase of the Arcam A2X. 108
Table 21. Process time and energy demand for the cooling phase of the Arcam A2X. 109
Table 22. Time and energy demand for phases (1), (2), (3) and (5) for the Markforged Mark Two. * This value was computed equal to 0.01 Wh, however, only the significant digits were reported. 112
Table 23. Printing energy, time and mass for not reinforced samples manufactured on the Markforged Mark Two. 113
Table 24. Printing energy and time for reinforced samples manufactured on the Markforged Mark Two. 113
Table 25. Printing mass results for reinforced samples manufactured on the Markforged Mark Two. 113
Table 26. Values of the “a” coefficient in Eq. 4 for the Stratasys F370. 116
Table 27. Values of the “C_i” coefficients in Eq. 5, expressed in MJ/min, for the Stratasys F370. 119
Table 28. Values of the “C_i” coefficients in Eq. 7 for the Stratasys F370. 119
Table 29. Values of the “C_i” coefficient in Eq. 13 and Eq. 14, expressed in MJ/h, for the Arcam A2X. 125
Table 30. Values of the “C_i” coefficients in Eq. 15 for the fibre and matrix curve, expressed in MJ/min. 129
Table 31. Results of the JOBs used to validate the regression laws of the Markforged Mark Two. 133
Table 32. Results of the model for the energy prediction of 3D printed composites with the Markforged Mark Two. 135
Table 33. Energy demand share of each machine subunit as a percentage of the total energy demand for the AM machines investigated in this work. 137

List of Figures

Figure 1. Conceptual framework of the thesis. 17
Figure 2. Gantt chart of the activities. 19
Figure 3. Sustainable development paradigm for the Anthropocene, according to [2]. 24
Figure 4. Implementation of the "6R methodology" in the industrial practice (Adapted from [50]). 28
Figure 5. AM processes classified according to ASTM standards [20]. 34
Figure 6. SEC data available in the literature for conventional and automatic composite manufacturing techniques, expressed in MJ/kg (oil equivalent). *Compression moulding techniques which use SMCs and BMCs. **Only the laser input energy to the process is considered. 44
Figure 7. (a) Scheme and extension to a function-oriented analysis of (a) the brand-new scenario and of (b) the remanufacturing scenario. 50
Figure 8. Hypothetical example of product technology substitution. Adapted from [141]. 52
Figure 9. Bathtub curve and failure modes. 53
Figure 10. Effect of dependability on the physical lifetime of the product. 54
Figure 11. Markovian modelling of the remanufacturing process. 57
Figure 12. Markovian modelling of the behaviours of the users. 59
Figure 13. Mock-up of the described case study. Adapted from [152]. 63
Figure 14. Focus of the steps of the manufacturing and remanufacturing scenarios. 65
Figure 15. (a) Distribution of the users for each life and (b) effect on the scrap flows of each corresponding remanufacturing loop. 70
Figure 16. Product flows for each Node of the remanufacturing Markov chain: (a) first remanufacturing and (b) last remanufacturing. "Average case" scenario. 71
Figure 17. Product flows for key-Nodes of the remanufacturing Markov chain: (a) shares for each remanufacturing loop and (b) cumulative trends. 72
Figure 18. (a) Distributions of the target share for each life (f_P) and (b) cumulative trends. 73

Figure 19. CED to remanufacture one blade as function of the remanufactured material percentage and CED for the manufacturing of a brand-new blade. MJ is intended for MJ (oil equivalent). 74
Figure 20. Energy percentage share of the different steps to produce one blade in both scenarios. 75
Figure 21. (a) Energy demand shares for each remanufacturing loop for key-Nodes of the remanufacturing Markov chain and (b) cumulative energy trends. .75
Figure 22. (a) Cumulative energy trends for the two scenarios for each life and (b) final CED (considering the overall variability). 76
Figure 23. Energy demand shares for each remanufacturing loop for key-Nodes of the remanufacturing Markov chain: (a) set #1 of remanufacturing percentages, (b) set #2 of remanufacturing percentages. 78
Figure 24. Cumulative energy trends for the two scenarios for each life: (a) set #1 of remanufacturing percentages, (b) set #2 of remanufacturing percentages. ..79
Figure 25. Final CED of the remanufacturing and brand-new scenarios (considering the overall variability): (a) set #1 of remanufacturing percentages, (b) set #2 of remanufacturing percentages. 79
Figure 26. Effect of the initial distribution of the users: (a) distribution of the users for each life and (b) effect on the scrap flows of each corresponding remanufacturing loop. 80
Figure 27. Effect of the initial distribution of the users: (a) distributions of the target share for each life (f_P) and (b) cumulative trends. 80
Figure 28. Effect of the initial distribution of the users: (a) energy demand shares for each remanufacturing loop for key-Nodes of the remanufacturing Markov chain and (b) cumulative energy trends. 81
Figure 29. Effect of the awareness campaigns for the users: (a) distribution of the users for each life and (b) effect on the scrap flows of each corresponding remanufacturing loop. 81
Figure 30. Effect of the awareness campaigns for the users: (a) distributions of the target share for each life (f_P) and (b) cumulative trends. 82
Figure 31. Effect of the awareness campaigns for the users: (a) cumulative energy trends for the two scenarios for each life and (b) final CED (considering the overall variability).....82
Figure 32. Effect of the behaviours of the users: (a) distributions of the target share for each life (f_P) and (b) cumulative trends. 83

Figure 33. Effect of the behaviours of the users: (a) cumulative energy trends for the two scenarios for each life and (b) final CED (considering the overall variability).....83
Figure 34. Flowchart highlighting the methodology of Chapter 3.....86
Figure 35. Selected geometries for the Stratasys F370. 87
Figure 36. Experimental setup (a) and additively manufactured components (b) on the Stratasys F370. 88
Figure 37. Different infill strategies within the GrabCAD Print software for a simple cube. 89
Figure 38. Designed JOB for the Arcam A2X. 92
Figure 39. Selected geometries for the Markforged Mark Two.....97
Figure 40. Experimental setup and additively manufactured components on the Markforged Mark Two. 99
Figure 41. Data acquisition and identification of the main process subphases for the Stratasys F370 (JOB 3). 100
Figure 42. Infill strategies as a function of the component material computed with the GrabCAD Print software. 103
Figure 43. Data acquisition and identification of the main process subphases for the Arcam A2X (JOB 1). 104
Figure 44. Printing phase: data acquisition and identification of the different machine subunits for the Arcam A2X (JOB 3).....107
Figure 45. Printing phase: data acquisition of the electron beam and identification of the layer production subphases (JOB 3).....108
Figure 46. Data acquisition and identification of the main process subphases for the Markforged Mark Two (JOB 24). 110
Figure 47. Extruder path for the CF layers of geometry “D” for the different inclinations.....114
Figure 48. Printing phase: correlation between energy and time for the Stratasys F370.....115
Figure 49. Printing phase: energy and mass results for samples manufactured on the Stratasys F370.....116
Figure 50. Effect of process parameters on the printing time and the energy demand of the Stratasys F370.....117
Figure 51. Empirical approach applied to the printing phase of the Stratasys F370. 119
Figure 52. Experimental test for model validation of the Stratasys F370.....120

Figure 53. Experimental analysis between energy and time for the vacuum generation phase of the Arcam A2X.....121
Figure 54. Experimental analysis between energy and time for the printing phase of the Arcam A2X. 122
Figure 55. Experimental analysis between energy and time for the cooling phase of the Arcam A2X. 122
Figure 56. Process subphase times as percentages of the total demand of the Arcam A2X.....123
Figure 57. Process subphase energies as percentages of the total demand of the Arcam A2X.....124
Figure 58. Empirical approach applied to the Arcam A2X at the unit process level and to the printing phase. 126
Figure 59. Printing phase: correlation between energy and time for the Markforged Mark Two. 127
Figure 60. Printing energy and mass for not reinforced samples manufactured on the Markforged Mark Two. 127
Figure 61. Time and energy demand for the reinforced samples (JOBs 23-34). 128
Figure 62. Empirical approach applied to the Markforged Mark Two for the matrix and fibre deposition. 131
Figure 63. Experimental tests for model validation of the Markforged Mark Two. 132
Figure 64. Comparison between SEC and DR_a data from literature and from this study. 138
Figure 65. Example of a product (a) produced with conventional processes and (b) relative redesigned for AM.....145

Nomenclature of key variables

F	Function target to be achieved from one product for the comparative LCA performed in Chapter 2 (e.g., the satisfaction of an overall lifetime for a turbine blade).
P	Population of products considered for the comparative LCA performed in Chapter 2 (e.g., set of turbine blades present in one of the stages of an aeronautic engine).
F_P	Overall function target to be achieved from all products belonging to the population "P". This variable is defined as the product between "P" and "F".
PA_i	Number of remanufactured products which were used under the prescribed working conditions during their previous "i" life.
L_A	Physical lifetime guaranteed from the brand-new products and from the remanufactured products for their next "i+1" life which were used under the prescribed working conditions during their previous "i" life.
PB_i	Number of remanufactured products which were not used under the prescribed working conditions during their previous "i" life.
L_B	Physical lifetime guaranteed from the remanufactured products for their next "i+1" life which were not used under the prescribed working conditions during their previous "i" life.
SA_i	Number of scraps belonging to the remanufactured products which were used under the prescribed working conditions during their previous "i" life.
SB_i	Number of scraps belonging to the remanufactured products which were not used under the prescribed working conditions during their previous "i" life.
BN_{i+1}	Number of brand-new products needed for the next "i+1" life of the remanufacturing scenario. This variable is defined as the sum of "SA_i" and "SB_i" in the previous "i" life.
f_{Pi+1}	Share of the overall function target "F_P" which is achieved in the next life "i+1", considering the distribution of "PA_i", "PB_i", "SA_i", "SB_i" during the previous "i" life.
p_{ij}	State transition probability which connects Node "i" to Node "j" of a Markov chain system.
M_R	Probability matrix of the remanufacturing process modelled with a Markov chain approach.
M_U	Probability matrix of the market evolution modelled with a Markov chain approach.
R_i	Row vector which defines the "i_{th}" condition of the remanufacturing process modelled with a Markov chain approach after each use phase.

R_0	Row vector which defines the "zero" condition of the remanufacturing process modelled with a Markov chain approach after each use phase.
U_i	Row vector which defines the "i_{th}" condition of the market distribution modelled with a Markov chain approach.
U_1	Row vector which defines the market distribution modelled with a Markov chain approach for the first life of the comparative LCA performed in Chapter 2.
SEC	Specific Energy Consumption, defined as the ratio between the energy demand at the unit process level (i.e., considering both productive and not productive phases) and the printed mass.
SPE	Specific Printing Energy, defined as the ratio between the printing energy (i.e., neglecting the not productive phases) and the printed mass.
DR_a	Average Deposition Rate, defined as the ratio between the printed mass and the needed time at the unit process level.
DR_{aprint}	Average Deposition Rate for the printing phase, defined as the ratio between the printed mass and the printing time.
SPE_{Matrix}	Specific Printing Energy referred to the matrix deposition (including that related to the purge corner part in case of reinforced sample) of a sample made with the CFF technology.
$SPE_{CF(K)}$	Specific Printing Energy referred to the reinforcement deposition of a sample made with the CFF technology.
SPE_{JOB}	Modelled Specific Printing Energy referred to the deposition of a sample (i.e., the matrix, the reinforcement and the mass related to the purge corner part in case of reinforced sample) made with the CFF technology.
$DR_{aprintMatrix}$	Average Deposition Rate for the printing phase referred to the matrix deposition (including that related to the purge corner part in case of reinforced sample) of a sample made with the CFF technology.
$DR_{aprintCF(K)}$	Average Deposition Rate for the printing phase referred to the reinforcement deposition of a sample made with the CFF technology.
E_{FDM}	Overall energy demand to perform the FDM process (i.e., considering both productive and not productive phases).
E_{EBM}	Overall energy demand to perform the EBM process (i.e., considering both productive and not productive phases).
E_{bed}	Energy demand to prepare the powder bed of the EBM machine.
E_{vacuum}	Energy demand to reach the vacuum pressure needed to switch on the electron beam of the EBM machine.
E_{build}	Energy demand during the build phase (i.e., electron beam alignment, heating of the start table, and printing phase) of the EBM machine.
$E_{alignment}$	Energy demand to perform the alignment of the electron beam.
E_{table}	Energy demand to bring the start plate to the target temperature to start the printing phase for the EBM process.
$E_{cooling}$	Energy demand needed during the cooling phase of the EBM process.
$E_{cleaning}$	Energy demand needed to clean the build chamber of the EBM machine before the start of a new JOB.

E_{CFF}	Overall energy demand to perform the CFF process (i.e., considering both productive and not productive phases).
E_{Matrix}	Energy demand to deposit the entire matrix material (including that related to the purge corner part in case of reinforced sample) of a sample produced with the CFF technology.
$E_{CF(K)}$	Energy demand to deposit the reinforcement of a sample produced with the CFF technology.
m_{Matrix}	Mass of the entire matrix material (including that related to the purge corner part in case of reinforced sample) of a sample produced with the CFF technology.
$m_{CF(K)}$	Mass of the reinforcement of a sample deposited with the CFF technology.
m_{JOB}	Overall mass (i.e., matrix, reinforcement and the mass related to the purge corner part in case of reinforced sample) of a sample deposited with the CFF technology.
e_{Corner}	Energy demand to deposit a layer of the corner purge part with the CFF technology.
n	Number of layers until the last reinforced one for a sample deposited with the CFF technology.

Introduction

In the study entitled “The trajectory of the Anthropocene: The Great Acceleration” [1], Will Steffen et al. show socio-economic and earth system trends from 1750 to 2010. Starting from the post war world II, a great acceleration is visible in these key parameters and after the 1950 there is a clear evidence that fundamental changes in the functioning of the Earth System are guided by human activities. As consequence of this phenomenon, the attention to the efficient use of energy and resources is grooving among the political authorities. At worldwide level, the G7 Summit Declaration of June 2015 launched the G7 Alliance on Resource Efficiency with the aim to promote Circular Economy (CE), Remanufacturing and Recycling concepts as strategic actions [7]. Similar initiatives are pursued from the EU Commission with the action “Closing the loop - An EU action plan for the CE” [17] and from China with its “Five Year Plan” development [18,19]. A report produced by Ellen MacArthur Foundation with the McKinsey Center for Business and Environment and the SUN Institute, strongly recommends the need to switch to a CE system for Europe in order to remain competitive in the manufacturing sector at global level [8].

On the other hand, it is necessary to contextualise the CE logics with the current manufacturing paradigm. According to [9], there are four manufacturing paradigms from before common era until the contemporary time: (a) craft production, (b) mass production, (c) mass customised production and (d) direct digital manufacturing (DDM). Craft production was typical of artisan societies, in which products were manufactured by experts mainly for their local community. The products were thought for specialised task and even if they could be different, they all shared similarities in the way they were produced. With the beginning of the 20th Century, mass production was dominated from standardised products and the consumers (which could also be from outside the national borders) had limited or none influence on their design. Even if the mass production and the mass customisation (which characterized the second part of the 20th Century, from the post war world II) paradigms share similarities (as better discussed in [9]), in the latter system the design of the products is highly influenced from the users. Finally, in the DDM paradigm of the 21st Century, the design requirements are

directly created by a network of different people. Once one of these highly personalised products is created, it can be directly produced, and its design remains for future improvements or alterations according to the desires of new actors. According to [9], the transition from one manufacturing paradigm to another is influenced from the parallel evolution of the enabling technology and of the enabling hardware. Among these, the Additive Manufacturing (AM) technology is considered as one of the drivers for the migration to DDM. In fact, with AM, CAD files and open-source printer software, products can be directly manufactured close to the customer and directly derived from digital models [9,10]. A description of some of the most noticeable applications of AM is provided in the following paragraph, in order to contextualise these technologies in the nowadays world.

The role of Additive Manufacturing

AM describes a set of manufacturing technologies which produce a part with a layer by layer strategy from a 3D CAD model [20]. Charles Hull invented the first additive manufacturing system, known as Stereolithography (SLA), in 1983, and its format file called Standard Triangulation Language (STL). If initially AM was confined to rapid prototyping, rapid tooling and rapid casting, soon it became a technology to manufacture near net shape and net shape products. AM is nowadays considered as breakthrough technology to consolidate the Industry 4.0 in the modern firms [21], and more in general, as a driver of the direct digital manufacturing paradigm [9]. AM techniques allow the fabrication of complex shapes without the use of specific production tools, reducing the economic lot size to the single unit and allowing the mass customisation [22]. Some examples come from the medical sector with orthodontic implants and prostheses. For instance, Renishaw collaborates to a cranial surgery of a 68-year-old female patient with a meningioma using the Laser Powder Bed Fusion (L-PBF) technology. A cutting guide was produced to highlight the cutting area on the skull and then a cranial plate was placed to protect the area after the operation [23]. Similarly, producers of AM systems as Renishaw and EOS applied L-PBF to increase the production efficiency in dental frameworks without losing accuracy [23,24]. An example of orthopedic applications is given from EOS with a novel 3D-printed tracheal splints to treat a tracheobronchomalasia using the Selective Laser Sintering (SLS) process [24]. 3D Printed acetabular cups can be also made with metal powder-

based AM techniques to obtain an open-pore (cellular or lattice) structure that can promote bone ingrowth and prevent a later-stage loosening of the implant [25]. Moreover, the re-design for AM allows the topological optimisation of structural parts and facilitate the light-weighting [26,27]. The topology optimisation can also achieve an optimised thermal flow dissipation: in fact, conformal channels cooling can reduce the cycle time of injection moulding [28]. GE realised the world's first engine with extensive use of AM producing their Advanced Turboprop with a reduction of components from 845 to just 11 [29]. Optisys redesigned a large, multi-part antenna assembly into a palm-sized, lighter, one-piece, 3D-printed metal antenna. The manufacturing conventional methods were brazing and plunge EDM. On the other hand, Optisys achieved the following benefits with AM: part count reduction from 100 pieces to a 1 integrated assembly, weight savings of over 95%, lead time reduced from 11 months to 2 months, production costs reduced by 20-25% and non-recurring costs reduced by 75%. In aeronautic, Electron Beam Melting (EBM) is used from GE to produce turbine blades with a new generation of metal alloy for AM which is titanium aluminide. Comparing with the previous casting process applied to nickel-based alloys, an increase of productivity is achieved as well as a reduction of the final component mass [30]. AM techniques are also used for sport applications: lightweight continuous carbon fibre products on demand such as bike frames and tennis rackets are currently made by AREVO with an Fused Deposition Modelling (FDM) based technique [30]. Other benefits are present in automation. For instance, bionic systems inspired to elephant proboscis are made via SLS with huge saving on the unit costs compared to injection moulding [24]. Flexible grippers are produced with SLS, SLA or Multi Jet Fusion (MJF) [31]. Architectural design is carried out with AM: 3D Printed Canal House with FDM are produced in Amsterdam [32]. Finally, examples of 3D Printing for jewellery are given from EOS for gold goods [24].

Conceptual framework of the thesis

Figure 1 shows the conceptual framework of this thesis.

Chapter 1 starts with a meditation on the study entitled “The trajectory of the Anthropocene: The Great Acceleration” [1]. It generates the awareness for the needs of works in the direction of a sustainable development. In paragraph 1.1.1, the concepts of the "Earth’s Life Support System" [2,3] and, as consequence, those of "Absolute Sustainability" [4] and of the "IPAT equation" [5,6] are given

to contextualise this study in the modern concept of sustainability. As seen in the first section of this introduction, the Circular Economy approach is currently seen as a key economic model to face the sustainability challenge of the contemporary world. Therefore, paragraph 1.1.2 goes into the details of the CE, describing is basic principles. The investigation of the circular economy actions gave the following RQ1:

Research Question 1 (RQ1). With a Circular Economy point of view, how to assess the remaining useful lifetime of products and how to perform a LCA study under a function-oriented analysis?

This work includes into its first research question (RQ1) the boundary constrains of the current manufacturing paradigm, as visible in Figure 1, even if the proposed methodology can be extended to other manufacturing techniques. As discussed in [9], the current manufacturing paradigm of the direct digital manufacturing is based on the presence of Additive Manufacturing systems. Therefore, paragraph 1.1.3 aims to contextualise the CE logics by means of AM techniques [11,12]. Chapter 1 performs a literature review, which was used to investigate the state-of-the-art gaps and to formulates the aims of the thesis connected to the RQ1 in an iterative way, a visible from Figure 1.

The LCA methodologies require data closely related to the considered case study to fill their analysis. This need gave the following RQ2:

Research Question 2 (RQ2). How to evaluate the energy efficiency of a manufacturing technology at the unit process level and which can be a good methodology to achieve this goal?

The literature showed practices already available for conventional processes (e.g., machining, injection moulding). On the other hand, these studies are not available for AM techniques. Moreover, the boundary constrains of the current manufacturing paradigm require an investigation of the advantages and disadvantages that AM can also bring regarding the sustainability at its unit process level. As matter of fact, AM techniques are characterised from low productivity and high energy demand, especially in comparison with bulk and subtractive techniques [13–16]. Chapter 1 performs a literature review (see paragraph 1.2), which was used to investigate the state-of-the-art gaps and to formulates the aims of the thesis connected to the RQ2 in an iterative way, a visible from Figure 1.

The aims of this thesis are reported at the end of the entire literature review performed in Chapter 1 (i.e., in paragraph 1.3).

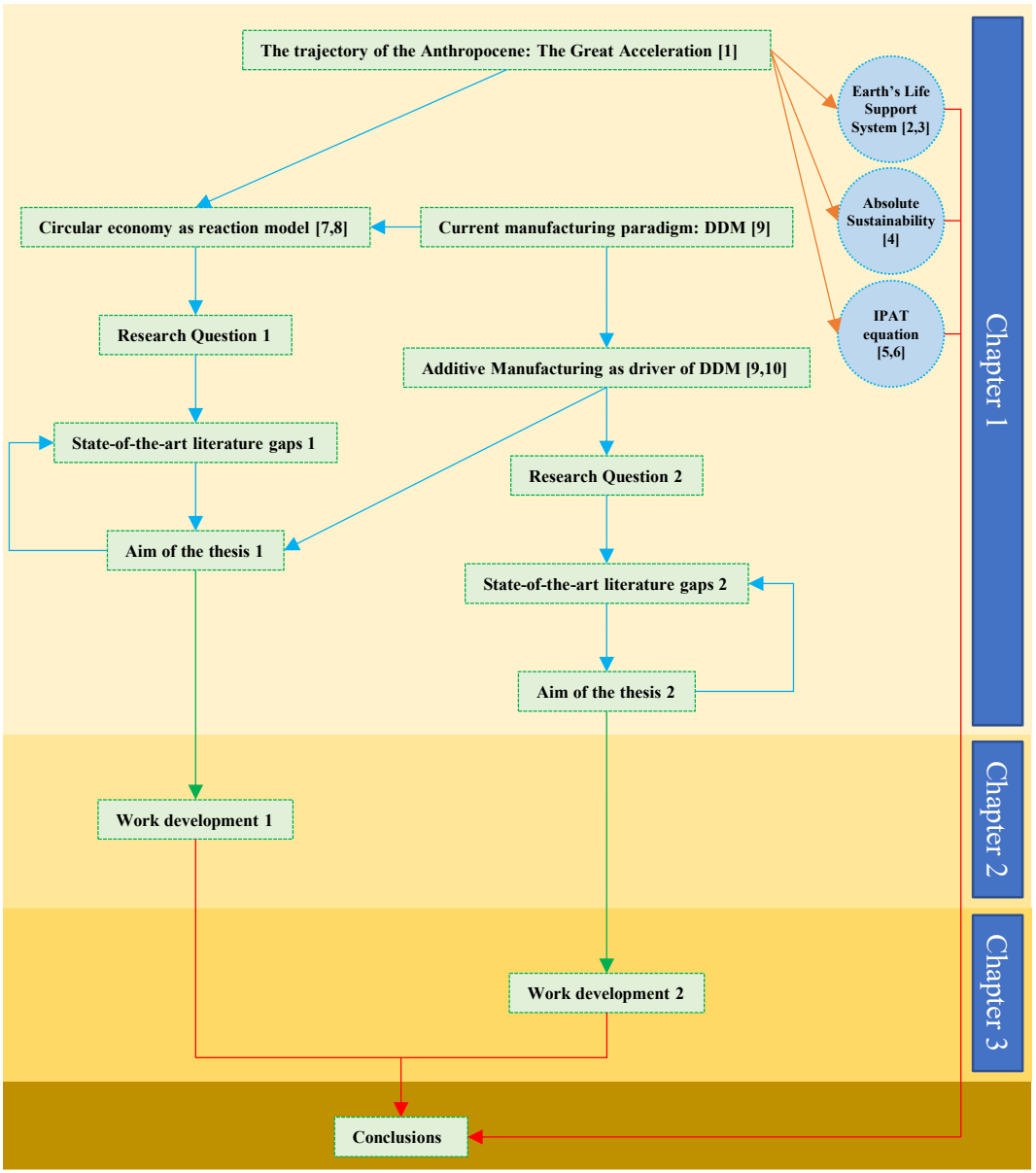

Figure 1. Conceptual framework of the thesis.

As visible from Figure 1, Chapter 2 and Chapter 3 run independently the investigation of RQ1 and RQ2, respectively, with a different methodology. For sake of clarity, a summary of the two methodologies is reported for each Chapter (see Table 3 and Figure 34, respectively for Chapter 2 and Chapter 3).

The conclusion section summarises the results of this work and reports their limits and possible future improvements. Moreover, it discusses the connections between the topics investigated in Chapter 2 and in Chapter 3. The methodologies and the results of the present study could be extended to other manufacturing techniques. In fact, finally considerations are made both for the unit process level and for a CE point of view on how to choose a manufacturing process rather than another in order to actually select a sustainable alternative.

Gantt chart of the activities

Figure 2 reports a Gantt chart of the studies and of the research activities carried out during the PhD at Politecnico di Torino, including the visiting period at the University of New South Wales (UNSW). A division into the main performed tasks is given.

According to the requirements given by Politecnico di Torino, an educational path needs to be followed by the students of the PhD School. This was taken by the author of this thesis from the beginning of the PhD until June 2019. The attended courses are listed in the following:

- Additive manufacturing and reverse engineering: innovation, advances and sustainability (35 h);
- Additive Manufacturing in Bioengineering and Surgery (20 h);
- Advanced techniques for quality measurement (25 h);
- Advanced topics in the finite element method (20 h);
- Communication (5 h);
- Design and analysis of industrial experiments (25 h);
- Entrepreneurial Finance (5 h);
- Forensic investigation techniques and job safety analysis contributions in the occupational safety & health risk assessment and management (10 h);
- Industrial welding processes (15 h);
- Management of product design processes (20 h);
- Mechanics, properties and high-resolution characterization of surfaces (20 h);
- Occupational accidents root causes analysis and prevention (5 h);
- Polymeric additive manufacturing (20 h);
- Project management (5 h);
- Public speaking (5 h);
- Public Speaking II (12 h);
- Research integrity (5 h);
- Responsible research and innovation, the impact on social challenges (5 h);
- Statistical methods in design, production and verification processes (30 h);
- Structural joints: design, processes and manufacturing (30 h);
- The new Internet Society: entering the black-box of digital innovations (6 h);
- Time management (2 h);
- Tools and technologies for product development (25 h);
- Writing Scientific Papers in English (15 h).

Regarding the scientific activity, initially it focused on the study of the energy efficiency at the unit process level of AM techniques (Chapter 3). The experimental work was carried out in collaboration with the Integrated Additive Manufacturing (IAM) laboratory of Politecnico di Torino. An initial study of the literature (paragraph 1.2 of Chapter 1) was required, and it was performed from November 2017 to January 2018. Then, the DOE for the investigation of the selected AM processes in this thesis was structured, as visible from Figure 2. The relative experimental activity was carried out almost during the totality of the first and the second year of the PhD, as shown in Figure 2. The details of these two tasks are reported in Chapter 3.

A research period abroad of 9 months was done at the Sustainability in Manufacturing & Life Cycle Engineering Research Group @ UNSW. This period was useful to give a higher point of view to the research, contextualising the activity performed at Politecnico di Torino in the concepts reviewed in paragraph 1.1 of Chapter 1 and in the modelling elaborated in Chapter 2. More in details, the review of the literature, concerning these topics, was performed from October 2019 to February 2020 and the modelling was carried out from December 2019 to June 2020.

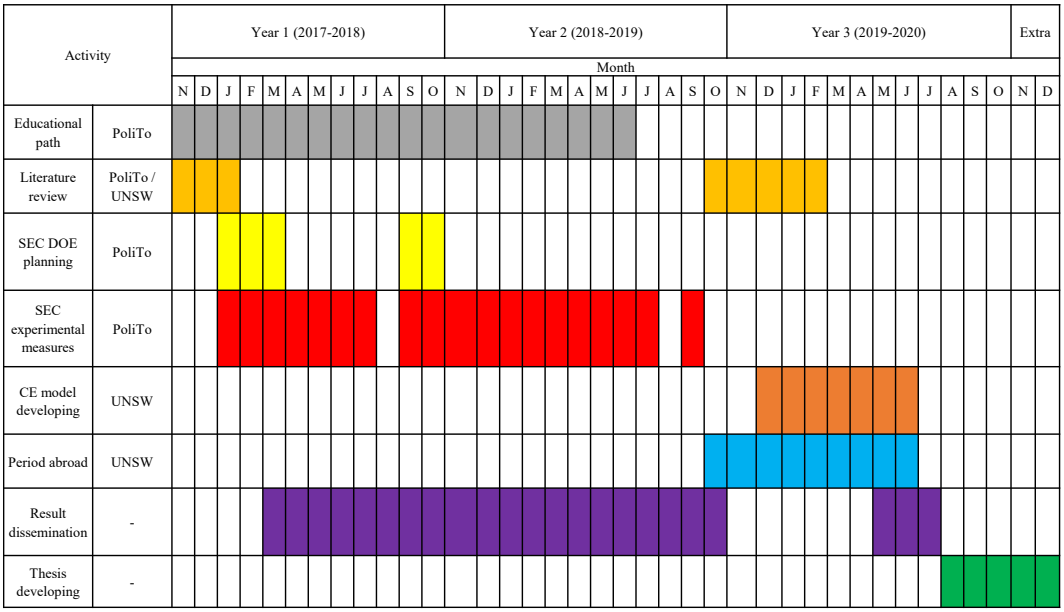

Figure 2. Gantt chart of the activities.

One of the difficulties of this work was the connection between the investigated topics. In fact, they space from the unit process level (i.e., with a

highly focalised point of view on the process) to a broader evaluation of complex mechanisms, such as those present in a CE context.

Another was given by the effect of the COVID-19 pandemic, which slowed down the developing of this thesis. This required two extra months to complete it, as visible from Figure 2.

Finally, regarding the result dissemination activity, it is possible to see the "Papers related to the PhD research activities" section of this thesis to consult the produced work and Figure 2 to see the required time.

Chapter 1

Literature review

1.1 The Circular Economy challenges

In this paragraph the concept of the Earth's Life Support System as well as that of Anthropocene are introduced. The basic concepts of Circular Economy (CE) are given and placed into the three dimensions of sustainability [2,3]. Finally, the paragraph highlights the space that Additive Manufacturing (AM) covers in the current manufacturing paradigm (i.e., the direct digital manufacturing - DDM [9]) and describes the advantages achievable with the adoption of additive techniques for production in a CE system.

1.1.1 The Earth's Life Support System

In the study entitled "The trajectory of the Anthropocene: The Great Acceleration" [1], Will Steffen et al. show socio-economic and earth system trends from 1750 to 2010. The investigated socio-economic trends are: (a) population, (b) real GDP, (c) foreign direct investment, (d) urban population, (e) primary energy use, (f) fertiliser consumption, (g) large dams, (h) water use, (i) paper production, (j) transportation, (k) telecommunications and (l) international tourism. On the other hand, the investigated earth system trends are: (a) carbon dioxide, (b) nitrous oxide, (c) methane, (d) stratospheric temperature, (e) surface temperature, (f) ocean acidification, (g) marine fish capture, (h) shrimp

aquaculture, (i) nitrogen to coastal zone, (j) tropical forest loss, (k) domesticated land and (l) terrestrial biosphere degradation. Starting from the post war world II, a great acceleration is visible in these key parameters. Moreover, after the 1950 there is a clear evidence that fundamental changes in the functioning of the Earth System are guided by human activities, because they are not connected to the range of variability of the Holocene (which was considered as the current geological epoch, approximately began 11700 years before present). Therefore, the 1950 defines the start date for the Anthropocene, which is the term introduced from Paul J. Crutzen and Eugene F. Stoermer to describe a new geological era in which the human activities have a clear environmental impact on the Earth and have the capabilities to change it [33]. A new model to intend sustainability was proposed in [2,3] to realises a sustainable development paradigm for the Anthropocene. According to those works, the wide used "three pillars" approach, which separates social, ecological, and economic goals, cannot face the challenges of the Anthropocene. According to Johan Rockström in [2], the "three pillars" approach has driven a fragmented assessment of the development process, where economic growth overcomes natural and human resources. Therefore, there is the need of an integrated point of view that reconnects human development with the biosphere. *Reporting the words in* [2]*, in such new paradigm (shown in Figure 3):*

"the economy is seen as a means to achieve social goals generating prosperity within the limits of the Earth. Establishing an economy that functions as "an open sub-system of a finite and nongrowth ecosystem" will require the collective effort of nations, businesses, citizens, and institutions".

In this sense, the concept of "Absolute Sustainability" is given in [4]: there are limits for man-made pollution in our planet, which have to be seen as absolute boundaries posed by the Earth's Life Support System (i.e., the finite natural resources and the limited capacity of the environment to absorb pollution). According to the 2015 update on planetary boundaries [2,3], which together define the Earth's Life Support System, four out of nine boundaries have been transgressed. Two are in the high-risk zone (biosphere integrity and interference with the nitrogen and phosphorous cycles), while other two are in the danger zone (climate change and land use change).

The IPAT equation assesses the overall environmental impact (I), based on the work of Erlich and Holdren [5] and Commoner [6], which has to stay within the Earth's Life Support System. The equation evaluates the environmental impact (I) as product of the human population (P), the human affluence (A) and

the technology factor (T). As analysed in [34], according to the Intergovernmental Panel on Climate Change (IPCC) [35], in 2050 there is the need to reduce the emissions due to man related activities of greenhouse gases by between 30-70% of the current level to gain a reasonable probability to stay below the 2 degree target (which was agreed for the global temperature increase at the COP21 meeting in Paris 2015). Moreover, the global population (P) is predicted to reach 9.75 billion in 2050 [36]. The global average affluence (A) is expected to increase by a factor equal to 2. The technology factor T has to approximately decrease by a factor 10 to compensate the increase in P and A in order to achieve a 70% reduction in I. As described in [34], in the IPAT equation present a coupling between A and T. In fact, the reducing of several orders of magnitude in T over the last centuries have been more than neutralised by gaining increases in consumption (A). The environmental impact (I) can be evaluated using Life Cycle Assessment (LCA) techniques, and they are typically used to compare the impact of products and technologies [37].

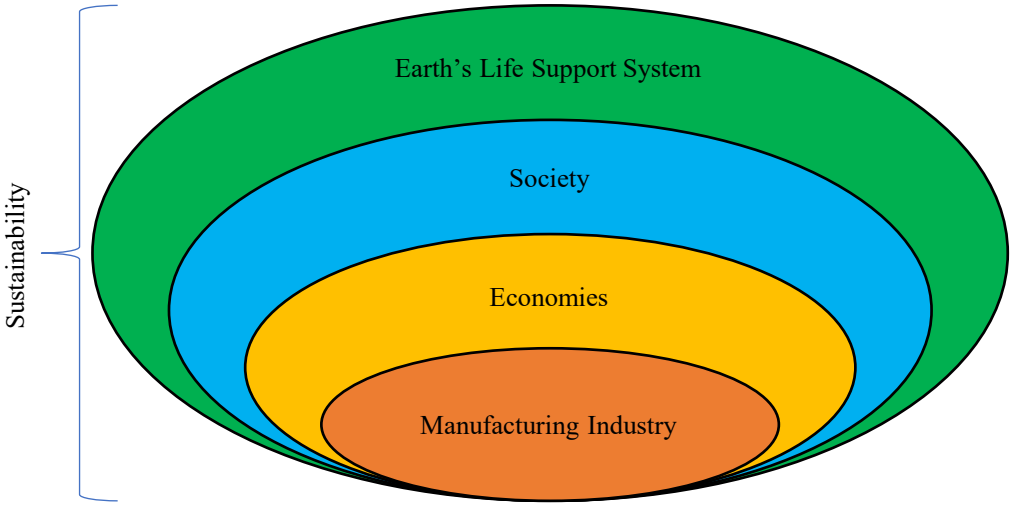

Figure 3. Sustainable development paradigm for the Anthropocene, according to [2].

1.1.2 Pillars of the Circular Economy

As described in the report of McKinsey Global Institute and McKinsey Sustainability & Resource Productivity Practice, the average resource price (based on arithmetic average of four commodity sub-indexes: food, non-food agricultural raw materials, metals and energy) has increased significantly since the turn of the 21st Century. In fact, an overall decreasing trend can be noticed between 1900 and

2000 (except for the period around the substantial event of the past, e.g., the World War I, World War II and the 1970s oil shock) [38]. On the other hand, the increasing trend of the present Century is still going on as described from McKinsey Global Institute in [38] for the main resource markets. Pushed from these planet changes and the new sustainable development paradigm for the Anthropocene, the attention to the efficient use of energy and resources is grooving among the political authorities. The 1987 report "Our common future" from the UN Commission for Environment and Development, sustainability was defined as central pillar for the development of humanity [36]. More recently, the G7 Summit Declaration of June 2015 launched the G7 Alliance on Resource Efficiency with the aim to promote the CE, Remanufacturing and Recycling concepts as strategic actions [7]. In the same year, the UN defined the 17 Sustainable Development Goals (SDG) to transform our world, promoting prosperity while protecting the planet [39]. Similar initiatives are pursued from the EU Commission with the action "Closing the loop - An EU action plan for the CE" [17] and from China with its "Five Year Plan" for development [18,19]. Finally, a report produced by Ellen MacArthur Foundation with the McKinsey Center for Business and Environment and the SUN Institute, strongly recommends the need to switch to a CE system for Europe in order to remain competitive in the manufacturing sector at global level [8].

According to [40], the traditional linear economy model (i.e., a system who relies on the logic of "take - make - dispose"), cannot face the sustainability challenges of the world. As highlighted in [41], the CE concepts find their origins in several schools of thought and they cannot be tracked back to one single author or date. In fact, they show relationships with the theory of "Regenerative Design", introduced by Lyle in the late 70s. This theory brings the idea to link sustainable development to the concept of resource regeneration [42]. Moreover, the economic basis for a transition from a linear system to a non-linear model was originally introduced by Stahel in 1981 [43] and further elaborated with the idea of "Cradle-to-Cradle" design in 2002 [44]. The concept of "Industrial Ecology", as detailed in [45], has also links to the CE strategy. More recently, the "Blue Economy" concept, elaborated by Pauli [46], describes a system in which the resources are connected in cascading systems and the waste of one product is the input to generate a new cash flow. The Ellen MacArthur Foundation defined the modern concept of Circular Economy with four different mechanisms for value

creation that offer higher opportunities comparing with the linear strategy [47]. *Reporting the words in* [41]*, they are:*

"The power of inner circle: the closer the product gets to direct reuse, i.e.,, the perpetuation of its original purpose, the larger the cost savings will be in terms of material, labour, energy, capital and the associated externalities.

The value of circling longer: value created by keeping products, components, and materials in use longer within the Circular Economy. This can be achieved by enabling more cycles or by spending more time within a single cycle.

The power of cascaded use: value created by using discarded materials from one value chain as by-products, replacing virgin material in another.

The power of pure circles: uncontaminated material streams increase collection and redistribution efficiency while maintaining quality."

Jawahir et al. [40,48], proposed the so-called "6Rs model" to define the "Sustainable Manufacturing", which extends the traditional "3R model" based on the Reduce, Reuse, Recycle practices with three additional actions namely Recover, Redesign, and Remanufacture. The "3Rs model" represents the foundation for the "Green Manufacturing" elaborated in the 1990s from the "Lean Manufacturing" philosophy, which is based on the "1R model" (Reduce) [49]. According to [40], referring to the production of the single product or component, *Reduce* aims to the reduced use of energy, materials and other resources during pre-manufacturing, manufacturing and the use phase, as well as to the reduction of emissions and waste during these three first stages of the life cycle. More in general at system level, it refers to the reduction of the overall environmental impact due to the proper implementation of the "6Rs model". *Reuse* refers to the reuse of the entire product, or its components, after its first life-cycle, for subsequent life-cycles, to reduce the usage of virgin resources and the related emissions and waste flows for the production of newer products and components. On the other hand, *Remanufacture* refers to the re-processing of already used products to restore their original state or to have a like-new form by means of the reuse of as many parts as possible without the loss of functionality. *Redesign* includes all the activities which aim to redesign the next generation products, which would use components, materials and resources recovered from the previous life cycle, or previous generation of products. *Recycle* involves the process of converting material that would otherwise be considered waste into feedstocks for new products. *Recover* refers to the process of collecting products

at the end of the use stage, therefore, it includes practices as disassembling, sorting and cleaning.

According to [41,50], the following actions are present in the practice for the implementation of the "6R methodology" in the industrial practice (Figure 4):

Maintenance: it defines all the strategies which aim to preserve the functional condition of a product. This practice directly involves the user of the product.

Repair: it refers to the correction of specified faults in a product. Repair aims to return a product or component purely to a functioning condition after a failure has been detected, either during service or after discard. This practice can also directly involve the user of the product.

Product Reuse: it represents a generic term which includes all the operations that allow a product to be put back into service, thanks to a distribution system, essentially in the same form, with or without repair or remediation.

Remanufacturing for function restore: it returns a used product to at least its original performance with a warranty that it fulfils a function similar to the original part. *Remanufacturing for function up/downgrade*: in case of upgrading, it provides new functionalities to products through remanufacturing, which aim to extend products' value life. In case of downgrading, the remanufactured product will be delivered to a secondary market with lower performance requirements. *Component Reuse*: it returns the components to be reused to the manufacturing level in order to incorporate them in a new product.

Closed-loop recycling: it refers to the recycling of a material which does not show degradation of its properties (upcycling). *Open-loop recycling*: it refers to the recycling of a materials which shows a degradation of its properties (downcycling). Therefore, in the second case, the recycled material will be only usable for applications which demand lower performances.

The implementation of these actions requires different de-/re-manufacturing systems capabilities, as the examples reported in [41] testify. An analysis of remanufacturing practices in Japan is given in [51], focusing on photocopiers, single-use cameras, auto parts, printer ink cartridges and toner cartridges. An example of de-manufacturing systems is the pilot plant installed at ITIA-CNR, the Institute of Industrial Technologies and Automation of the Italian National Council for Research [52]. An application of that plant to the recycling of products with complicated material mixtures, including key-metals and rare earths, such as electronic and automotive waste is provided in [53]. The authors in [54] proposed a design method for semi-destructive disassembly with split lines to

facilitate the de-manufacturing process. Other authors in [55], highlighted the importance of cognitive robotics in disassembly of products and reported their application with the vision-based disassembly rig applied to LCD screens.

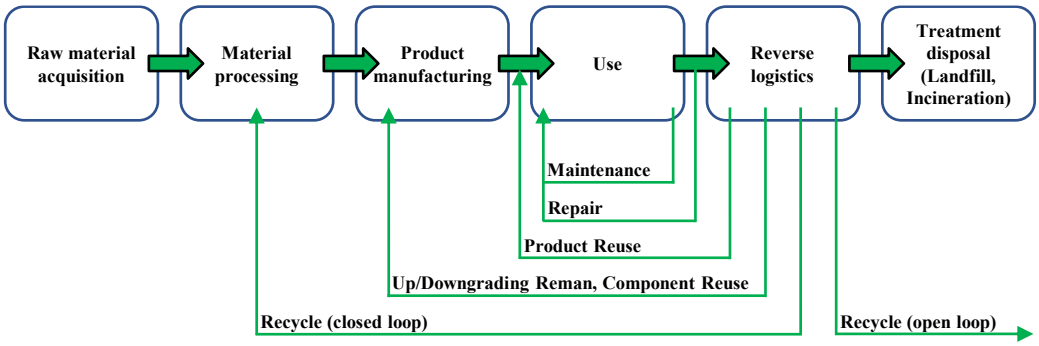

Figure 4. Implementation of the "6R methodology" in the industrial practice (Adapted from [50]).

1.1.3 Additive Manufacturing and Circular Economy

As highlighted in the introduction section of this thesis, the current manufacturing paradigm is defined as direct digital manufacturing (DDM). It describes a new era of manufacturing in which the design requirements are directly created by a network of different people [9]. It aims to a high customisation of the products and it allows the decentralised production of objects close to the customer and directly derived from digital models [9,10]. Additive processes are considered as drivers of this manufacturing paradigm for their intrinsic characteristics and therefore, the attention to the contextualisation of these techniques in the new model of the circular economy is grooving. Different authors from both the academic and the industry context, proposed a research agenda to determine enablers and barriers for AM to embrace the CE philosophy [56]. Six main area of investigations were considered, which are: (a) product, service and system design, (b) material supply chains, (c) information structure and flows, (d) entrepreneurial responses, (e) business model transformations and (f) education and skills development. Moreover, the authors in [57] highlighted different fields of analysis to study the alignment between AM and the concepts of CE: (a) material savings, (b) flexible manufacturing strategies, (c) hard repair and maintenance intervention, (d) extended products life span and (e) design based economy. In [58] the authors described as AM can be used to locally manufacture new goods from local sources of recycled plastic waste. In particular, in the same paper the authors brought the case of the London metropolitan area,

where system conditions already exist in the form of material flows, technology policy, and facilities to evaluate 3D printing's viability as driver of a CE at the local level. Regarding this topic, the authors in [59] identified the key potential of Fused Deposition Modelling (FDM) to produce satisfying plastic parts which incorporate recycled fibre as reinforcement. Focusing on the remanufacturing applications of AM, in [60,61] the authors compared the capabilities of AM Laser-based processes (as Direct Energy Deposition - DED) with those of other techniques as GTAW/TIG, Electro Spark, HVOF and PTAW. The advantages of AM were mainly found in the lower heat input, the less warpage and distortion, the excellent metallurgical bonding, the excellent mechanical performance, the high precision of resulting geometry and the precise thermal control. A review of the remanufacturing applications of DED to different case studies (e.g., mould, die, rails, vessels, crankshaft, marin piston, gas turbine compressor, low-pressure turbine blades and turbine airfoils) is also provided in [12,60], considering materials as steels and Ni-based superalloy. Applications of laser metal deposition to re-fill milled grooves are given in [62] using stainless steel and a titanium-alloy. The authors succeed to rebuild different U- or V-groove shapes without defects as long as the groove was wide enough to allow the powder jet accessibility. An example of remanufacturing via powder bed process is given in [11] for the Siemens's gas turbine burner, where damaged burner tips were first machined and then placed into a Laser Powder Bed Fusion (L-PBF) machine. In such cases an extensive use of reverse engineering is needed to rebuild the damaged volume, as highlighted in [63,64].

The reduction of the energy and the material resource usage was demonstrated with LCA studies aiming to compare conventional technologies and AM processes, such as Electron Beam Melting (EBM) [65,66], L-PBF [67,68] and Wire Arc Additive Manufacturing (WAAM) [69,70]. More in detail, the re-redesign for AM can actively contribute to reduce the environmental impact of the additive processes achieving a strong light-weighting, respect to conventional processes. Moreover, the CE practice of recycling allows a further reduction, comparing with a linear model, especially for processes with a worst material usage efficiency (e.g., machining) [67] and for materials with a high embodied energy (e.g., titanium alloys) [66]. In [63], the authors evaluated the suitability of remanufacturing for a turbine blade made of Inconel 625, considering the component percentage to be remanufactured as input variable and using the Cumulative Energy Demand (CED) and the overall CO_2 emissions as key metrics

of the assessment. For the CE approach, remanufacturing technologies as DED, GTAW and PTA were considered. On the other hand, for the linear economy model, investment casting was considered for the brand-new manufacturing of the entire component. Fixing the remanufacturing percentage, the authors in [63] computed a higher environmental input for GTAW and PTA respect to DED. Moreover, the AM process was also considered able to give better mechanical performances comparing with those of other remanufacturing techniques. Comparing the CE and the linear approach, the DED process should be preferred for remanufacturing percentages below the ranges 15-24% and 18-28% for the case study in [63], respectively for the CED and the overall CO_2 emissions. The authors in [71], investigated the environmental impact to remanufacture the tip portion of a burner, used in a Siemens industrial gas turbine: L-PBF was compared with conventional machining plus welding. The tip portion of a burner is made of a Nickel based alloy and it is positioned on a burner tip spacer, which is made of a stainless-steel alloy. Sankey diagrams were used to show the energy and resources flows for both scenarios. The authors conducted a sensitivity analysis in which they evaluated the benefits arising from recycling actions, starting from 0% (no recycling, i.e., all metal scraps go to landfill deposit) to theoretically 100% (all metal scraps go back to metallurgy processes). Furthermore, two recycling modes were considered, namely down-cycling (all types of scraps are collected in one vessel and cannot be separated, therefore, only stainless-steel can be recovered, considering the case study in [71]) and equal quality recycling (scraps are collected and recycled separately for each alloy, aiming to recover the scraps in the original composition as far as possible). An overall lower material flow was noticed for the AM approach, in fact, the Abiotic Depletion Potential (ADP), which indicates the mineral resource depletion, showed a lower value for AM as long as the recycling rate was kept lower than around the 80%. The Global Warming Potential (GWP, mainly attributed to the CO_2 emissions in [71]) indicator and the CED gave higher values for the conventional approach for all the investigated recycling rate range. More in detail, the trends for the AM approach as function of the recycling rate showed a flat tendency, due to the minimised material flow of the additive approach.

Among the possible actions in the industrial practice for the implementation of the "6R methodology", in this thesis the attention is focused on remanufacturing. It is a CE action particularly connected the manufacturing level, as visible in Figure 4, and this suits better the background of the author of this

thesis. This work particularly focuses on additive techniques, due their importance for the current manufacturing paradigm. The DED process is chosen to investigate the energy savings that can be achieved with the implementation of a circular economy model based on remanufacturing because it is a promising technology to achieve this goal, as noticeable from the literature review performed above. On the other hand, the EBM process is considered for the comparison with a linear economy approach, because it currently represents a mature technique at industrial level.

1.2 The unit process level of AM

As far as the energy efficiency at the unit process level of a manufacturing process is concerned, the state-of-the-art literature offers a parameter to synthesise this useful information, i.e., the Specific Energy Consumption (SEC). It is defined as the energy demand at the unit process level (i.e., considering both productive and not productive phases) to produce the unit mass of material. SEC is often used in literature to address the energy efficiency of a manufacturing technology. Some examples are given for machining processes [72], injection moulding [73] and even for AM techniques [13,14]. If from one side, the state-of-the-art literature is plenty of works for the characterisation of conventional processes, on the other hand, there is a lack of studies to define the energy efficiency of additive techniques. In this paragraph, particular attention is given to the unit process level of AM processes in order to provide a base knowledge of the achievable energy efficiency. The study of these technologies is particularly interesting, since two disadvantages of AM make them less competitive respect to bulk and subtractive techniques: the low productivity and the high energy demand [13–16]. Only few works have investigated this aspect, defining new parameters specially designed for additive techniques. The Specific Printing Energy (SPE) is defined as the ratio between the printing energy (i.e., neglecting the not productive phases) and the printed mass [74,75]. To evaluate the deposition efficiency, the average Deposition Rate (DR_a) is defined as the ratio between the printed mass and the needed time [74,75]. This variable can be defined according to the printing phase (DR_{aprint}) or to the entire unit process level (DR_a).

According to the ASTM F2792 - 12a (Standard Terminology for Additive Manufacturing Technologies) [20] the panorama of the additive technologies can be divided in seven categories. As visible from Figure 5, they are binder jetting,

directed energy deposition, material extrusion, material jetting, powder bed fusion, sheet lamination and vat photopolymerization. The ASTM Committee F42 on Additive Manufacturing Technologies proposes this distinction because it allows to discuss about a category of machines, rather than giving an extensive list of commercial variations of a process methodology. More information regarding the standardisation activities in additive manufacturing, carried out from ISO and ASTM, can be found in [76]. *Reporting the words in the ASTM F2792 - 12a, the following definitions of the AM categories is given. Vat photopolymerization: an AM process in which liquid photopolymer in a vat is selectively cured by light-activated polymerization. Material extrusion: an AM process in which material is selectively dispensed through a nozzle or orifice. Material jetting: an AM process in which droplets of build material are selectively deposited. Binder jetting: an AM process in which a liquid bonding agent is selectively deposited to join powder materials. Powder bed fusion: an AM process in which thermal energy selectively fuses regions of a powder bed. Directed energy deposition: an AM process in which focused thermal energy is used to fuse materials by melting as they are being deposited. Sheet lamination: an AM process in which sheets of material are bonded to form an object.*

The first AM process, i.e., the Stereolithography (SLA) technique, was invented by Charles Hull in 1983 and it belongs to the vat photopolymerization category. This process uses a laser source to cure the liquid polymeric resin and it is currently applied in 3D printers of 3D Systems [77] and Stratasys [78]. On the other hand, the Digital Light Processing (DLP) uses a digital light to achieve this goal. Among the AM technologies which use the material extrusion principle, the Fused Deposition Modelling (FDM) process was the first invented. This technique, first patented by Stratasys [78], can use a plastic feedstock material either in a wire or in a disk shape. Considering the material jetting principle, in the Drop On Demand (DOD) process the fluid (e.g., plastic or wax) is selectively expelled from different jet nozzles according to the feature requirements of the layer. Some of the principal techniques which belongs to DOD are MultiJet Printing (MJP) from 3D Systems [77] and PolyJet from Stratasys [78]. In both cases, the polymer is cured with UV light. In binder jetting the printhead selectively deposits a liquid binding agent onto a thin layer of powder particles (e.g., plastic, metal, sand or gypsum). Examples of 3D printers which use this principle are given from 3D Systems [77]. Considering the powder bed fusion category, the Multi Jet Fusion (MJF) technique was developed from HP [79] to

produce components starting from plastic or metal powders. In this case, the heating input is given from resistors. The Selective Laser Sintering (SLS) process is currently used from EOS [24] to produce polymer components. The laser heat source is also applied to melt metal powders defining the family of the Laser Powder Bed Fusion (L-PBF) processes. Different industries, such as EOS [24], General Electric [29] and Renishaw [23] produce 3D printers which apply this principle. Considering the electron beam heat source, the Electron Beam Melting (EBM) process was first patented from Arcam and it is currently used from General Electric [29] to melt metal powders. The direct energy deposition category includes the Direct Energy Deposition (DED) process which uses a laser heat source and the Electron Beam Additive Manufacturing (EBAM) technique which uses an electron beam. This technology category is currently under developing and few examples of industries can be given, such as Prima Industrie [80], Optomec [81] and Sciaky Inc [82]. Finally, Mcor Technologies [83] developed applications of the sheet lamination AM category.

It is necessary to mention that Figure 5 offers a window of AM techniques which are currently well established and does not go into the details of new processes or variants of existing technologies currently under development. In fact, in the last few decades a big effort has been continually given to the developing of AM. Therefore, the capabilities of the single process evolve very fast. For instance, the Fused Filament Fabrication (FFF) and the Laminated Object Manufacturing (LOM) can produce composite products at industrial level. In particular, among the two-extrusion head FFF systems, Markforged [84] patented and developed the Continuous Filament Fabrication (CFF) process in which a continuous fibre is deposited layer by layer. Another example can be given from the FDM technique, which can be also used to deposit ceramics and metals dispersed in a polymeric base feedstock, eventually with some postprocessing. Furthermore, most of the techniques shown in Figure 5 can produce composite objects, at least at laboratory level [85,86].

Among these processes, some of them are selected for the unit process level study in this thesis. The FDM technology is chosen because it is widely spread in the world, not only at industrial level, but also at domestic level, due to its relative simplicity. The EBM process is selected as well because it is a mature technique considered as promising industrial technology for the production of components made of high strength alloy, due to the high specific energy of the electron beam and because the vacuum working condition of this technique reduces the melting

temperature point of these alloys. Finally, the CFF process is proposed because it can be positively used to produce composite products at industrial and domestic level. In the following, a deep description is provided for the selected technologies for the empirical studies on the unit process level of AM together with a critic evaluation of the state-of-the-art literature about their energy and time efficiency.

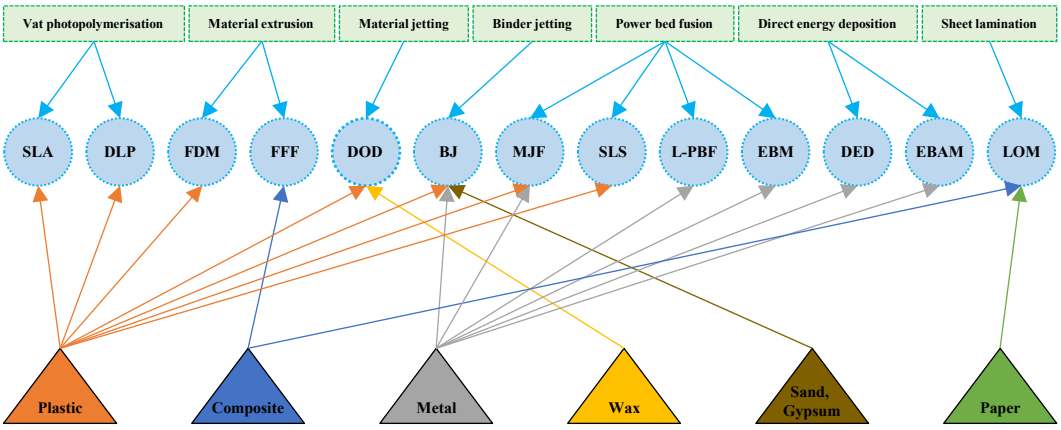

Figure 5. AM processes classified according to ASTM standards [20].

1.2.1 Fused Deposition Modelling

Among the AM techniques which process plastics, the material extrusion process patented by Stratasys as Fused Deposition Modelling (FDM) is widely used for the low costs and simplicity of the equipment and the capability to process different materials, even if nano-reinforced [87] or characterised by a high melting point (as PEEK [88]). This process has already proved to be competitive respect to the conventional technologies which process plastics [89,90], particularly if optimisation of the process parameters is performed [91]. After the expiration of the FDM patents in 2008, many low-cost FDM systems have been proposed worldwide. Usually, these machines are addressed as 3D printers. Due to the availability of FDM systems, it is worth to quantify their environmental impacts.

The FDM technology

The FDM technology is based on the extrusion of a polymer through a heated nozzle. In some cases, the start plate of the machine is prepared to facilitate the adhesion of the 3D printed parts. Then the extruders are powered to reach the process temperature. If the build chamber and the start plate can be heated up, they are also powered in this phase. The calibration phase occurs bringing the start

plate and the extruders to the initial position. Finally, the printing process can start. Typically, 3D printers have a three-axis structure and one extruder, while the start plate and the build chamber are not heated. There are two standard sizes for the diameter of the plastic wire, around 1.75 mm or 3 mm. The nozzle diameter varies from 0.10 mm to 0.70 mm. Further machine subunits as multiple extruders, heaters for the start plate and the build chamber increase the cost of the system. On the other hand, industrial FDM machines have a heated build chamber and advanced mechanic solutions to guarantee better positioning accuracy and higher speed. Industrial FDM machines have at least two extruder heads, respectively for the build material and its support. The calibration operations and the material change need to be done manually for low cost systems. Set-up operations are automatic for industrial machines and the material change is simpler because the materials are supplied in chipped cartridges. Most of the 3D printers are open-source systems and for the above-mentioned characteristics they are sold at prices starting from some hundreds of euros. Instead, prices for industrial systems starts from above 15000 euros. The build volume can be different according to the application. For instance, cheap 3D printers can start from about 10 cm per side, while industrial machine provided from Stratasys reach $914.4 \times 609.6 \times 914.4$ mm^3. Finally, possible layer thickness can vary from 0.127 mm to 0.508 mm.

Energy efficiency of the FDM process

Table 1 reports the correlation between the SEC and DR_a data reviewed in literature for the FDM technology. Luo et al. [92] compared the energy efficiency of different Stratasys machines (FDM 1650, FDM 2000, FDM 8000 and FDM Quantum). The SEC data in [92] were also referenced in further research [13,15,93,94]. Mognol et al. [95] studied the influence of the component orientation on the overall energy consumption of FDM for the Stratasys FDM 3000 and ABS. Only the volume results are reported in [95] for the material flow data. Therefore, the printed masses were estimated in this work considering a specific density of the material equal to 1.04, as typical for ABS.

Machine	Material	Mean operational power [W]	SEC [electric MJ/kg]	DR_a [kg/min]	Reference
Stratasys FDM 1650	ABS	1320	1247	$6.35 \cdot 10^{-5}$	[92]
Stratasys FDM 2000	ABS	2200	416	$3.18 \cdot 10^{-4}$	[92]

Stratasys FDM 8000	ABS	2200	83	$1.59 \cdot 10^{-3}$	[92]
Stratasys FDM Quantum	ABS	11000	589	$1.12 \cdot 10^{-3}$	[92]
Stratasys FDM 3000	ABS	570	228 - 447 *	$1.41 \cdot 10^{-4}$ - $7.55 \cdot 10^{-5}$ *	[95]
Stratasys FDM 400mc (Single part)	PC	2450	536	n.a.	[96]
Stratasys FDM 400mc (Full build)	PC	2450	519	$3.17 \cdot 10^{-4}$	[96]
Stratasys FDM 400mc (Single part)	PC	2450	738	$2.07 \cdot 10^{-4}$	[97]
Stratasys FDM 400mc (Full build)	PC	2450	693	$2.13 \cdot 10^{-4}$	[97]
Stratasys Dimension SST 1200es	ABS	580	171 - 219	n.a.	[16]
Stratasys Dimension 768 SST	ABS P400	1100	689	$7.65 \cdot 10^{-5}$	[15]
Stratasys Dimension SST	n.a.	1100	n.a.	n.a.	[98]
Makerbot Replicator 2X	ABS	125 *	28 - 53	$1.64 \cdot 10^{-4}$ - $2.91 \cdot 10^{-4}$ *	[94]
MakerBot Replicator 2X	ABS	125 *	23 *	$3.34 \cdot 10^{-4}$ *	[99]
3D Systems RapMan 3.2	ABS	n.a.	19 *	$1.66 \cdot 10^{-4}$ *	[99]
Stratasys Mojo	ABS	n.a.	40 *	$2.31 \cdot 10^{-4}$ *	[99]
HP DesignJet 3D	ABS	n.a.	77 *	$3.85 \cdot 10^{-4}$ *	[99]
Stratasys Dimension Elite	ABS	n.a.	127 *	$2.55 \cdot 10^{-4}$ *	[99]

Table 1. Electric energy and time efficiency data available in the literature for FDM. The values marked with "*" have been computed in this work. Full build is intended for the saturation of the start plate.

The quantity of material needed for the support structures was found to be the main driver on the energy demand. On the other hand, the height of the printed component appeared to be of secondary importance. The paper of Mognol et al. [95] was also referred in subsequent works [13,94,100]. In [96,97] the effect of the machine build capacity utilisation on SEC was highlighted. A Stratasys FDM 400mc machine was used to produce parts made of polycarbonate. A slight

variation in the SEC value was noticed between the conditions of single capacity and full capacity utilisation because of the low energy requests from the not productive phases of FDM. These results were also referred in [13,15,94,101]. Some authors [15,16,94,98] focused on the characterisation of the power profile of different FDM machines (i.e., Stratasys Dimension SST 1200 es, Stratasys Dimension 768 STT, Stratasys Dimension SST and MakerBot Replicator 2X) and identified the main sub-phases of the process. In [94] the correlation between SEC and the component geometry was studied on the MakerBot Replicator 2X with ABS material. The higher values were found for components with a higher height, because of the longer not productive time due to the higher layer number. In [99] the performances of five different FDM machines (i.e., MakerBot Replicator 2x, 3D Systems RapMan 3.2, Stratasys Mojo, HP DesignJet 3D and Stratasys Dimension Elite) were evaluated under the technical, economic, and environmental perspective. The results reported in [94,99] were further elaborated in this work to compute the SEC factors.

1.2.2 Electron Beam Melting

In 1993 the Electron Beam Melting (EBM) was patented. The process uses the principle of melting electrically conductive powder layer by layer to manufacturing three-dimensional bodies [102]. As EBM process is replacing traditional processes like casting, a crucial issue concerns the assessment of its sustainability, and thus the environmental burdens associated with it. Specific studies that consider the CED to produce a part by means of EBM processes, from the powder production to post-processing, have highlighted that the manufacturing step is one of the main contribution that has to be taken into account [66,103].

The EBM technology

EBM is a powder bed fusion AM process in which an electron beam (EB) is used to selectively melt metal powder [104]. Initially, the EB uniformly preheats the start plate. Then, a rake system distributes a uniform powder layer, which is preheated completely by several smooth beam passages at a high beam current and high scan speed. The preheating of both the start plate and the powder bed is performed up to a specific temperature, which depends on the printed material. The preheating of the powder bed consists of two subsequent steps. First, the

powder bed is uniformly preheated by a series of beam passages. The preheated area corresponds to the maximum rectangular area that contains all the parts that will be melted. The powder is then further heated in an area that corresponds to a predefined offset of the actual melting zone. The preheating phase sinters the particles, preventing the so-called smoke effect and creating a neck connection between the particles that improves thermal conductivity [102]. Thanks to this partial sintering, the powder bed has a certain strength [105] which allows the nesting of the parts along the building direction and the reduction of supports. Different melting strategies can be used to melt the contour and inner parts of the section that has to be melted. A MultiBeam^{TM} [106] strategy is generally used for the contour [107], while a hatching strategy is used for the inner part [106]. After the melting phase, an additional step, called postheating [108], is introduced. The aim is to keep the build at the correct temperature. In this step, the layer can either be cooled down or further heated, depending on the total amount of energy supplied during the previous steps [109]. The entire process is performed in a vacuum environment that is generated by turbomolecular pumps [110]. Moreover, after the start of the electron beam, a small amount of inert helium gas is added to avoid the build-up of electrical charges in the powder and to ensure thermal stability of the process. After the build task has been completed, the entire build is cooled down inside the machine to 80 °C. The features that can be processed by EBM are usually grouped into support structures, lattice structures and the so-called bulk material. The differences are mainly due to the function of the part and the relative heat distribution during the process. Due to their specific geometries and functions, the process parameters for the support and the lattice structure differ from those of the bulk one. A set of process parameters is called a theme. Three themes are generally used for each material in the EBM process. An additional theme is used for the preheating step. The process parameters for the postheating are usually the same as those used for the second preheating step [111].

Energy efficiency of the EBM process

Baumers et al. [112] compared the specific energy demands of EBM with that of Laser Powder Bed Fusion (L-PBF). The comparison was made producing a JOB with a single component. An additional JOB was performed replicating components until the start plates of the two machines were completely saturated.

The latter experiment only led to the saturation of the building capacity for a height that corresponded to the benchmarking one, and a saturation along the height of the build chamber was not investigated. Moreover, components produced by EBM are attached directly to the start plate without the need of support structures. The authors showed that the EBM required a lower SEC than that of L-PBF because of the thicker layer thickness and the higher energy per unit area provided by the electron beam. The saturation of the start plate led to a reduction in SEC for both processes because of the amortisation of the fixed energy terms of the not productive phases. Kellens et al. [13] computed a SEC value of 375 electric MJ/kg from the work of Paris et al. [103] (Table 2). Baumers et al. [96] carried out a similar study to that in [112] in which a larger number of AM technologies were considered. The results for the EBM process showed that energy efficiency increased remarkably once the number of parts in the JOB had been increased. The SEC value of a single component (Table 2) for the EBM process was 177 electric MJ/kg, while it dropped to 61 electric MJ/kg when the start plate was saturated. Since the volume in the EBM process can also be fully saturated along the building direction, the energy efficiency can easily be enhanced. Baumers et al. [113] compared EBM and L-PBF, considering the nesting of 5 different components to saturate the machine start plate. The EBM machine (Arcam S12) showed a lower energy consumption than the L-PBF one (EOSINT M270). The ratio between the energy and the mass resulting from Baumers's study led to SEC values of 118.46 electric MJ/kg and 258.56 electric MJ/kg for Arcam S12 and EOSINT M270, respectively. Baumers et al. [114] distinguished different energy terms during the EBM process at a layer level: the spreading of the powder bed, preheating and melting. The Arcam A1 machine was analysed under the full capacity condition, in a similarly way as in Baumers et al. [96,112], using a bulk component. The results on the SEC values agreed with those reported in [96,112] (Table 2). The effect of the complexity of the component shape on the energy demand of EBM was also investigated. The complexity of the JOB was described in that experiment theme by means of the mean connectivity value (MCV) of each layer. This parameter acts as an indicator of the distance between the different areas that have to be melted which belong to the same cross section of the component. MCV decreases if the cross section of a component has various areas to be melted that are far from each other. According to [114], the lower MCV is the higher the complexity of the section becomes. The results showed that there was no correlation between MCV and the energy

demand during the melting phase. This result can be tracked back to the fact that the EB scan speed can reach 8 km/sec, therefore the JOB complexity is reasonably independent from the MCV. Baumers et al. [115] proposed models to estimate the time and the energy needed for powder bed-based AM processes. The authors considered all the idle phases (i.e., atmosphere generation) as well as each fixed time for each layer (i.e., the time necessary to spread the powder layer). The active time and energy were considered as a linear function of the area that had to be melted. As the literature review has highlighted, most of the findings about the SEC values derived from Baumers' works which represent the state of the art in [13–15,93,94,101,115,116]. According to Baumers et al. [96], the EBM technology was the fastest AM technique, with a DR_a equal to 0.13 kg/h for the Arcam A1 EBM machine under a full capacity condition. Table 2 summarises the SEC and the overall average values obtained from literature studies in which Ti6Al4V powders had been processed.

Machine	Mean operational power [kW]	SEC [eletric MJ/kg]	DR_a [kg/h]	Reference(s)
Arcam A1 (Single component)	2.01	177	0.04 *	[112]
Arcam A1 (Full capacity)	2.22	61	0.13 *	[112]
Arcam A1 (Single component)	2.01	177	n.a.	[96]
Arcam A1 (Full capacity)	2.22	61	0.13	[96]
Arcam S12 (Full start plate)	n.a.	118 *	0.07 *	[113]
Arcam A1 (Full capacity)	2.22	60	0.13	[114]
Arcam	n/a	375	n/a	[13,103]

Table 2. Electric energy and time efficiency data available in the literature for EBM applied to Ti6Al4V. The values marked with "*" have been computed in this work. Full capacity is intended for the saturation of the start plate.

1.2.3 Continuous Filament Fabrication

Fibre reinforced polymers showed the potential to easy replace metal components in a large number of applications [117]. The U.S. Department of Energy estimated an overall Carbon Fibre (CF) market in 2010 of about 39.9 million lbs, where 9.9 million lbs for wind energy, 6.6 million lbs for aerospace, 2.2 million lbs for automotive and 1.7 million lbs for pressure vessels [118]. For glass fibres, the estimated overall glass fibre market for 2010 was of 1567.4 million lbs, where 485.9 million lbs for automotive, 62.7 for wind turbine, 94.0 for aerospace and 94.0 for pressure vessels [119]. The global composite market is estimated to reach $40.2 billion by 2024 and it is forecasted to grow at a Compound Annual Growth Rate (CAGR) of 3.3% from 2019 to 2024, with an

estimated market of the end products of $114.7 billion by 2024 [120]. Even if AM is relatively new, it has been giving proves of its high capabilities to produce reinforced composites [121]. However, a lack of studies which aim to assesses the energy efficiency performances of AM technologies was noticed in the literature. The following paragraph aims to describe the Fused Filament Fabrication (FFF) technology, which is a promising AM technique for composite manufacturing. Then, a state-of-the-art literature about the energy efficiency of well-established processes for composite production is provided.

The CFF technology

AM processes based on the extrusion principle to produce composites can use both solid filament or paste/liquid form. In the first case, the system is called Fused Filament Fabrication (FFF) while if a fluid-like feedstock is used as supporting material the process is called Liquid Deposition Modelling (LDM). FFF can process both discontinuous (with different fibre sizes as nano, micro and milli) and continuous reinforcement in a thermoplastic matrix [85,122]. For FFF, fibre and matrix can be supplied separately from the matrix and then are mixed directly through one printing head. The fibres can be coated in situ with a liquid resin or it can be already pre-impregnated with a compatible resin [85,122]. For LDM, the reinforcements are in the form of discontinuous fibres and they are dispersed in the resin feedstock. Different discontinuous reinforcements have been investigated as silicon carbide (SiC) whiskers, carbon fibres, glass fibres, and CNT [85].

Among the two-extrusion head FFF systems, Markforged patented and developed the Continuous Filament Fabrication (CFF) process in which a continuous fibre is deposited layer by layer. The reinforcement filament commercialised by Markforged to perform the CFF process are Carbon Fibre (CF), Fibreglass (FG), Kevlar® (KV) and High-Strength High-Temperature (HSHT) fibreglass. The matrix filament is Nylon PA6 or a Nylon PA6 filament reinforced with chopped carbon, commercial called Onyx. The fibre filament is coated and englobed in a thermoplastic matrix of PA6 [84]. When the machine is switched on, it waits the operator to load the code of the JOB and the order to start the process. During this time window, the operator applies a glue stick onto the start plate for a better adhesion of the 3D printed part. Then, the machine heats the matrix and fibre extruders to the process temperatures. The matrix extruder

deposits a purge tape along the major side of the start plate to evacuate the surplus of material remained outside of the dry box. The duration and the action sequences of the printing window depend on the component features and process parameters. In case of reinforced samples, a purge corner part is deposited before each layer until the last reinforced one. Otherwise, this part is missing if no fibre is deposited. In case of not reinforced layers, the printing sequence is: (a) deposition of the perimeter and then (b) deposition of the inner area. On the other hand, for the reinforced layers the printing sequence is: (a) deposition of the fibre, (b) deposition of the perimeter and (c) filling of the gaps between perimeter and fibre. Once the JOB is completed, the operator removes it from the start plate and cleans the glue stick left. The procedures described in case of reinforced and not reinforced samples is not dependent from the selected materials.

Energy efficiency of other processes to manufacture composites

Figure 6 shows an overview of the literature about the SEC values of well-established techniques to manufacture fibre reinforced parts. To uniform the data found in the literature, some of them were converted from electric energy to oil equivalent energy, as proposed in [123] using a conversation factor equal to 0.38 according to the European average [67]. For the sake of clarity, Figure 6 highlights the range between 0 and 90 MJ/kg. For the autoclave process a wide range was measured for the SEC value, from 20 MJ/kg to 141 MJ/kg [124–128]. Moreover, two studies (which are not reported in the graph) provided higher values equal to 386 MJ/kg [129] and 600 MJ/kg [130]. Thermoplastic resins require a higher processing energy (47 MJ/kg) if compared to the thermoset resin (141 MJ/kg) because of the need to reach the melting point [127]. Reductions of the energy demand can be achieved if the autoclave curing is replaced by high energy X-ray curing [131], microwave curing [132,133] or nanostructured carbon nanotube (CNT) out-of-oven conductive curing [134]. Spray-up techniques show SEC values (8-16 MJ/kg) [118,119,124–126,130] comparable to those for hand lay-up techniques (8-19 MJ/kg) [118,119,130], due to the same approach when the layers of composite materials are overlapped. However, Spray-up process requires slightly lower values because of its automated tools. Compression moulding techniques which use a hot press and need a cold load as Sheet/Bulk Moulding Compounds (SMCs, BMCs) show low SEC values (3-18 MJ/kg) [118,119,125] and indicate an interesting alternative to the autoclave processes,

especially in case of high production volume. Thermoforming processes which use a cold press and hot loads as Glass Mat Thermoplastics (GMTs) require higher SEC (30-79 MJ/kg) [118,119] respect to those typical for the previous mentioned techniques. This may be related to the higher compactness of hot press systems and the resultant lower energy losses. In fact, for thermoforming processes, the load is heated outside of the press. SEC values ranging between 12 MJ/kg and 37 MJ/kg are needed for other cold press processes in which the resin and the reinforcement are directly mixed while they are in the mould, and no heat source is provided before or during the curing [118,119,124,126,130]. Respect to the use of hot presses, the SEC values for cold press-based techniques are higher because the curing needs to be performed under pressure for a longer time. Lower SEC were found for the preform matched die processes (around 10 MJ/kg) [124–126,130]. Finally, for Cold Diaphragm Forming (CDF) the use of a thermoplastic resin with high melting point as well as the long curing cycle time leads to a SEC value of 85 MJ/kg [127]. The injection processes have lower SEC values and higher production rates than those for the autoclave technology. The lower SEC values of Vacuum Assisted Resin Injection (VARI) processes (3-11 MJ/kg) [118,119,124–126,130] compared with those for Resin Transfer Moulding (RTM) technologies (3-81 MJ/kg) [118,119,124–128,130] could be explained by the lower pressure required by VARI even if higher heat dispersion may occur due to the use of a single mould. For RTM, Katsiropoulos et al. [126] reported a higher value for thermoplastic resins (81 MJ/kg) than for thermoset resins (27 MJ/kg). The filament winding process and the pultrusion technologies show the lowest energy demands [118,119,124–126,128,130]. The filament winding technology showed slight lower SEC values (3-8 MJ/kg) than those of the pultrusion technique (3-10 MJ/kg).

For Automated Tape Laying (ATL) and Automated Fibre Placement (AFP) processes a lack of data regarding the energy consumption was found in literature for the different fibre placement systems and heating solutions. A range of 19-38 MJ/kg was found in [135] for the deposition of unidirectional carbon reinforced PPS tapes onto carbon woven fabric reinforced PPS laminates providing the heat with a laser source and using different placement velocities and laser powers. However, this range only considers the laser input energy to the process and higher SEC should be expected if the laser efficiency and the energy demand of the other systems would be also included. Brecher et al. [136] evaluated the laser assisted ATL process for unidirectional CF tape on substrates made of PA6

reinforced with chopped glass fibre rovings. The overall electric specific energy for unit length varied in the range 204-544 J/mm.

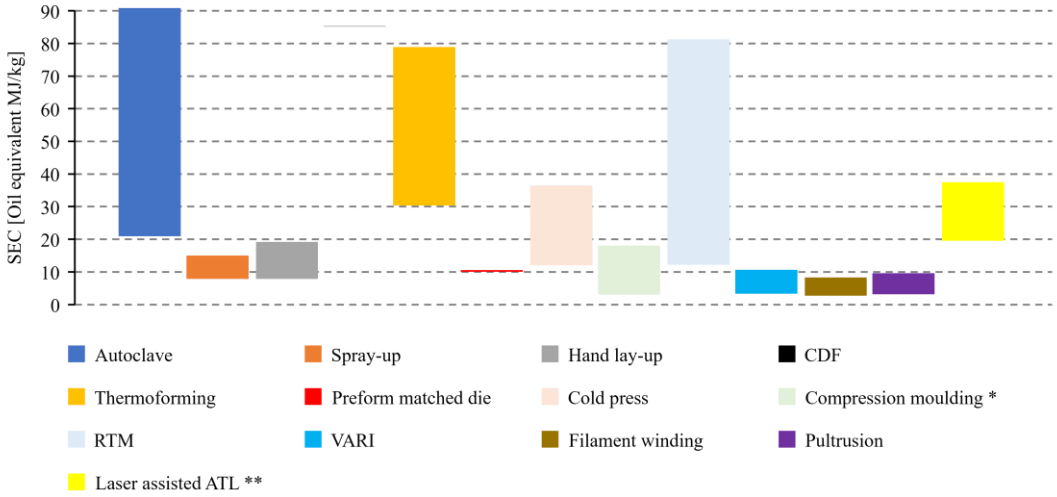

Figure 6. SEC data available in the literature for conventional and automatic composite manufacturing techniques, expressed in MJ/kg (oil equivalent). *Compression moulding techniques which use SMCs and BMCs. **Only the laser input energy to the process is considered.

1.3 Research questions and aims of the thesis

At the end of this critical literature review provided in this Chapter, the aims of this work are listed and discussed in the following, starting from each RQ.

Research question 1 (RQ1). With a Circular Economy point of view, how to assess the remaining useful lifetime of products and how to perform a LCA study under a function-oriented analysis (e.g., the satisfaction of a target, such as an overall lifetime for a turbine blade, or of an overall number of injected components to be produced with a mould)?

As far as paragraph 1.1 is concerned, the study of the state-of-the-art literature produced the following research gaps:

1. The reviewed studies lay on LCA methodologies which focus on the single production of the product and do not pursue the comparison for the further lives the product may have with the application of the CE;
2. The implications of the reliability property on the iterated products represent a central topic still to be addressed.

Aims of the thesis regarding RQ1. Chapter 2 attempts to fill the state-of-the-art literature gaps as follows:

- A LCA methodology is proposed to extend the existing analysis to the multiple lives of the product while taking into account reliability;
- Under function-oriented boundaries, the environmental impact of the CE strategies which lay on remanufacturing is compared with that of the linear economy model;
- Two AM processes (namely, DED for the remanufacturing approach and EBM for the linear economy system) are selected for the comparison;
- A case study from the aeronautic industry is used for the numerical quantification of the analysis;
- A sensitivity analysis is conducted for the main variables of the methodology, which are highlighted in Chapter 2;

Research question 2 (RQ2). How to evaluate the energy efficiency of a manufacturing technology at the unit process level and which can be a good methodology to achieve this goal?

The study of the state-of-the-art literature (see paragraph 1.2) regarding the AM techniques produced the following research gaps:

1. Considering the FDM and the EBM processes:

- A wide variation of the SEC can be noticed for both technologies (i.e., between 20 and 1200 electric MJ/kg for FDM, and between 60 and 375 electric MJ/kg for EBM);
- The relationships between the SEC and the architecture of the machine and the architecture of the process control were never investigated;
- For FDM the effects of (a) the printed material and of (b) the main process parameters (such as the layer thickness, the infill strategy and the position of the part on the build table) are still to be investigated. For EBM all the studies considered one single component or saturation of only the start plate. Therefore, (a) no studies have been conducted to investigate the effect of nesting along the building direction, (b) all the literature studies considered the analysis of energy efficiency only during the melting of bulk material.

- Finally, the importance of the part geometrical complexity and its effects on the process energy efficiency are neglected.

2. Considering the production of composite by means of AM, there is a lack of studies regarding their energy efficiency. Therefore, it is not even possible to have a qualitative information, as happens for other AM technologies.

Aims of the thesis regarding RQ2. Chapter 3 attempts to fill the state-of-the-art literature gaps as follows:

- An innovative methodology is proposed for the quantitative evaluation of the energy efficiency of AM, connecting this variable to the deposition efficiency by means of an empirical regression law;
- Well-known AM techniques as FDM and EBM are considered as case study to perform the empirical work and to solve the relative research gaps reported above;
- The approach is also applied to the CFF process. Moreover, the energy efficiency of the CFF technology is compared with that of the reviewed well-established processes for composite production to highlight the role that AM can have in this manufacturing sector;
- For each investigated AM machine, the energy demand of each machine subunit is evaluated respect to the overall energy demand to highlight the weight of the share needed to melt the feedstock material;
- The investigated AM processes are compared to each other to highlight the validity area of a given technology in the bidimensional space which has the energy and the deposition efficiency as input variables;
- Finally, the relationships between the results of the proposed model, the quality criteria and the concepts of the design for AM (DfAM) are discussed.

Chapter 2 and Chapter 3 run independently the investigation of RQ1 and RQ2, respectively, with a different methodology. For sake of clarity, a summary of the two methodologies is reported for each Chapter (see Table 3 and Figure 34, respectively for Chapter 2 and Chapter 3).

The conclusion section summarises the results of this work and reports their limits and possible future improvements. Moreover, it discusses the connections between the topics investigated in Chapter 2 and in Chapter 3. The methodologies and the results of the present study could be extended to other manufacturing techniques. In fact, finally considerations are made both for the unit process level and for a CE point of view on how to choose a manufacturing process rather than another in order to actually select a sustainable alternative.

Chapter 2

The Circular Economy challenges

2.1 Methodology

This Chapter attempts to solve the literature gaps reported in Chapter 1 focusing on how to address the implications of the reliability property for iterated products and on how to extend the existing LCA methodologies to a function-oriented analysis.

To enter into the detail of the comparative LCA, the scenario in which the product is dismissed, once it ends is life, and a brand-new product is produced (see Figure 7) is compared with a scenario that applies the remanufacturing action of CE aiming to achieve multiple lives for the original manufactured product (see Figure 7). Since the benefits arising from recycling are high, as shown in the literature for some practical case studies [66,67], they are taken into account for both scenarios with one of the methods proposed from Hammond and Jones in [137]. In this way, it is possible to directly evaluate the effects of only remanufacturing. The Cumulative Energy Demand (CED) metric is evaluated in this work. On the other hand, the cumulative carbon dioxide emission metric is neglected since this metric keeps the same trend of the CED, as shown in [68] for different practical case studies.

For the brand-new manufacturing strategy, the LCA takes into account (a) the production of the raw material (i.e., the extraction of the ores for the primary material production and the processing of the scraps for the secondary material

production), (b) the pre-manufacturing stage (to transform the raw material in the shape needed from the subsequent manufacturing technology), (c) the manufacturing technology itself (needed to manufacture the product) and all the post-manufacturing processes that the product may need (see Figure 7). Once the first product is manufactured (dark grey path) is goes to the use phase (light grey path). It performs its function for a share of the overall target (F) and then it is dismissed and recycled (light green path). All the subsequent brand-new products follow the same path until the target is satisfied. Finally, for each mass flow is also included the relative energy demand needed to transport it.

For the remanufacturing scenario, the proposed LCA methodology considers the manufacturing (dark grey path) and the use (light grey path) of the original manufactured product, as for the brand-new manufacturing scenario (see Figure 7). For the subsequent lives of the product, the remanufacturing is taken into account by means of (d) the production of the raw material (including primary and secondary production), (e) the pre-manufacturing stage (which has to be coherent with the selected re-manufacturing technology), (f) the remanufacturing technology itself (needed to restore the initial function of the product) and all the post-manufacturing processes that the product may need. After each use the remanufactured product is brought back to stage (f) (upper dark green path) where feedstock material (that followed the initials steps of raw material production and of pre-manufacturing) is processed (dark grey path). Then, the product is ready to start again the use phase (lower dark green path). Once the target is achieved, it is recycled as for the brand-new manufacturing scenario (light green path). For both scenarios, the scraps produced in the manufacturing/remanufacturing plant (e.g., chips and supports) are recycled (light green path). Finally, for each mass flow is also included the relative energy demand needed to transport it.

Considering the single iteration for both scenarios, the benefits arising from recycling should be addressed only once and not double counted. In fact, focusing on the methods proposed from Hammond and Jones in [137] to take into account the recycling benefits, it is possible to use: (a) the recycled content approach (which allocates the full benefits of material recycling to the input side of a product system), (b) the substitution method (which allocates the full benefit of recycling at end of life) and (c) the 50:50 method (which is exactly half way in between the previous two methods). The recycled content approach is applied in this comparative LCA.

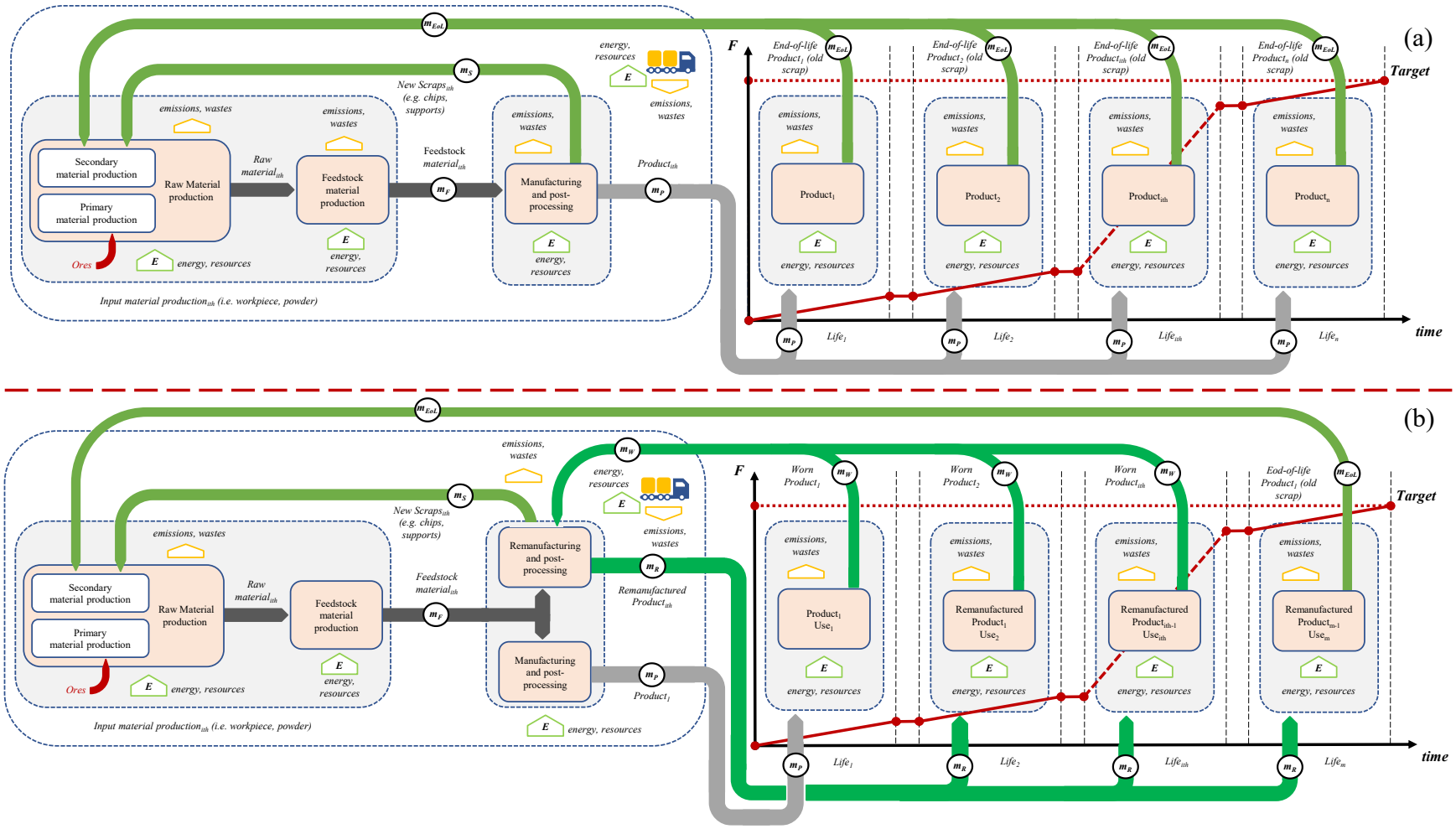

Figure 7. (a) Scheme and extension to a function-oriented analysis of (a) the brand-new scenario and of (b) the remanufacturing scenario.

Therefore, the overall input material flow needed for each new life has a percentage of recycled material (the so called "upstream flow of recycled material in the current supply"). On the other hand, the benefits arising from the recycling of the process scraps (such as supports and chips masses) or from the products at their end-of-life are neglected because they will be included in the next iteration.

Both scenarios, have in common the functional unit of the comparative LCA, i.e., the achievement of the same function target (F). For instance, it can be the satisfaction of an overall lifetime for a turbine blade, or the satisfaction of an overall number of injected components to be produced with a mould. As reviewed in [138], dies and moulds can fail for different reasons (such as thermal cracking, wear, plastic deformation, gross failures, soldering and corrosion) even if the target production is not satisfied yet. Therefore, the damaged product needs to be remanufactured or to be replaced with a brand-new one in order to fulfil the designed target.

A population of products (P) is considered for both scenarios. The comparison between brand-new and remanufacturing scenario is carried out for "P" products, instead of only for one. The target function "F" has to be achieved for each product belonging to the population "P". Therefore, the overall target function to be achieved (F_P) is given by the product between "P" and "F".

2.1.1 Work assumption 1: Physical lifetime and technology lifetime

As discussed in [139], a product can be retired from the market even if it has a remaining physical lifetime. The current physical lifetime of a product is defined as the difference between the operating life and the usage life. The operating life is the time that the product or the component is expected to have a failure or disruption which cannot resume any of its normal operations. In other words, it represents the designed engineering life. The usage life indicates the actual age measured in operating time (e.g., hours, cycles, kilometres) that a product or component has been used. The usage life is a critical parameter to evaluate. For instance, according to [139] possible methods for its assessment are statistical techniques, regression analysis, Kriging techniques, vibration analysis and artificial neural networks. For a better understanding of the problem, applications of these techniques are given in ([140] and references therein). On the other hand, the technology lifetime indicates the time in which the product or component

holds a dominant market share due to its technology superiority. The transition from an old product to a newer one can be described as shown in Figure 8 by means of an hypothetical example of product technology substitution [141].

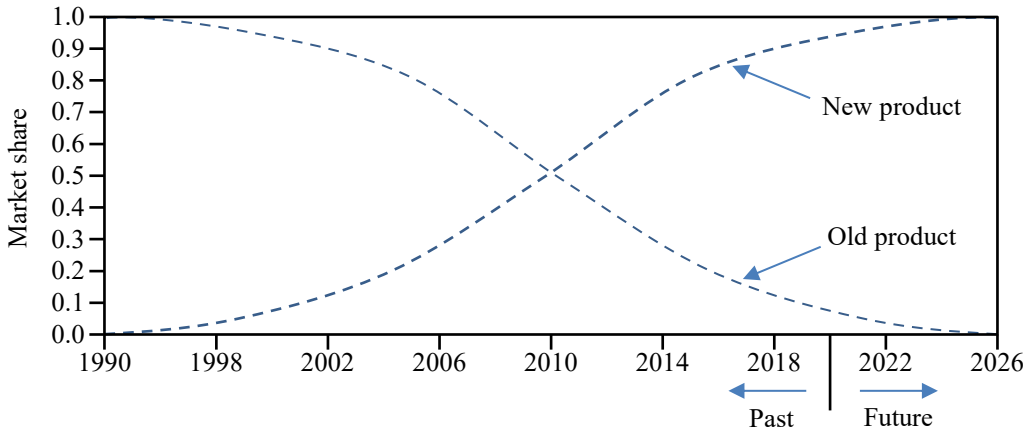

Figure 8. Hypothetical example of product technology substitution. Adapted from [141].

Therefore, the remaining useful life can be estimated as the minimum between the physical lifetime and technology lifetime. For instance, the authors in [142] evaluated the optimum circulating time for a product. In particular, a product should be kept in the market with multiple lives thanks to the CE strategies as long as the technology improvement will make more profitable the manufacturing of a brand-new product with lower environmental impact.

In this study, it is assumed that the product under study holds the 100% of the market (i.e., when its market share is close to one). Any other new version of the product has a negligible market share for the entire time range covered from the analysis. In other words, the product technology lifetime is much higher than the physical lifetime. Therefore, the remanufacturing or the brand-new manufacturing of the product are the unique ways to satisfy the target function “F”.

2.1.2 Work assumption 2: Bathtub curve and failure modes

The Bathtub curve offers the failure rate that may occur during the time, from the production of a product to its use phase. Three main failure modes are commonly considered: (a) early or infant mortality, (b) constant or random failure and (c) wear out failure. The (a) infant mortality refers to the failure of the product just after or during its manufacturing (e.g., due to impurities in the starting ores, errors in the process parameters, or during the installation of the product just at

the beginning of its use phase [143]). The (b) constant failure is caused from random problems (e.g., extreme heavy loading, ground movement, or third-party interference [143]). Finally, the (c) wear out failure is due to the aging of the product (e.g., [143] and references therein). As visible in Figure 9, the observed failure is the sum of the three failure modes.

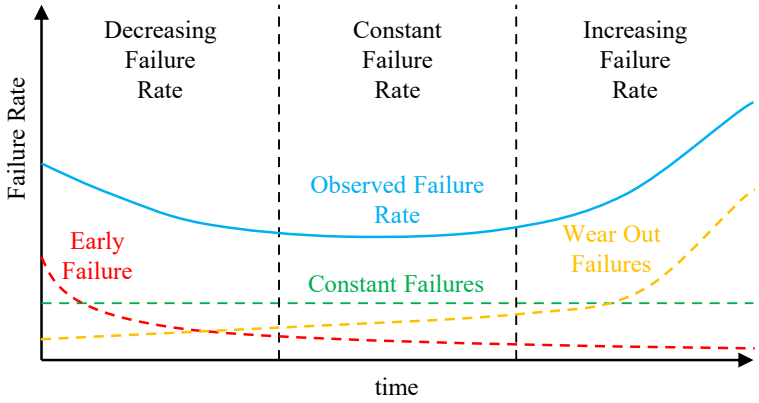

Figure 9. Bathtub curve and failure modes.

Usually, once the problems which cause the (a) early mortality are corrected, they do not appear again, therefore a decreasing trend in visible in Figure 9. The first window is also referred as Burn-in period. The time window referred to the constant failure rate, is also known as useful life period.

In this study, (a) infant mortality is neglected, assuming that there are not impurities in the starting ores, errors in the process parameters, or during the installation of the product. Moreover, also (b) random failure is neglected, assuming the absence of random interferences. Therefore, the product fails only due to its aging, i.e., when its usage life reaches its operating life. This work assumption applies to both brand-new and remanufacturing scenarios.

2.1.3 Work assumption 3: Availability, Capability and Dependability

The quality of a remanufactured product may induce hesitation for many consumers regarding its capacity to provide the expected performance as that of a new one. To overcome this aspect, remanufacturers often use marketing strategies to increase certainty about product quality [144]. When a product is remanufactured, it should be as well as new in order to be reintroduced in the market. In other words, the remanufacturing process (and more in general, all the

other ancillary activities needed to bring back the product to the use phase) should guarantee the reliability property for the circulated product. *In this sense, the reliability property is defined as "the ability of a product or system to perform its intended function"* [145]. In this work, three properties of reliability are considered: (a) availability, (b) capability and (c) dependability. The (a) availability property requires that the circulated product should be ready to perform its function every time that the user needs it as happens for the brand-new one. The (b) capability property requires that the circulated product should perform its function as good as the brand-new one. Finally, the (c) dependability property requires that under the same operating conditions, the circulated product should last as long as the brand-new one.

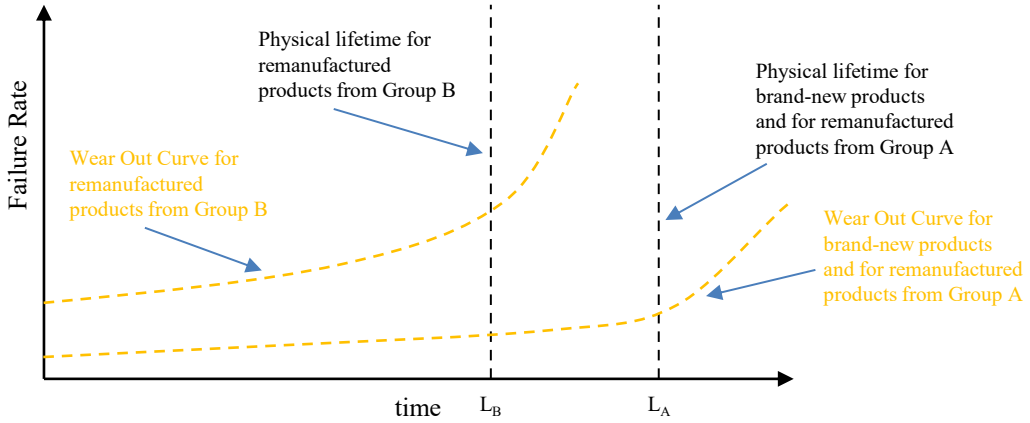

Figure 10. Effect of dependability on the physical lifetime of the product.

In this study, it is assumed that the (a) availability and the (b) capability properties are satisfied for any life of the remanufactured product. On the other hand, as the use conditions of the product during its previous life are unknown, it is difficult to evaluate their effect on the next life and to predict the extension of the operating life that the product gains thanks to the remanufacturing process. Moreover, also the usage life of the products can experience an acceleration even if the same operating conditions are present. For this reason, it is difficult to guarantee the (c) dependability property. Therefore, in this study, it is assumed the presence of two types of user:

1) User A: which defines the user who used the remanufactured products under the prescribed working conditions during their previous "i" life. Therefore, these remanufactured products (PA_i) will guarantee the same physical lifetime (L_A) of the brand-new products during their next "i+1" life (see Figure 10).

2) User B: which defines the user who did not used the remanufactured products under the prescribed working conditions during their previous "i" life. Therefore, these remanufactured products (PB_i) will guarantee a lower physical lifetime (L_B) respect to that of the brand-new products during their next "i+1" life (see Figure 10).
In this study, it is assumed that the same physical lifetime (L_A) is guaranteed for all the brand-new products, since they have to be used only once and there are not users that may have affected their properties in the current life.

2.1.4 Work assumption 4: A Markov chain approach to model the remanufacturing process

A Markov chain-based model is used to address the internal steps of the remanufacturing process for each life. *According to the Oxford Dictionary, Markov chain is defined as "a stochastic model describing a sequence of possible events in which the probability of each event depends only on the state attained in the previous event"*. It this sense, the Markov chain-based models describe systems "without memory" of their past history, because only the current event influences the future state. These models have extensive applications to different areas, as visible from the literature. For instance, they are applied as decomposition method to evaluate the performance of transfer lines where machines can fail in multiple modes [146], to evaluate the output variability in production systems [147], in the design and management of reconfigurable assembly lines in the automotive industry [148]. Markov chain models are also applied to describe the overall manufacturing step of a product, in order to consider and prioritise the different steps (such as turning, milling and drilling) [149]. Considering examples closer to the topic of this work, a multistage manufacturing process with inspection, rejection, and rework can be also modelled with a Markov chain model in [150].

Taking as example, the steps proposed in [151] for the repairing of industrial electronic parts, a Markov chain-based model is applied in this study to evaluate the dynamics that occurs inside the remanufacturing plant for each life. Moreover, the Markov chain is applied to introduce in this study: (a) the presence of products directly coming from the previous use phase which show not good enough conditions to start the remanufacturing step (i.e., the remanufacturing process would not be able to restore their physical lifetime) and (b) the possibility that the

remanufacturing process would fail its task to restore the products. Considering Figure 11, the following nodes are present:

- Node 1: receiving of the products (from both Group A and Group B) coming from the previous use phase;
- Node 2: first detect station, which is applied only to products belonging to Group B, since they conditions are unknown and need to be checked. On the other hand, product belonging to Group A do not need this step, since they were used according to the prescribed working conditions which are known;
- Node 3: first remanufacturing station (products belonging to Group A directly reach this node);
- Node 4: first test station, which is needed to verify the condition of the remanufactured products at Node 3;
- Node 5: second detect station for products which do not satisfy the test performed at node Node 4;
- Node 6: second remanufacturing station, which is applied to the products that in the second detect station (Node 5) are considered to be eligible for a second remanufacturing;
- Node 7: second test station, which is needed to verify the condition of the remanufactured products at Node 6;
- Node 8: only products that satisfied the tests performed at Node 4 and Node 7 arrive to this Node and will be shipped in order to start the next life;
- Node 9: products which arrive here from Node 1 (i.e., those belonging to Group A), Node 2 (i.e., those belonging to Group B) and Node 7 (i.e., those which belong to Group A or Group B and that have failed the first and also the second reman) are considered as scraps. The term "SA_i" defines the overall number of scraps belonging to Group A due the distribution of the users during the previous "i" life. Similarly, the term "SB_i" defines the overall number of scraps belonging to Group B due the distribution of the users during the previous "i" life. Therefore, brand new products (defined as "BN_{i+1}", which is the sum of "SA_i" and of "SB_i") are necessarily needed to fulfil the overall number of products (i.e., the quantity "P") for the next "i+1" life.

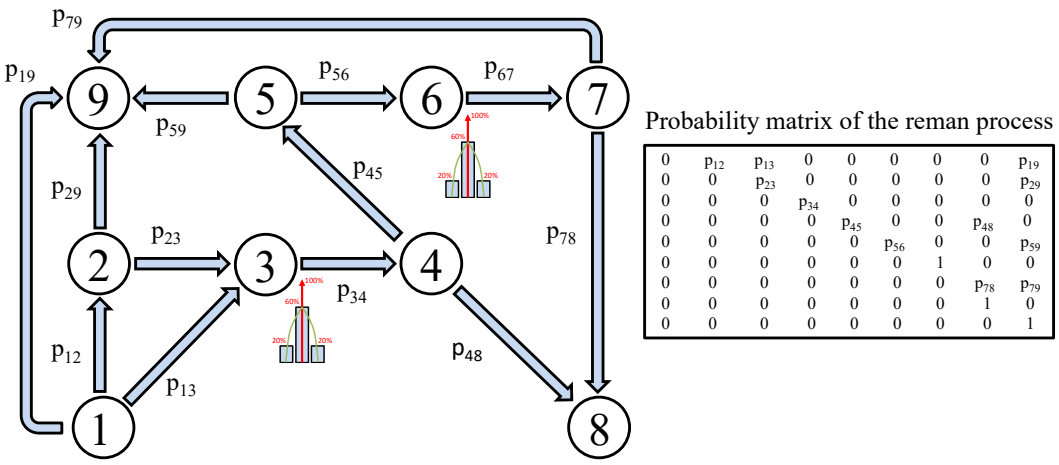

Figure 11. Markovian modelling of the remanufacturing process.

In Figure 11, the terms "p_{ij}" (defined as "state transition probability") describe the probability that the products present at Node "i" have to move to Node "j" in the next step. In this sense, the subscript "i" defines the starting Node, while the subscript "j" defines the arriving Node. These terms can vary from a minimum value equal to zero (none of the products present at Node "i" move to Node "j") to a maximum value equal to one (all the products present at Node "i" move to Node "j"). The terms "p_{ij}" are placed in a matrix called "Probability matrix" of the remanufacturing process (M_R), visible in Figure 11. In "M_R", the "i" row refers to the product flows which start from the "i" Node. Similarly, the "j" column refers to the product flows which reach the "j" Node.

In Markov chain models, a Node is called "Absorbing Node" when it has the state transition probability "p_{ii}" (i.e., the term in the diagonal of "Probability matrix") equal to "1". In this study, there are two "Absorbing Nodes", respectively Node 8 and Node 9. In fact, when a product reach Node 9 it is considered as scrap, and when it reaches Node 8 its remanufacturing process is considered as ended.

Moreover, the internal structure of the Markov chain used to describe the remanufacturing process should be thought in order to avoid "infinite internal circulations" (i.e., the "Absorbing Nodes" should be reached in a finite number of steps). In fact, based on economic considerations, only a finite number of circulations is allowed. According to [151], instead of connecting Node 4 with Node 2 (that could create infinite internal circulations), three other Nodes are introduced (Node 5, Node 6 and Node 7) in order to have maximum two remanufacturing stations. The overall number of internal steps is up to the

structure of the modelled Markov chain, i.e., to the internal connections and number of Nodes. For the modelled system in Figure 11 this number is equal to 7.

The evaluation of the product flows inside the modelled remanufacturing process is performed for each life. Therefore, taking as reference the generic remanufacturing, the row vector "R_i" defines the condition of the Nodes of the modelled remanufacturing process in the "i" Markovian step. Considering the structure of "M_R", "R_i" shows 9 columns. In "R_i", the "j" column refers to the amount of product present in Node "j". Dividing "R_i" for the population "P", the numerical terms present in "R_i" goes from a minimum of zero (i.e., none of the products is present in the considered Node) to a maximum of one (i.e., all the products are present in the considered Node). At the end of each life, when "R_i" describes the "zero" condition of the remanufacturing process (i.e., when the products reach Node 1 from their previous use stage and all the other Nodes are not processing any product), only the first column shows the number "1", while all the others show the number "0". In this case, the vector "R_i" is defined as "R_0". By means of "M_R" and "R_i", the evolution paths of the products which initially reached Node 1 from their previous use is defined until the totally of the products reach the two "Absorbing Nodes". According to the Markov chain-based models and the rules of the multiplications between matrices, the "i+1" condition of the Nodes is computed starting from their "i" condition using the relative "Probability matrix", as shown in Eq. 1.

$$\textbf{Eq. 1} \qquad \mathbf{R_{i+1} = R_i \cdot M_R}$$

2.1.5 Work assumption 5: A Markov chain approach to model the behaviours of the users

Instead of considering a constant distribution of the products between Group A and Group B, a Markov chain-based model is also used to discriminate the products for each life of the assessment until the overall function target of the comparative LCA (F_P) is reached. As visible in Figure 12, the state transition probability "p_{AA}" defines the probability that the products used in the previous life according to the prescribed working conditions have to be used again in the same way in the next life. On the other hand, the term "p_{AB}" defines the probability that the products used in the previous life according to the prescribed working conditions have to be used under the not prescribed working conditions in the next life. Similar considerations can be applied to the state transition probabilities

"p_{BB}" and "p_{BA}". The value of these probabilities can be set according to a forecast of the market and of the product's users. They can be constant if a unique trend is expected during the investigated time window. On the other hand, they can eventually vary for each iteration in order to assess a dynamic evolution of the market as effect of awareness campaigns for the users of the products. A "Probability matrix" of the market evolution (M_U) can be defined for the remanufacturing scenario, as shown in Figure 12. In this study, a constant value of its "state transition probabilities" is considered in order to evaluate an evolution of the market given from a unique trend.

The row vector "U_i" defines the distribution of the market (i.e., the number of A and B products) for the generic "i" life. Considering the structure of "M_U", "U_i" shows 2 columns. Dividing "U_i" for the population "P", the numerical terms present in the "j" column of the vector "U_i" goes from a minimum of zero (none of the products belongs to Group "j") to a maximum of one (all the products belong to Group "j"). The initial distribution of the market characterises the first life and it is needed to start the analysis of the remanufacturing scenario. In this case, the vector "U_i" is defined as "U_1". By means of "M_U" and "U_i", the evolution paths of the products for each life iteration are defined until the final function target of the comparative LCA (F_P) is reached. According to the Markov chain-based models and the rules of the multiplications between matrices, the "i+1" condition of the market is computed from their "i" condition using the relative "Probability matrix", as shown in Eq. 2.

$$\mathbf{U_{i+1} = U_i \cdot M_U} \qquad \textbf{Eq. 2}$$

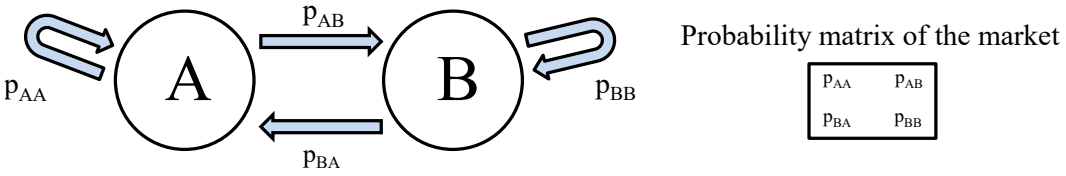

Figure 12. Markovian modelling of the behaviours of the users.

2.1.6 MATLAB and Excel codes

This paragraph aims to describes the iterations processes performed in this Chapter from the point of view of the used numerical codes. In particular, the MATLAB R2019a software was used for this task. Appendix A, reported at the end of this thesis, shows the MATLAB code used to compute the Markovian steps

of the market evolution for each life. Appendix B, reported at the end of this thesis as well, shows the MATLAB code used to compute the Markovian steps of the remanufacturing process of each life.

Considering Appendix A, first the variable "P" in introduced. Then, the matrix "M_U" and the row vector "U_1" are reported. As shown in Eq. 2, the row vector "U_i" is computed for each life "i" with a for-loop considering a max iteration number "p".

The initial condition for the distribution of the products in the modelled remanufacturing process (R_0) requires that all the products are present in Node 1 (i.e., the receiving Node). However, as previously discussed, the distribution of the products belonging to Group A and to Group B changes for each life. Therefore, the terms "p_{12}", "p_{13}" and "p_{19}" change their numerical value as well for each market distribution. Considering Appendix B, these terms are computed for each life. However, some assumptions are fixed: (a) all products belonging to Group B go from Node 1 to Node 2 because they need to be controlled, (b) the 95% of products belonging to Group A go from Node 1 to Node 3 (because they are considered as products in good and known conditions) and the 5% of products belonging to Group A go from Node 1 to Node 9 (because they are considered as scraps from the previous life). In Appendix B, the matrix "M_R" is computed for each iteration and the internal flow of the remanufacturing process are computed by means of Eq. 1, until all the processed products reach Node 8 or Node 9 for the generic "i" life. A for-loop is used to achieve this goal. In this case the iteration number is set to "m", which is defined as the iteration number for the Markovian remanufacturing process. As discussed above, "m" is equal to 7 according to the Markovian structure of the remanufacturing process modelled in this Chapter. This task is performed for each life, therefore the described for-loop is located inside another for-loop considering a max iteration number equal to "p".

Finally, the results of both MATLAB codes are imported into an Excel file. For each life, the modelled remanufacturing process gives a number of products which are considered as scraps (those of Node 9) and that will be replaced from brand-new products. These brand-new products will guarantee the entire physical lifetime (L_A) in the next life.

Considering the distribution of the market during the previous life "i" (i.e., the variables "PA_i" and "PB_i") and the integration of brand-new products for the next life "i+1" (i.e., the variable "BN_{i+1}", which is the sum of the terms "SA_i" and "SB_i"), the share of the overall target function (F_P) which will be gained during

the next life "i+1" (f_{Pi+1}) is computed according to Eq. 3. This evaluation is performed for each life until the overall function target (F_P) is achieved.

$$\textbf{Eq. 3} \qquad f_{Pi+1} = L_A \cdot (PA_i - SA_i + BN_{1+i}) + L_B \cdot (PB_i - SB_i)$$

2.1.7 Summary of the methodology

This paragraph aims to summarise the assumptions made in this Chapter. Table 3 reports a distinction between the work assumptions valid for the brand-new scenario and those valid for the remanufacturing approach.

Summary of the comparative LCA methodology		
Base concepts	A population of products (P) is considered for both scenarios	
	The target function "F" has to be achieved for each product belonging to the population "P"	
	The recycled content approach is applied in this comparative LCA for both scenarios [137]	
Work assumption	Brand-new scenario (Figure 7 - a)	Remanufacturing scenario (Figure 7 - b)
WA1	Physical lifetime much longer than technology lifetime (i.e., the product under study holds the 100% of the market) (Figure 8)	
WA2	Infant mortality and random failure are neglected; wear out failure is considered (Figure 9)	
WA3	Reliability: availability and capability are satisfied; dependability is affected from the use conditions in the previous life of the product	
	Dependability: is satisfied from all products since they are brand-new for each iteration	Dependability: products used under the prescribed working conditions and products that were not are considered due to the users' habits (Figure 10)
WA4	-	The remanufacturing process is modelled with a Markov chain approach (Figure 11)
WA5	-	The behaviours of the users are modelled with a Markov chain approach (Figure 12)
Appendix A	-	MATLAB code to compute the Markovian steps of the market evolution for each life
Appendix B	-	MATLAB code to compute the Markovian steps of the remanufacturing process for each life: - The terms "p_{12}", "p_{13}" and "p_{19}" change their numerical value for each market distribution; - All products belonging to Group B go from Node 1 to Node 2; - Almost the totality (95%) of products belonging to Group A go from Node 1 to Node 3. The remaining products (5%) go from Node 1 to Node 9;

Table 3. Summary of the methodology applied in Chapter 2.

2.2 Case study and Data Inventory

In this paragraph, a turbine blade is used as case study for the application of the methodology proposed in this Chapter. This case study comes from the work [152], where the authors assessed the physical lifetime for the blades of a High-Pressure Turbine (HPT) of commercial aircraft engines. The physical lifetime was determined using the Johnson-Weibull analysis, which evaluates the field data coming from the investigation of sixteen HPT blade sets. According to the case study reported in [152], the blade section is approximately 71 mm in height and has a cord length at the tip of approximately 37 mm. Moreover, the height from the blade root to the blade tip is approximately 118 mm. Figure 13 shows a mock-up of the described case study, which was designed using the software Solidworks 2019 for this thesis. For sake of simplicity, the cooling channels that typically characterise these blades are omitted in the mock-up. A volume of 30576.87 mm^3 is computed by means of Solidworks 2019. The population (P) of the turbine blades is set to 82 units, which is the number contained in the investigated turbine [152].

The work of [152] gave a physical lifetime for each blade equal to *10^4 hours*. This value is assumed in this study for each brand-new blade and for each remanufactured blade that during its previous use phase was used according to the prescribed working conditions (L_A). On the other hand, a conservative reduction of the *20%* for this value is assumed in this study for the products belong to Group B (L_B). A variation of *±10%* of the physical lifetime is considered for all products belonging to Group A and Group B to perform a sensitivity analysis of the results giving respectively the "best case" and the "worst case" scenario respect to the brand-new manufacturing strategy.

Considering an overall operating use phase of 30 years for a long-distance aircraft [153], for both scenarios the overall target for each blade would be *10^5 hours*. This value is computed considering an average duration for one flight cycle equal to 5 hours (e.g., according to [152] a long-haul, coast-to-coast airline operation in the continental United States typically runs between 4 to 6 hours per cycle) and two cycles per day for almost the totally of the year.

The "state transition probabilities" for "M_R" and for "M_U" are respectively assumed in this work as shown in Table 4 and Table 5.

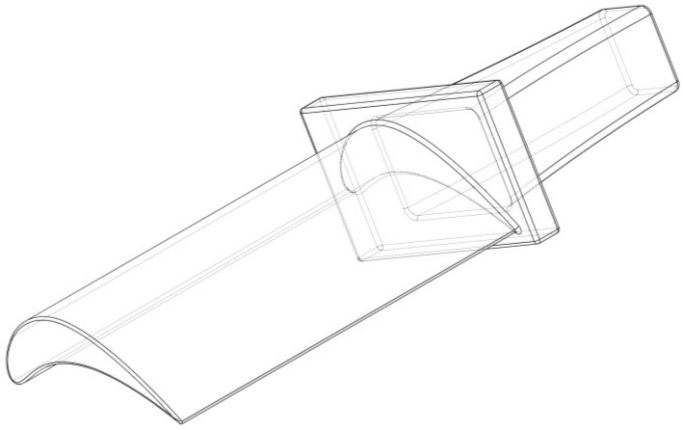

Figure 13. Mock-up of the described case study. Adapted from [152]**.**

For what exposed above regarding the evolution of the market distribution and the structure of "M_R", the terms "p_{12}", "p_{13}" and "p_{19}" do not show a numerical value in Table 4. For Node 2, it is assumed that the *80%* of the processed products, which all belong to Group B, reaches the first remanufacturing station (Node 3). The remaining *20%* is considered as scraps from the previous life and therefore it reaches Node 9. Considering the first test station (Node 4), it is assumed that the *95%* of the remanufactured products (coming from both Group A and Group B) passes it and reaches the shipping station (Node 8). On the other hand, the term "p_{45}" is assumed equal to *0.05* to reduce the number of products which does not pass the test and goes through a second iteration. Considering Node 5 (second detect station), it is assumed that the *95%* of the controlled products goes to Node 6 (second remanufacturing station) and the remaining *5%* is considered as scraps. The *95%* of the tested products in Node 7 reaches the shipping station (Node 8) because it is assumed that the second remanufacturing fixes its last problems. On the other hand, the *5%* reaches the scrap station.

Considering "M_U", the "state transition probabilities" are thought to guarantee a virtuous evolution of the market in which the number of products used under the prescribed working conditions will increase during the subsequent iterations. The assumed initial condition of the market ("U_1") considers that the *90%* of the products belongs to Group B. While the remaining *10%* belongs to Group A.

-	To Node 1	To Node 2	To Node 3	To Node 4	To Node 5	To Node 6	To Node 7	To Node 8	To Node 9
From Node 1	0	p_{12}	p_{13}	0	0	0	0	0	p_{19}

From Node 2	0	0	0.80	0	0	0	0	0	0.20
From Node 3	0	0	0	1	0	0	0	0	0
From Node 4	0	0	0	0	0.05	0	0	0.95	0
From Node 5	0	0	0	0	0	0.95	0	0	0.05
From Node 6	0	0	0	0	0	0	1	0	0
From Node 7	0	0	0	0	0	0	0	0.95	0.05
From Node 8	0	0	0	0	0	0	0	1	0
From Node 9	0	0	0	0	0	0	0	0	1

Table 4. "State transition probabilities" for "M_R".

-	To Group A	To Group B
From Group A	0.80	0.20
From Group B	0.50	0.50

Table 5. "State transition probabilities" for "M_U".

2.2.1 Materials and Technologies

The case study of this Chapter typically requires a nickel-base superalloy, as discussed in [152]. However, different commercial nickel-base superalloys are available in the market. Therefore, the NiCr20Co18Ti material is considered, according to the remanufacturing study performed in [63] for a turbine blade.

The brand-new manufacturing scenario considers Electron Beam Melting (EBM) as technology to produce each set of blades. As visible in Figure 14, the EBM machine receives the feedstock material (produced by means of the atomisation process) for the new set of blades. The blades are removed from the start plate of the EBM machine by means of wire Electrical Discharge Machining (wire-EDM). Then, the Hot Isostatic Pressure (HIP) treatment is applied to each blade and finally machining is considered to reach the needed surface finishing. On the other hand, the remanufacturing scenario considers the Direct Energy Deposition (DED) technology to restore the initial shape of the blades that can be remanufactured (the scraps are integrated with brand-new blades, using the EBM path discussed above). As visible from Figure 14, the worn product coming from the previous life is cleaned and a machining step is applied to prepare the working area on the blade.

Then, the DED stage receives the feedstock material (produced by means of the atomisation process) for the new set. The DED process is performed on the

worn blades and finally the HIP process and a machining step is considered. The contribute of the argon process is addressed for the atomisation of the NiCr20Co18Ti powder and to perform the DED process. On the other hand, the contribute of the helium gas is considered for the EBM machine. Finally, the contributes of the consumables for the machining step (e.g., the cutting tools and the cutting fluids), are also addressed.

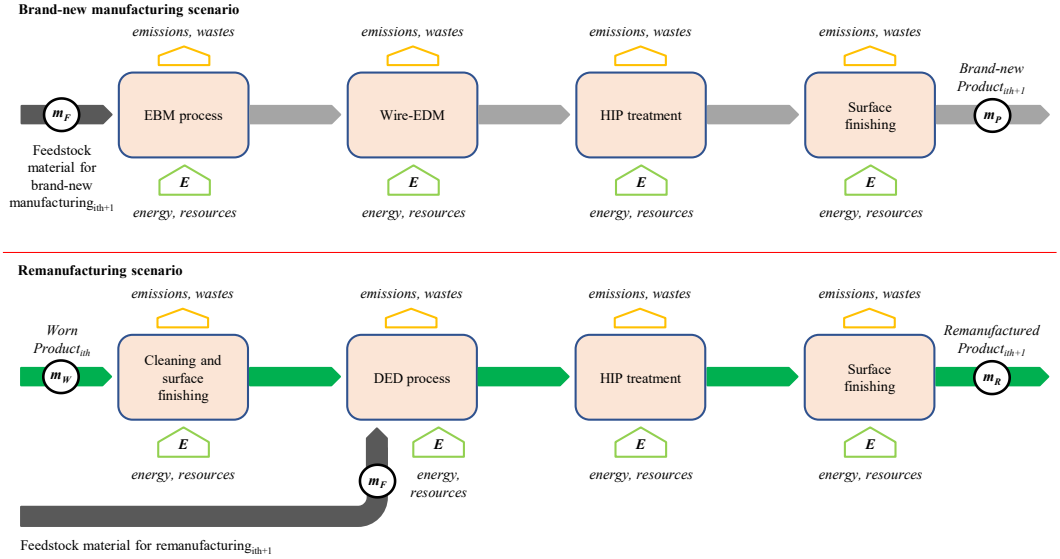

Figure 14. Focus of the steps of the manufacturing and remanufacturing scenarios.

The energy demands and the mass flows detailed in Figure 14 are addressed using the LCA methodology elaborated from Priarone and Ingarao in [37,65]. In particular, this Chapter remands to the works referred in [37,65] for a better understanding of the formulas used to address the CED metric. That methodology offers good performances and successes to describe the differences among the main manufacturing technologies, such as machining, forming, casting and AM. Moreover, among the different reviewed LCA methodologies in [154], the one proposed in [37,65] gives results that are centred with the global average of the reviewed methods. Those works are extended in this Chapter to the multiple lives of a product needed to achieve a function target that transcends its single life.

Finally, to give a statistical value to the analysis, a distribution of the remanufacturing material percentage is chosen for the processed products of Node 3 (fist remanufacturing station) and Node 6 (second remanufacturing station). Lower percentages of remanufactured material are considered for Node 6, since it is assumed that this Node referees to minor problems and/or finishing operations

to perform in the products comparing with those needed in Node 3. The selected set of remanufacturing percentages (defined in the following as "*set #0*") is introduced as follows: the *12%*, *14%* and *16%* of the product material needs to be remanufactured respectively for the *20%*, *60%* and *20%* of the products (from both Group A and Group B) that pass through Node 3. Similarly, the *10%*, *12%* and *14%* of the product material needs to be remanufactured respectively for the *20%*, *60%* and *20%* of the products that pass through Node 6.

2.2.2 Data Inventory

Table 6 reports the input data necessary to evaluate the energy demand for one remanufacturing of the considered turbine blade and for one brand-new manufacturing of the entire product. *The conversion from electric MJ/kg to MJ/kg (oil equivalent) is done using 0.38 as conversion efficiency value, according to the European average* [67]. Finally, a *±10%* range is considered for the marked parameters in Table 6 (with "*") to cover their possible variability.

The first part of Table 6 focuses on the material eco-properties. The embodied energy for the material production (E_E) is computed considering the benefits arising from the upstream flow of recycled material in the current supply (equal to R = 30% [125]). The term E_E is computed applying the so-called 'recycled content approach' [137] using the energy for primary material production (E_V) and the energy for material recycling (E_R). Both terms are taken from the CES Selector database [125] for a nickel-based superalloy with similar composition of that of the NiCr20Co18Ti material.

The second part of Table 6 focuses on the atomisation phase. The energy for powder atomisation (E_A) is computed from the data available in [63] for the NiCr20Co18Ti material. On the other hand, the value of the input/output material ratio for powder atomisation (y_{GA}) is adapted from [103] due to the lack of data available in literature. The contribute of the gas embodied energy is also considered for the atomisation process of the NiCr20Co18Ti material. In particular, the consumption rate of the argon needed to produce 1 kg of powder (q_{Ar}) [71,155] is multiplied for the output powder mass from the atomisation unit. The argon embodied energy (E_{Ar}) is taken from the data reported in [155,156].

The third part of Table 6 focuses on the DED process. The specific energy consumption for the printing phase (SEC^{DED}) is multiplied for the deposited mass. The numerical value for the SEC^{DED} factor is taken from [63] for the

NiCr20Co18Ti material. In this study it is assumed that the area of the product to be remanufactured is first machined for a cutting deep of 3 mm to prepare the surface for the DED process. An allowance equal to the 10% of the remanufactured mass is assumed in this study for the subsequent machining phase. Moreover, a powder loss of the 40% should be considered for the DED process performed with the NiCr20Co18Ti material, according to [63]. Therefore, the deposited mass considers not only the remanufactured volume with the relative allowance, but also the powder lost (since the powder is melted regardless it reaches the target area or not). The contribute of the gas embodied energy is also considered for the DED unit process. In particular, the consumption rate of the argon gas (q_{Ar}) during the deposition phase is computed from the data available in [63] for the NiCr20Co18Ti material. The deposition time for the DED process is computed considering the powder flow rate for the NiCr20Co18Ti material (q_{Ni}^{DED}) [63]. The contribute of the pre-/post-settings is taken into account considering the product between the idle time (t_s^{DED}) and the idle power (P_{stb}^{DED}).

The fourth part of Table 6 focuses on the EBM process. Due to the available date in the literature, the unit process specific energy consumption (SEC^{EBM}) is considered for the EBM technology. Therefore, the contribute of the not productive phases (e.g., vacuum generation and cooling window) are included into this value. Moreover, the value of 160.53 MJ/kg was chosen among those available in the literature since it refers to a condition in which the machine start plate is saturated and the contribute of the fixed phases on the unit kg of printed material is reduced [112]. The material allowance and the support mass are both assumed in this study equal to the 10% of the product mass. The embodied energy of the helium gas is addressed for the printing phase, considering the helium consumption rate (q_{He}) [29]. The printing time is computed adapting the deposition rate for the printing phase available from the data reported in [103]. Moreover, the helium quantity for the cooling phase (q_{Cool}) is also included, as reported in the machine datasheet [29]. Finally, the embodied energy of the helium gas (E_{He}) is computed based on extraction from natural gas [157], since it requires much lower resources than extraction from the air [158].

The fifth part of Table 6 focuses on pre-/post-processes. The specific energy demand for surface cleaning (E_{Cle}) is considered before of each remanufacturing for the worn product [155,159]. The wire-EDM is taken into account only for the products produced via EBM, adapting the value reported in [65] for the specific

energy demand of the process (E_{EDM}). On the other hand, the HIP treatment is considered after the DED process and after the EDM step, using the specific energy demand of the process (E_{HIP}) for the NiCr20Co18Ti material [63].

The sixth part of Table 6 focuses on the machining process. Only the finishing machining is considered for the DED process. On the other hand, both rough (removing the 80% of the allowance) and finishing machining (removing the 20% of the allowance) are considered for the EBM process. The energy demands due to the machine tool for rough and finishing machining are addressed with the relative specific energy consumption parameter for the NiCr20Co18Ti material (i.e., respectively SEC_{RM}^{CM} and SEC_{FM}^{CM} [125]), which is multiplied for the relative machined mass. On the other hand, the energy demand due to the standby phases (pre-/post-settings and cutting tool changes) are addresses as reported in [70,109]. Moreover, the contributes of consumables as the cutting tool and the cutting fluid are included as shown in [70,109].

Material eco-properties			
Parameter	Physical unit	Numerical value	References
Recycle fraction in the current supply, R	-	30%*	[125]
Embodied energy for material production, E_E	MJ/kg	182.60	Computed as in [137]
Energy for primary material production, E_V	MJ/kg	245.00*	[125]
Energy for material recycling, E_R	MJ/kg	39.75*	[125]
Powder density, p_{Ni}	kg/m^3	8025.00	[125]
Parameters of the powder atomisation process			
Parameter	Physical unit	Numerical value	References
Energy for powder atomisation, E_A	MJ/kg	55.60*	[63]
Input/output material ratio for powder atomisation, y_{GA}	-	1.03*	Adapted from [103]
Argon density, p_{Ar}	kg/m^3	1.64	[160]
Consumption rate of the argon gas to produce 1 kg of powder, q_{Ar}	m^3/kg	3.30*	[71,155]
Argon embodied energy, E_{Ar}	MJ/kg	0.69*	[155,156]
Parameters of the DED process			
Parameter	Physical unit	Numerical value	References
Specific energy consumption for the printing phase of the DED process, SEC^{DED}	MJ/kg	1051.65*	[63]
Powder flow rate for the DED process, q_{Ni}^{DED}	kg/h	0.06*	[63]
Consumption rate of the argon gas, q_{Ar}	kg/h	0.94*	[63]
Time standby of the DED system, t_s^{DED}	h	1.00*	Assumed
Standby power of the DED system, P_{stb}^{DED}	kW	1.00*	Assumed
Parameters of the EBM process			
Parameter	Physical unit	Numerical value	References
Unit process specific energy consumption for EBM, SEC^{EBM}	MJ/kg	160.53*	Adapted from [112]
Powder printing rate for EBM, DR^{EBM}	kg/h	0.03*	Adapted from [103]
Helium density, p_{He}	kg/m^3	0.17	[160]
Consumption rate of the helium gas, q_{He}	l/h	1.00*	[29]
Helium quantity for the cooling phase, q_{Cool}	l	62.50*	[29]
Helium embodied energy, E_{He}	MJ/kg	1.58*	[157,158]

Parameters for pre-/post-processes			
Parameter	Physical unit	Numerical value	References
Specific energy demand for surface cleaning, E_{Cle}	MJ/kg	0.72*	[155,159]
Specific energy demand for wire-EDM, E_{EDM}	MJ/kg	37.00*	Adapted from [65,161]
Specific energy demand for HIP treatment, E_{HIP}	MJ/kg	8.54*	[63]
Parameters of the machining process			
Parameter	Physical unit	Numerical value	References
Specific energy consumption of the machine tool for rough machining, SEC_{RM}^{CM}	MJ/kg	1.54*	[125]
Material removal rate of the machine tool for rough machining, MRR_{RM}^{CM}	cm^3/sec	$5.54 \cdot 10^{-2}$*	Assumed
Specific energy consumption of the machine tool for finishing machining, SEC_{FM}^{CM}	MJ/kg	10.95*	[125]
Material removal rate of the machine tool for finishing machining, MRR_{FM}^{CM}	cm^3/sec	$3.46 \cdot 10^{-3}$*	Assumed
Standby power of the machine tool, P_{stb}^{CM}	kW	2.20*	[70]
Time standby of the machine tool, t_s^{CM}	h	0.50*	[70]
Time necessary for a cutting tool change, t_{cu}	min	2.00*	[70]
Life of the cutting tool, T	h	0.50*	[70]
Embodied energy of the cutting tool, E_{tool}	MJ/kg	400.00*	[162,163]
Consumption rate of the cutting fluid, q_L	kg/h	0.48*	[162,164]
Embodied energy of the cutting fluid, E_{lub}	MJ/kg	1.40*	[162,164]
Parameters for the transportation contribute			
Parameter	Physical unit	Numerical value	References
Specific energy demand for transportation, E_T	MJ/kg·km	$7.10 \cdot 10^{-4}$*	[37,123]
Travelled distance for one connection, d_i	km	200.00*	[37,123]

Table 6. Data inventory for the selected case study. A ±10% range of variability is considered for the parameters marked with "*". MJ is intended for MJ (oil equivalent).

The last part of Table 6 considers the contribute due to the transportation of the mass flows assessed in this study, as proposed in [37]. For the remanufacturing scenario, four travel distances are considered, namely: (a) the worn product is brought back to the remanufacturing station from the use place, (b) the feedstock mass needed for the remanufacturing is brought to the remanufacturing station, (c) the remanufactured product is conducted to the use place from the remanufacturing station and (d) the removed chips and allowances are brought from the remanufacturing station to the recycling plant.

For the brand-new manufacturing scenario, four travel distances are considered, namely: (a) the worn product is brought to the recycling plant, (b) the feedstock mass needed for the brand-new manufacturing is brought to the manufacturing station, (c) the brand-new product is conducted to the use place from the manufacturing station and (d) the removed allowances and supports are brought from the manufacturing station to the recycling plant.

2.3 Results

This section aims to report the main results of the comparative LCA between the two discussed scenarios. As reported above a ±10% variation is considered for the terms "L_A" and "L_B", which characterise the remanufactured products. This variation imposes a different number of iterations for the remanufacturing approach. Therefore, in the following graphs the "worst case" scenario for the remanufacturing approach is delimited from the red vertical line. On the other hand, the "best case" scenario for the remanufacturing approach is delimited from the green vertical line. Finally, the "average case" scenario for the remanufacturing approach is delimited from the orange vertical line. Starting from the "best case" scenario, 10 lives and 9 remanufacturing steps are needed to satisfy the overall function target (F_P). On the other hand, 11 lives and 10 remanufacturing steps are needed for the "average case" scenario and 12 lives and 11 remanufacturing steps are needed for the "worst case" scenario. Fixing the analysis (i.e., worst, average or best case scenario), the numbers of the remanufacturing loops are one unit lower those of the lives. In fact, once the products cumulate the overall target function (F_P), there is not a remanufacturing that follows the last life because the products are recycled.

Figure 15 (a) reports the evolution of the market distribution (i.e., the number of "PA" in blue and of "PB" in orange) during the overall time window of the analysis.

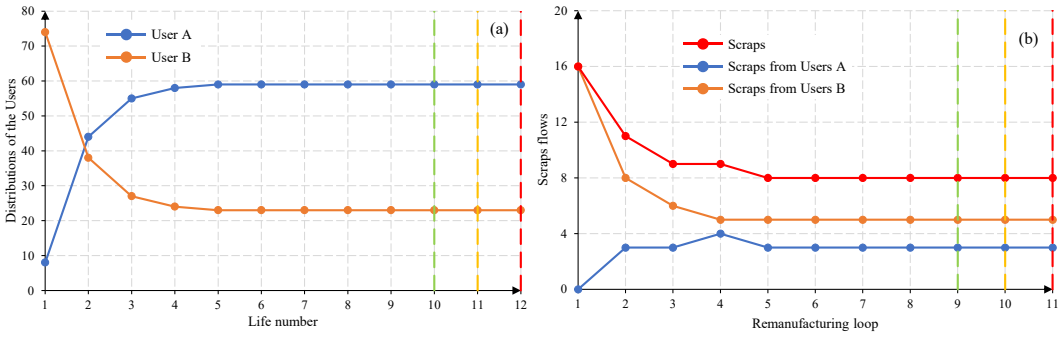

Figure 15. (a) Distribution of the users for each life and (b) effect on the scrap flows of each corresponding remanufacturing loop.

A quick variation of the initial condition is present in Figure 15 (a) in order to reach the asymptotic condition, as typical for Markovian models with constant "state transition probabilities". The number of products belonging to Group B reduces with the iterations because a virtuous evolution of the market was

assumed (see the "state transition probabilities" reported in Table 5 for "M_U"). Figure 15 (b) shows the overall number of scraps for each iteration in red. The scraps belonging to Group A and to Group B are also highlighted, respectively in blue and orange. Considering the "state transition probabilities" reported in Table 4 for "M_R", the products belonging to Group B are more likely to reach Node 9 respect to those belonging to Group A. Therefore, the trend for the overall scraps is mainly affected from the scraps belonging to Group B.

Focusing on the "average case" scenario, Figure 16 shows the product flows for each Node of the remanufacturing Markov chain for (a) the first remanufacturing and (b) the last remanufacturing (i.e., the tenth for the "average case" scenario). For each remanufacturing iteration all the products are present in Node 1 (receiving Node) for the initial condition (step "0").

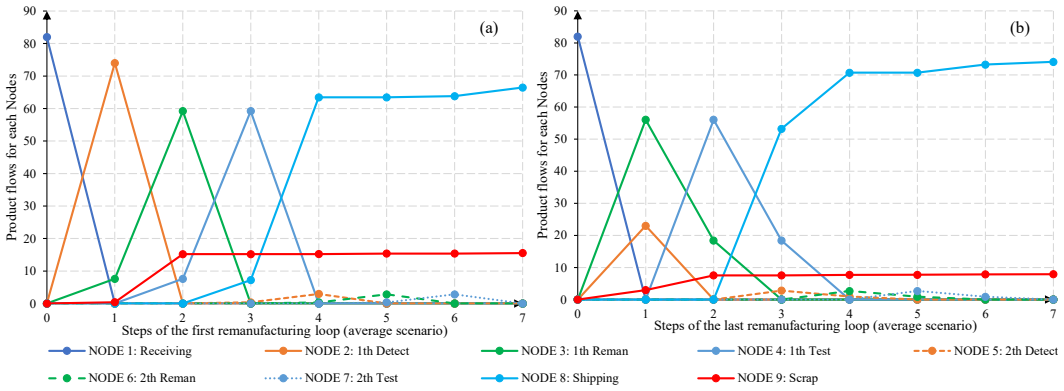

Figure 16. Product flows for each Node of the remanufacturing Markov chain: (a) first remanufacturing and (b) last remanufacturing. "Average case" scenario.

Then they are processed according to the distribution of the market due to the variation of the terms "p_{12}", "p_{13}" and "p_{19}". More in detail the terms "PA" and "PB" are respectively equal to 8 and 74 for the first iteration (i.e., equal to the initial condition "U_1"). On the other hand, these numbers change to 59 and 23 for the tenth loop. Considering these two distributions of the products, the terms "p_{12}", "p_{13}" and "p_{19}" are respectively equal to 0.902, 0.093 and 0.005 for the first iteration. While they respectively become 0.280, 0.684 and 0.036 for the last loop. These numbers explain why a higher number of products is processed in Node 2 for the first remanufacturing iteration respect to those in the tenth loop. As consequence of this, it is possible to observe a lower number of products in Node 3 for the first remanufacturing iteration than those for the last one. The second remanufacturing group of Nodes (composed from Node 5, Node 6 and Node 7)

processes few products due to the low value (0.05) assumed for the "p_{ij}" terms which feed it. Finally, the scraps are higher for the first remanufacturing, as also visible from Figure 15 (b).

Figure 17 shows the product flows for key-Nodes of the remanufacturing Markov chain, namely: Node 3 (first remanufacturing station, in green), Node 6 (second remanufacturing station, in green and dashed line) and Node 9 (scrap station, in red). In particular, Figure 17 (a) shows the shares for each remanufacturing loop while Figure 17 (b) highlights the cumulative trends.

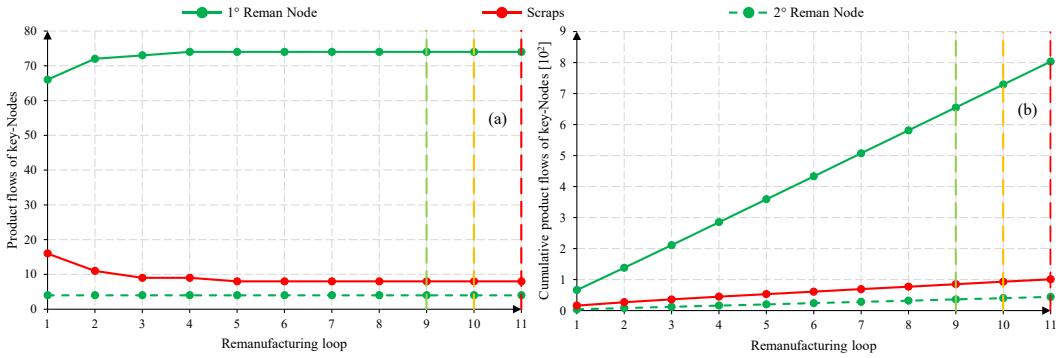

Figure 17. Product flows for key-Nodes of the remanufacturing Markov chain: (a) shares for each remanufacturing loop and (b) cumulative trends.

These results are used to compute the energy demands due to the remanufacturing process itself (i.e., the DED process) and the energy demands related to the manufacturing of the brand-new products (by means of EBM). In fact, the energy demands for only the remanufacturing process itself and for the manufacturing are included into this comparative LCA, as discussed in the previous section. On the other hand, the energy requirements to perform the operations at the detect and the test stations are not considered.

Figure 18 reports (a) the distributions of the target share for each life (i.e., the variable "f_P") of the remanufacturing scenario (in green) and compares it with those of the brand-new manufacturing scenario (in grey). Moreover, Figure 18 (a) highlights the shares of the products belonging to Group A (in blue) and those belonging to Group B (in orange). As discussed above, the products that reach the scrap station (Node 9) need to be replaced with brand-new ones. Therefore, the entire life (L_A) is considered for these new products and their shares are also included with those of the Group A. This last consideration applies also to the first life (i.e., when all the products are brand-new). Figure 18 (a) also reports the effect of the ±10% variability (visible with the dashed lines) which is considered for "L_A" and "L_B" for the remanufactured products. In the "best case" scenario the

remanufacturing approach is able to overcome the shares of the brand-new approach. This result can be technologically explained with the use of an appropriate coating that can be deposit by mean of the DED process and that strengthens the blade surface. On the other hand, the remanufacturing scenario shows the same share for all the loops of the analysis and this value overlaps that of the remanufacturing scenario only for the first life.

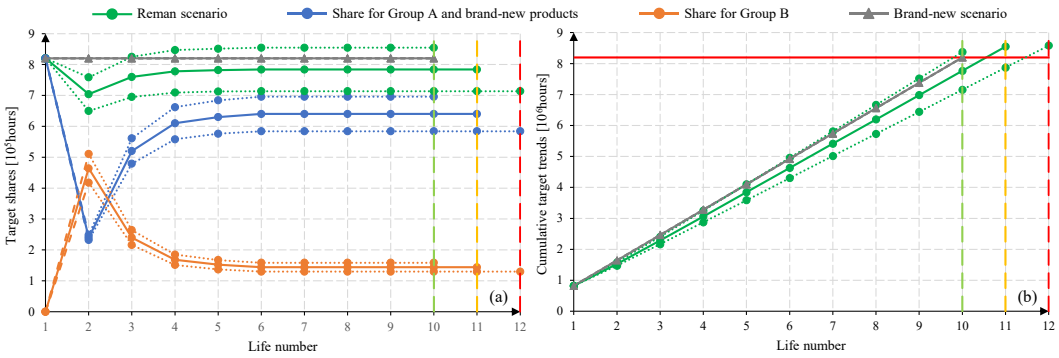

Figure 18. (a) Distributions of the target share for each life (f_P) and (b) cumulative trends.

Figure 18 (b) shows the cumulative trends for the brand-new scenario (in grey) and for the remanufacturing approach (in green). A linear trend is visible in the first case since constant shares are reported in Figure 18 (a) for the brand-new scenario. On the other hand, Figure 18 (a) shows a variation in the shares for the initial iterations until the asymptotic values are reached in Figure 15 for the product flows. Therefore, a slight not linearity is visible in Figure 18 (b) for the remanufacturing scenario only for the first part of the investigated life range.

In the following of this Chapter, the physic unit MJ is intended for MJ (oil equivalent) for all the results referred to the energy metric.

Figure 19 focuses on the CED needed to perform the remanufacturing of a single blade (in green), as function of the percentage of remanufactured material. The dashed green lines in Figure 19 refers to the ±10% range of variability considered for the input parameters marked with "*" in Table 6. Moreover, the point visible in Figure 19 for the remanufacturing of a single blade are computed for different material percentages with the aim to cover a possible remanufacturing domain (i.e., from 1% to 40%). A linear trend is kept since all the energy inputs are directly proportional to the remanufactured mass. This is mainly due to the lack of models in the literature which properly evaluate the energy consumption of AM production techniques (such as DED and EBM) at their unit process level. In fact, the state-of-the-art literature only offers constant

SEC values for the different AM technologies which do not consider the effect of the process and part designs, as highlighted in the paragraph 1.2 of Chapter 1.

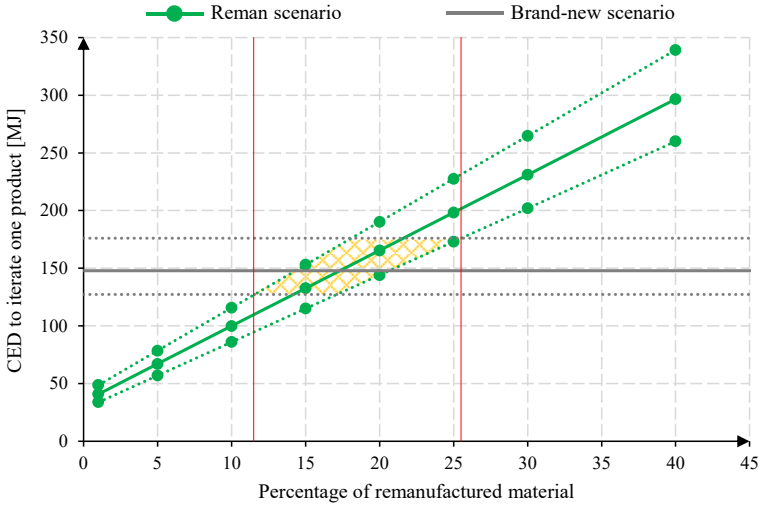

Figure 19. CED to remanufacture one blade as function of the remanufactured material percentage and CED for the manufacturing of a brand-new blade. MJ is intended for MJ (oil equivalent).

On the other hand, 147.89 MJ are computed for the manufacturing of a brand-new blade as average condition (grey line), with the highest value up to 175.91 MJ (upper dashed grey line) and a lowest one down to 127.19 MJ (lower dashed grey line). Considering the average results, the two continuous lines intersect eachother at around the 17% of remanufactured material. The maximum intersection range found for the remanufactured material percentage is given from 11.5%-25.5%, if the effect of the variability discussed for Table 6 is taken into account for both production routes. More precisely, Figure 19 shows the area of uncertainty shaded in orange.

Figure 20 highlights the energy percentage share of the different steps to produce one blade in both scenarios. These results are computed considering the average value for the data inventory reported in Table 6. In particular, it also reports the variation of the remanufactured material, evaluating the same percentage range shown in Figure 19. Considering the remanufacturing scenario, the weight of the remanufacturing step progressively rises with the percentage of material to be restored. Therefore, as far as this case study is concerned, the remanufacturing step should be seen as one field of action to improve the CED metric. Focusing on the brand-new manufacturing scenario, the manufacturing step holds a share which is about the 65% of that for the feedstock material production (i.e., the primary and secondary material production plus the

atomisation process). This difference is mainly due to the lower energy efficiency (i.e., one order of magnitude) at the unit process level of the DED process respect to that of the EBM technology (see Table 6). Moreover, the energy efficiency at the unit process level of the EBM process is comparable with the embody energy (considering the primary and secondary material production share, by means of the recycled content approach) of the selected alloy (see Table 6). Considering other steps, the heat treatment, the support removal (by means of Wire-EDM) and the transportation have negligible shares respect to the total.

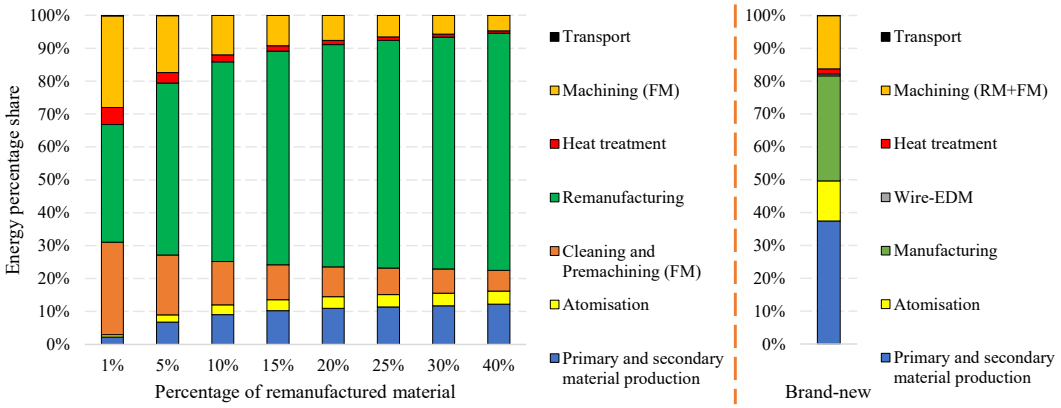

Figure 20. Energy percentage share of the different steps to produce one blade in both scenarios.

Figure 21 (a) shows the energy demand shares for each remanufacturing loop for Node 3 (first remanufacturing station, in green), Node 6 (second remanufacturing station, in green and dashed line) and Node 9 (scrap station, in red), while Figure 21 (b) reports the cumulative energy trends. These terms are computed using the products flows in Figure 17 and the energy demands for one remanufacturing and one brand-new manufacturing described for Figure 19. For these reasons, Figure 17 and Figure 21 show the same trends.

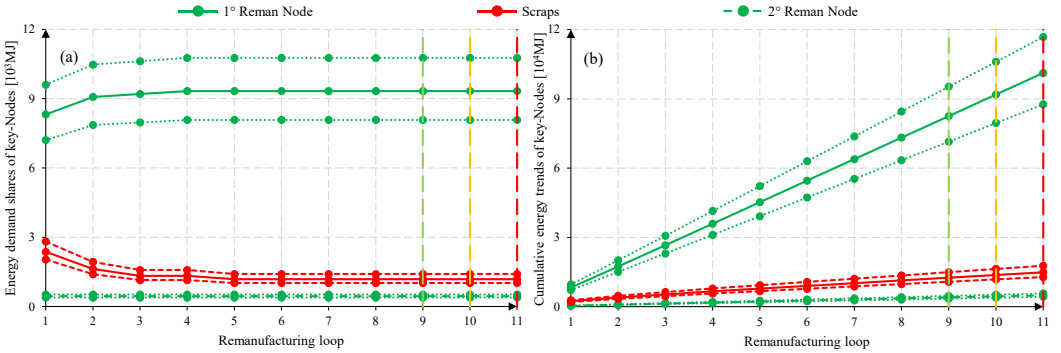

Figure 21. (a) Energy demand shares for each remanufacturing loop for key-Nodes of the remanufacturing Markov chain and (b) cumulative energy trends.

Figure 22 reports (a) the cumulative energy trends for the two scenarios for each life. The data reported for the remanufacturing approach were computed as the sum of the data reported in Figure 21 (b). In the "best case" scenario (green vertical line) the remanufacturing approach seems to be a better solution respect to the brand-new manufacturing for the considered percentages of remanufactured material (set #0). On the other hand, the higher number of loops needed from the remanufacturing approach for the "average case" (orange vertical line) and the "worst case" (red vertical line) scenarios make this route less convenient than the brand-new one.

Figure 22 (b) reports the CED needed from the two approaches at the final loop considering the "average case" scenario for the remanufacturing approach. The error bars consider the variability for the input data discussed for Table 6. Moreover, the error bars referred to the remanufacturing route also consider the variability given from the "best case" and "worst case" scenario (i.e., that for "L_A" and "L_B"). More in detail, the upper limit of the error bar is referred to the "worst case" scenario and the +10% for the marked input parameters in Table 6. On the other hand, the lower limit of the error bar is referred to the "best case" scenario and the -10% for the marked input parameters in Table 6. The results of Figure 22 (b) describe the breakeven condition between the two scenarios, for the input variables given in paragraph 2.2 and for the "set #0" of remanufactured material percentages.

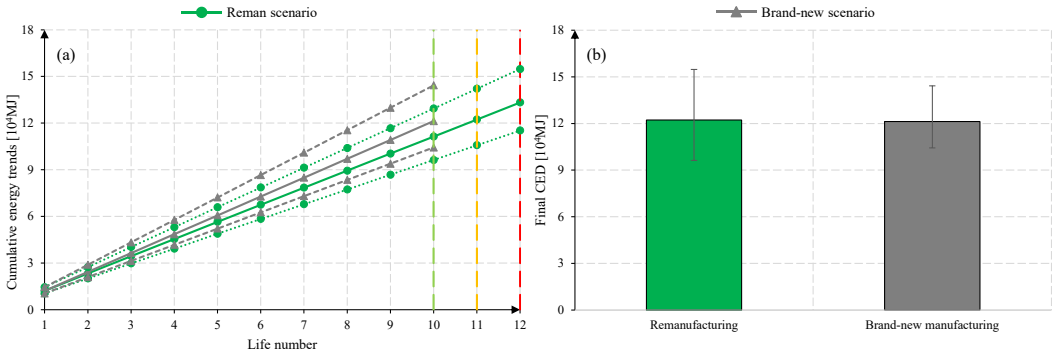

Figure 22. (a) Cumulative energy trends for the two scenarios for each life and (b) final CED (considering the overall variability).

2.4 Discussion

Considering the single production of one blade and its single remanufacturing, the breakeven condition for the remanufactured material percentage is given from

17% (with a maximum intersection range of 11.5%-25.5%), as highlighted from Figure 19. A similar result was found in [63], where investment casting was used as reference technology for the manufacturing process: in particular, the breakeven condition for the CED metric was given from around the 20% of remanufactured material (with a maximum intersection range of about 15%-24%). The lower result of this study (17% respect to about 20%) can be explained with a higher energy and resource efficiency of the EBM process respect to that of the investment casting process, as well as with a slight difference on the input data for the LCA analysis.

Focusing on a function-oriented analysis, Figure 22 reports that the breakeven condition is achieved for around the 14% of the remanufactured material (according to set #0). Therefore, a different breakeven value can be observed, considering the parameters of the analysis fixed in paragraph 2.2 of this Chapter. In particular, the different result is due to (a) the introduction of products which last for a lower physical lifetime (L_B) than others (L_A), (b) the presence of scraps which require to be replaced with brand-new products, (c) a not linear evaluation of the remanufacturing process which may require multiple internal iterations and to (d) a distribution of the products (i.e., those belonging to Group A and Group B) which changes during the time window of the analysis. This proves that appropriate tools are needed for not conventional LCA studies to take into account the higher complexity of the actions of the circular economy.

This Chapter performs the analysis considering different variabilities, e.g., those to model the physical lifetime for the remanufacturing scenario and the LCA input data marked with "*" in Table 6. Moreover, the function-oriented analysis cumulates the variability in the output of the multiple lives. Therefore, the technological knowledge of the selected steps (e.g., the atomisation process, the DED technique and so forth) as well as the truthfulness of the LCA input data are necessary needs to properly describe the applicability of the CE actions to AM. For instance, considering the AM unit process level, a proper evaluation of the SEC parameter should take into account the effect of the process and part designs, as highlighted in the paragraph 1.2 of Chapter 1.

The methodology proposed in this Chapter better quantifies the potentialities of a not linear approach as the CE. The introduced new variables in paragraph 2.1 of this Chapter have a deep impact in the results. Therefore, in the following a sensitivity analysis is performed for the main variables of the proposed methodology to better investigate its potentialities. More in details, the

investigated aspects are (a) the effect of the remanufactured material percentage, (b) the effect of the initial distribution of the users, (c) the effect of the awareness campaigns for the users and (d) the effect of the behaviours of the users.

2.4.1 Effect of the remanufactured material percentage

In this paragraph a sensitivity analysis is conducted in order to evaluate the effect of the remanufactured material percentage. Fixing all other parameters of the analysis as discussed in paragraph 2.2 of Chapter 2, two further sets of remanufacturing material percentages are considered as follows:

1) Set #1 of remanufacturing percentages: the 22%, 24% and 26% of the product material needs to be remanufactured respectively for the 20%, 60% and 20% of the products (from both Group A and Group B) that pass through Node 3. Similarly, the 20%, 22% and 24% of the product material needs to be remanufactured respectively for the 20%, 60% and 20% of the products that pass through Node 6.

2) Set #2 of remanufacturing percentages: the 4%, 6% and 8% of the product material needs to be remanufactured respectively for the 20%, 60% and 20% of the products (from both Group A and Group B) that pass through Node 3. Similarly, the 2%, 4% and 6% of the product material needs to be remanufactured respectively for the 20%, 60% and 20% of the products that pass through Node 6.

The remanufactured material percentages do not influence the product flows. On the other hand, they affect the energy requirements. Therefore, the different results of this sensitivity analysis are reported from Figure 23 to Figure 25.

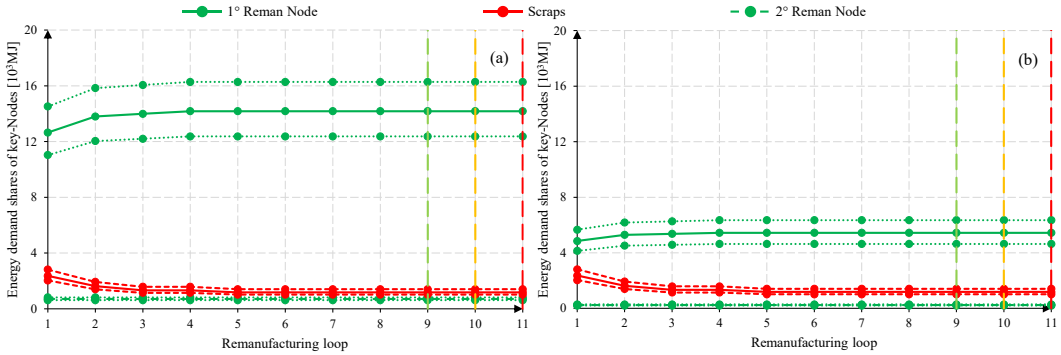

Figure 23. Energy demand shares for each remanufacturing loop for key-Nodes of the remanufacturing Markov chain: (a) set #1 of remanufacturing percentages, (b) set #2 of remanufacturing percentages.

In particular, Figure 23 distinguishes the energy demand shares for each remanufacturing loop for key-Nodes of the remanufacturing Markov chain: (a) set

#1 and (b) set #2. These results keep the same trends of those shown in Figure 21 (a) for the breakeven condition given from set #0. However, set #1 and set #2 give values respectively located above and below those for set #0.

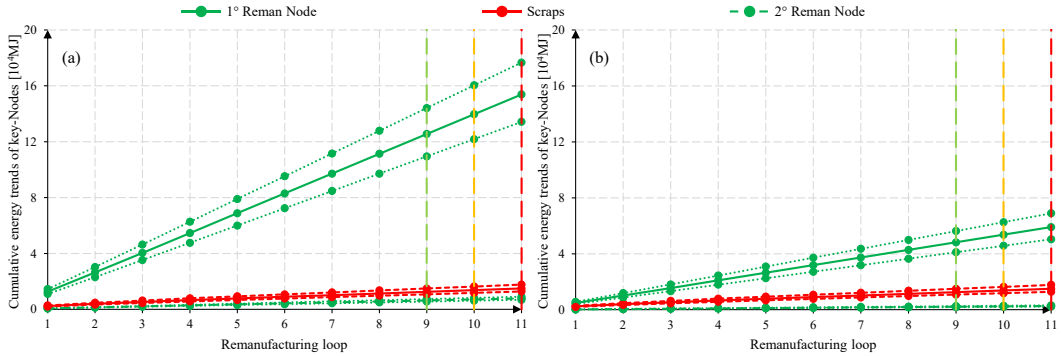

Figure 24. Cumulative energy trends for the two scenarios for each life: (a) set #1 of remanufacturing percentages, (b) set #2 of remanufacturing percentages.

Similar consideration can be applied for the results reported in Figure 21 (b) and for the cumulative energy trends for the two scenarios (Figure 24). Figure 25 highlights the final CED of the remanufacturing and brand-new scenarios (considering the overall variability): (a) set #1, (b) set #2. As it is possible to see, these two sets define conditions in which the error bars of the two scenarios are not overlapped.

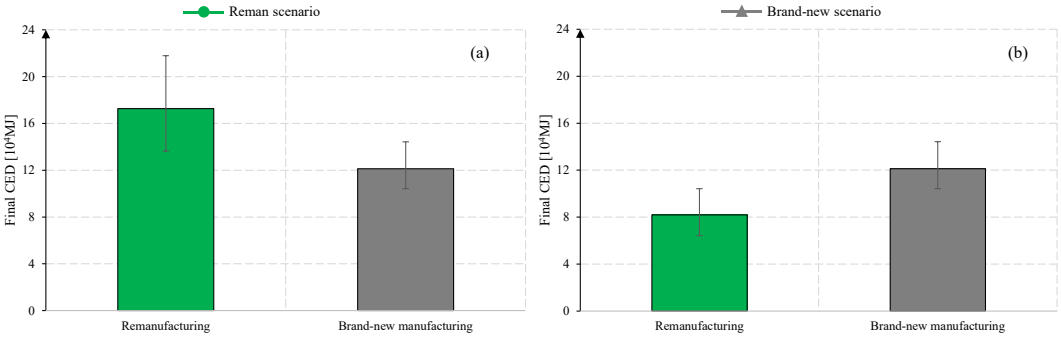

Figure 25. Final CED of the remanufacturing and brand-new scenarios (considering the overall variability): (a) set #1 of remanufacturing percentages, (b) set #2 of remanufacturing percentages.

2.4.2 Effect of the initial distribution of the users

In this paragraph a sensitivity analysis is conducted in order to evaluate the effect of the initial distribution of the users. Fixing all other parameters of the analysis as discussed in paragraph 2.2 of Chapter 2, the new vector "U_1" is modified as follows: 90% of the products are used according to the prescribed working conditions during their first use, while the remaining 10% of the products

belongs to Group B. The initial distribution of the users influences the product flows and with this all the subsequent results of the analysis. Therefore, the main results of this sensitivity analysis are reported from Figure 26 to Figure 28.

Figure 26 (a) reports the new distributions of the users which differs from those in Figure 15 (a). However, the same asymptotes are kept due to the same "state transition probabilities" of "M_U". Figure 26 (b) focuses on the scrap flows, which only for the initial remanufacturing loops are different respect to those in Figure 15 (b). The lower scraps of the initial steps are due the lower initial numbers of products belonging to Group B.

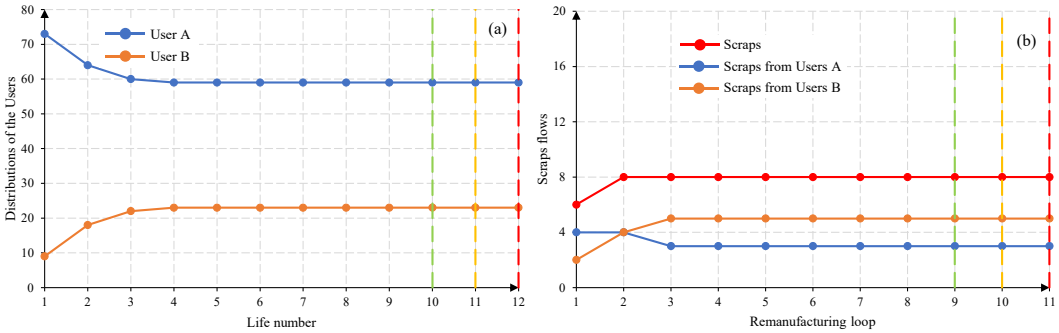

Figure 26. Effect of the initial distribution of the users: (a) distribution of the users for each life and (b) effect on the scrap flows of each corresponding remanufacturing loop.

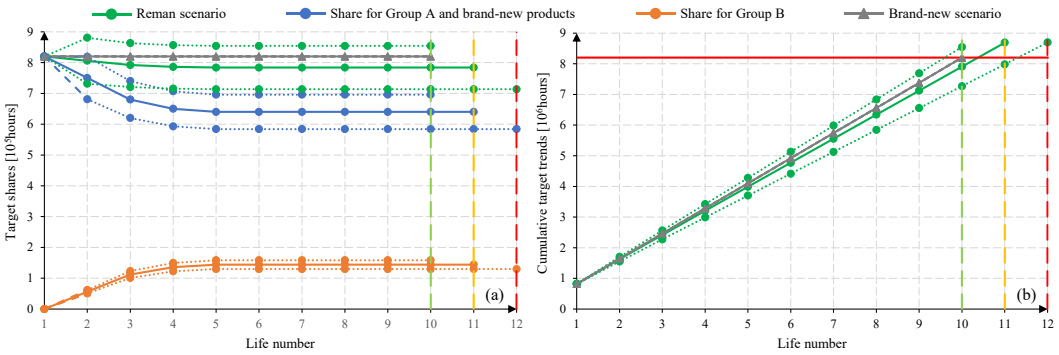

Figure 27. Effect of the initial distribution of the users: (a) distributions of the target share for each life (f_P) and (b) cumulative trends.

This difference leads to a higher value of "f_p" satisfied for the initial steps. In fact, the remanufacturing and the brand-new scenarios shows similar initial shares, as visible in Figure 27 (a). Figure 27 (b) reports the same initial trend for the two scenarios. However, a reduction in the inclination of the curve for the remanufacturing route can be distinguished for the further lives. Figure 27 (b) highlights that the same number of iterations is needed for the "worst case", "average case" and "worst case" scenarios, respect to those in Figure 18.

Therefore, the final energy demands will not be so different from those reported in Figure 22. However, different trends are reported in Figure 21 and Figure 28.

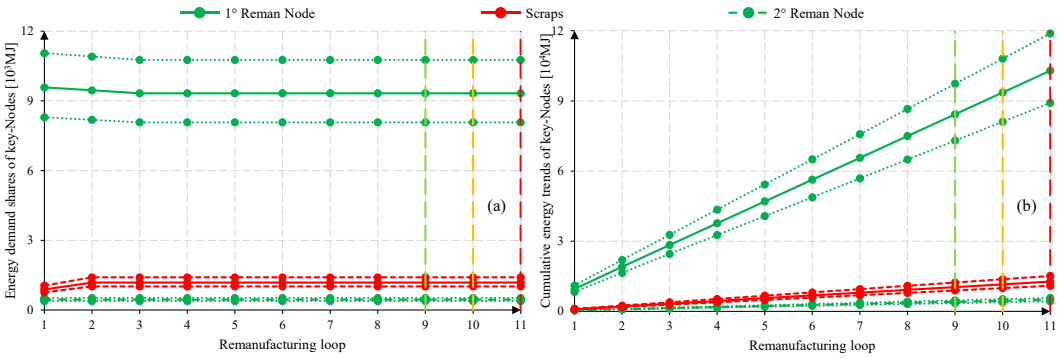

Figure 28. Effect of the initial distribution of the users: (a) energy demand shares for each remanufacturing loop for key-Nodes of the remanufacturing Markov chain and (b) cumulative energy trends.

2.4.3 Effect of the awareness campaigns for the users

In this paragraph a sensitivity analysis is conducted in order to evaluate the effect of the awareness campaigns for the users. Fixing all other parameters of the analysis as discussed in paragraph 2.2 of Chapter 2, the new matrix "M_U" is considered as highlighted in Table 7. The evolution of the user distribution influences the product flows and with this all the subsequent results of the analysis. The main results are reported from Figure 29 to Figure 31.

-	To Group A	To Group B
From Group A	0.50	0.50
From Group B	0.20	0.80

Table 7. "State transition probabilities" for the sensitivity analysis performed with "M_U".

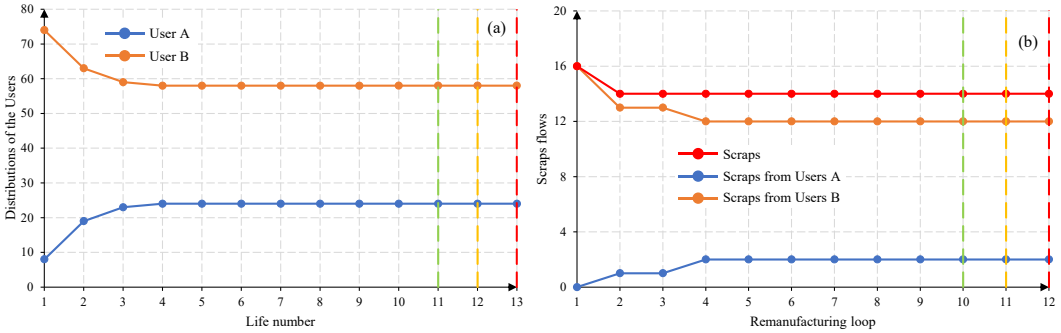

Figure 29. Effect of the awareness campaigns for the users: (a) distribution of the users for each life and (b) effect on the scrap flows of each corresponding remanufacturing loop.

Figure 29 reports the same initial conditions of those in Figure 15 for the distributions of the users and for the scraps. However, they differ for the trends and the final asymptotes. In particular, the new "state transition probabilities" for "M_U" privileges a negative evolution of the market which increases the users belonging to Group B. As consequence of this, a higher number of scraps is highlighted in Figure 29 (b).

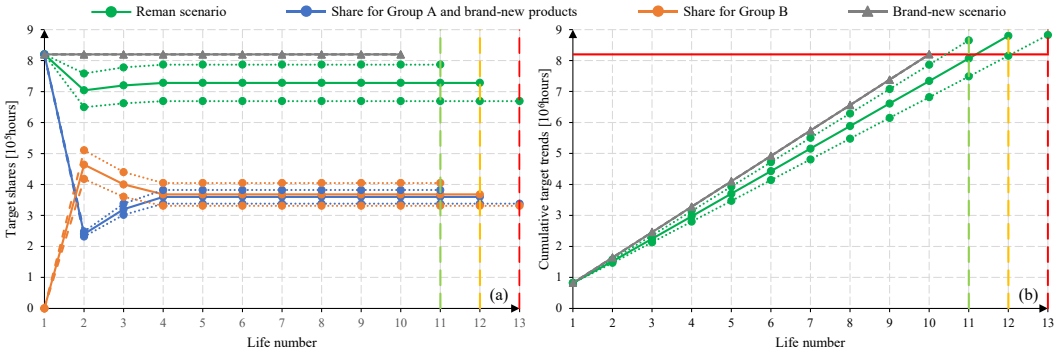

Figure 30. Effect of the awareness campaigns for the users: (a) distributions of the target share for each life (f_P) and (b) cumulative trends.

Moreover, Figure 30 shows a worsening of the remanufacturing loop number. In fact, starting from the "best case" scenario, 11 lives are needed to satisfy the overall function target (F_P). On the other hand, 12 lives are needed for the "average case" scenario and 13 lives are needed for the "worst case" scenario. In fact, Figure 30 (a) shows a reduction of the target share for each life (f_P) respect to those reported in Figure 18 (a). The main effect of this is the higher cumulative energy demand required from the remanufacturing approach respect to those of the brand-new scenario (Figure 31), even if the same remanufactured material percentages of those in Figure 22 are kept.

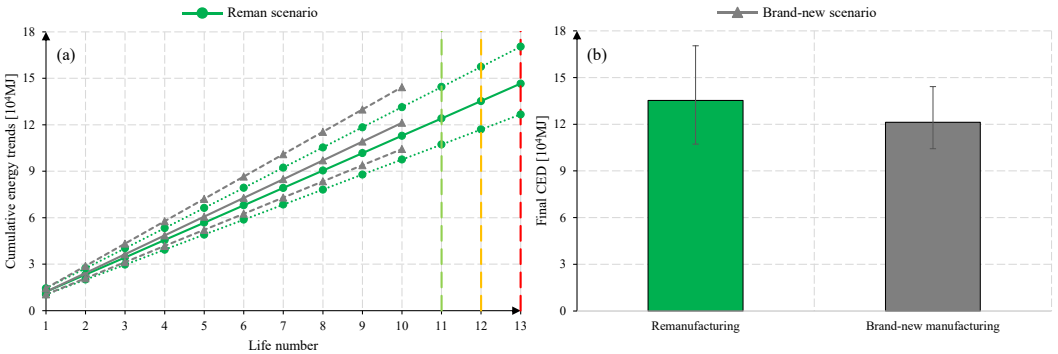

Figure 31. Effect of the awareness campaigns for the users: (a) cumulative energy trends for the two scenarios for each life and (b) final CED (considering the overall variability).

2.4.4 Effect of the behaviours of the users

In this paragraph a sensitivity analysis is conducted in order to evaluate the effect of the behaviours of the users. Fixing all other parameters of the analysis as discussed in paragraph 2.2 of Chapter 2, the new value of "L_B" is set to the 100% of "L_A". In this case, the same trends of Figure 15 are kept. However, the overall target function (F_P) may be achieved with a lower number of iterations due to the higher value of "L_B". Therefore, the main results of this sensitivity analysis are reported from Figure 32 to Figure 33.

Figure 32 (a) shows the distributions of the target share for each life (f_P), while Figure 32 (b) reports the cumulative trends. An improvement of the remanufacturing loop number is highlighted. In fact, starting from the "best case" scenario, 10 lives are needed to satisfy the overall function target (F_P).

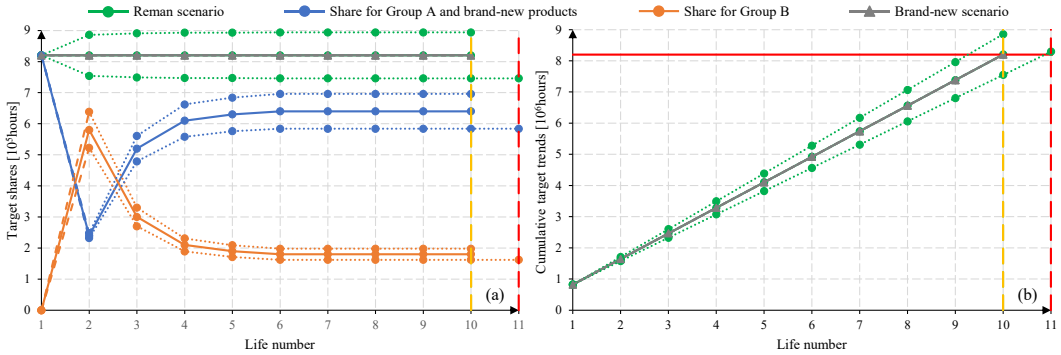

Figure 32. Effect of the behaviours of the users: (a) distributions of the target share for each life (f_P) and (b) cumulative trends.

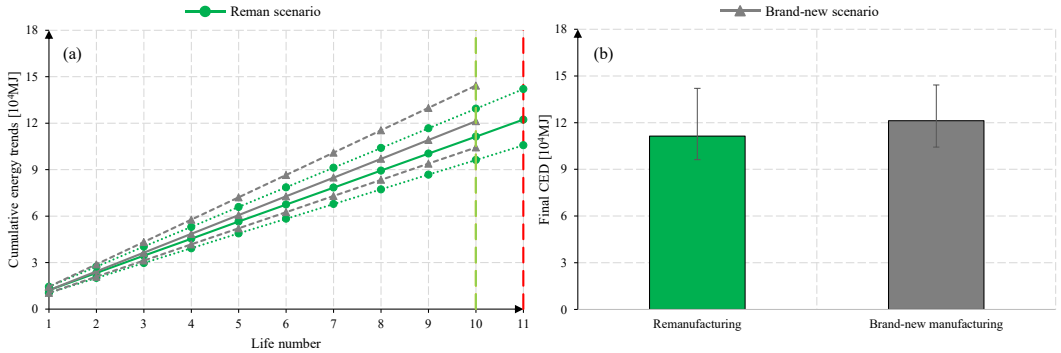

Figure 33. Effect of the behaviours of the users: (a) cumulative energy trends for the two scenarios for each life and (b) final CED (considering the overall variability).

On the other hand, 10 lives are needed for the "average case" scenario and 11 lives are needed for the "worst case" scenario. More in detail, the "average case"

scenario shows the same behaviour of the brand-new manufacturing approach. Figure 33 shows a lower cumulative energy demand required from the remanufacturing approach respect to those of the brand-new scenario, even if the same remanufactured material percentages of those in Figure 22 are kept.

Chapter 3

The unit process level of AM

3.1 Methodology

This Chapter aims to study the AM technology at its unit process level. In fact, it is necessary to have appropriate tools able to predict the energy requirement of the AM techniques to perform the analysis discussed in Chapter 2. Moreover, due to the high energy demand and low productivity of AM systems, it is worth to defines strategies for their improvement.

Three different processes are deeply investigated, namely Fused Deposition Modelling (FDM), Electron Beam Melting (EBM) and Continuous Filament Fabrication (CFF). Experimental tests were designed and performed for each investigated AM machines. The Stratasys F370 was selected for the FDM process, while the Arcam A2X and the Markforged Mark Two were respectively selected for EBM and CFF. For sake of clarity, the definition of the Specific Energy Consumption (SEC) is given again in this Chapter. SEC defines the energy demand at the unit process level (i.e., considering both productive and not productive phases) to produce the unit mass of material [72,73]. Another parameter to assess the energy efficiency of AM processes is the Specific Printing Energy (SPE), defined as the ratio between the printing energy (i.e., neglecting the not productive phases) and the printed mass [74,75]. On the other hand, the average Deposition Rate is the ratio between the printed mass and the selected time window. This variable can be defined according to the printing phase

(DR_{aprint}) or to the entire unit process level (DR_a) [74,75]. It is useful to remark that the defined parameters above describe a defined process window which is not instantaneous. Therefore, these parameters should be intended as significative of an average information regarding the time and energy efficiency of the AM techniques.

The methodology applied in this Chapter is schematised in Figure 34. First, the selected AM technology and AM system were studied in order to individuate its capabilities. For each case, different experiments were designed to achieve a wide variation of the process parameters, materials and designs. In the next paragraphs they will be reported in detail for each studied technology. The AM process time was measured during each test. All the profiles of current, voltage, power and energy were acquired by using a Fluke 435 Series II analyser. Then, the Fluke proprietary software (Power Log 430-II, Version 5.6) and Microsoft Excel were used to elaborate all the measured profiles and to compute the energy demands. The mass of each printed JOB was weighted by means of a Gibertini 1000 h-CM balance with a resolution of 0.01 g for the FDM and the CFF printed samples.

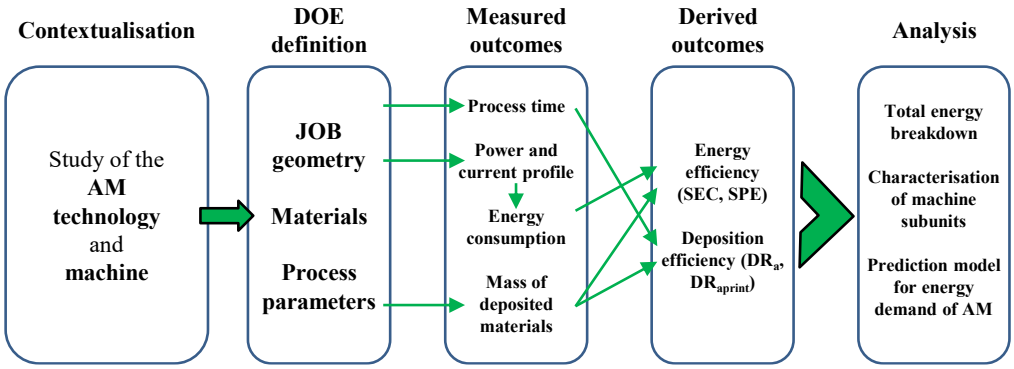

Figure 34. Flowchart highlighting the methodology of Chapter 3.

The nominal density of the material was also used for the reinforced samples made via CFF to assess the mass of their fibres. While for the JOBs realised via EBM, the mass of each printed JOB was computed considering the nominal density of the material and the volumes of the bulk, the support and the lattice parts. Then, data were analysed to compute the parameters referred to the energy efficiency (SEC and SPE) and to the deposition efficiency (DR_a and DR_{aprint}). The correlation between the process parameters, the material, the component designs and the energy and time efficiency of the studied AM systems is carried out. The characterisation of the main process subphases is performed for each AM systems

as well as for each machine subunits. Finally, an innovative empirical model for the energy demand prediction of AM systems is proposed for the first time in literature.

The studies showed in this Chapter for the FDM technology are also part of the published paper by the author of this thesis in [75]*. Similar consideration applies to the work for the EBM technology which is part of the published paper by the author of this thesis in* [74]*.*

Finally, the data which quantify energy entities in this Chapter directly refer to the machine electric consumption.

3.1.1 Fused Deposition Modelling

Figure 35 shows six components characterised by different geometrical complexity. These parts take into account the typical features that can be manufactured according to the capabilities of the FDM process. In particular, component "A" is a basket with a complex, thin and branched structure which is difficult to produce by means of conventional manufacturing routes such as injection moulding. The components "B" and "C" are brackets that were re-designed for AM using topological optimisation procedures.

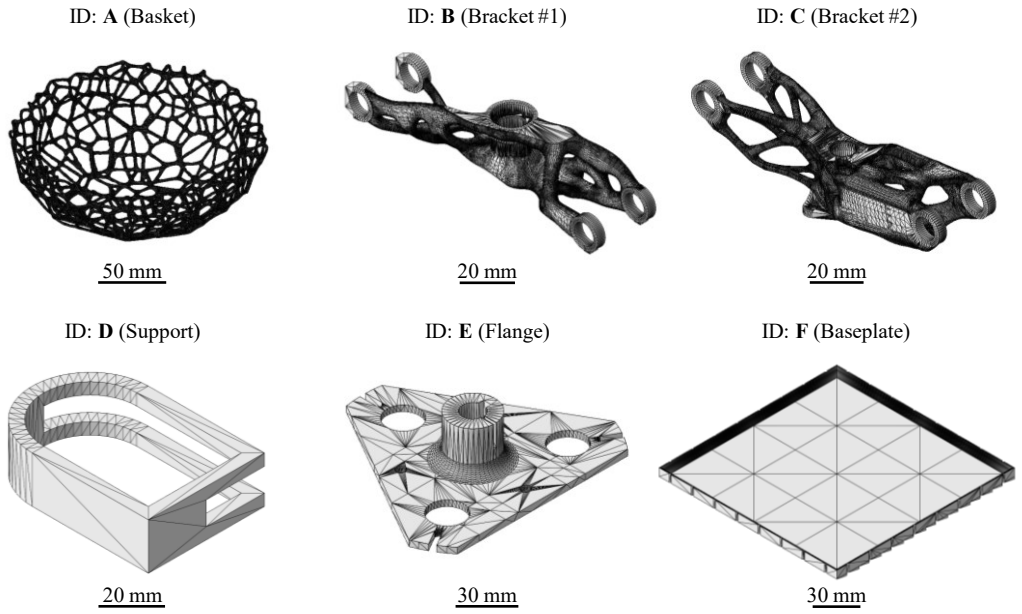

Figure 35. Selected geometries for the Stratasys F370.

The components "D", "E" and "F" are simple and massive geometries with different surface-to-volume ratios, that can still be suitable for AM in case of

batch sizes tending towards the single-part production. ABS or PC-ABS are the investigated materials. The PC-ABS manufactured parts and the experimental set-up are visible in Figure 36. The support structures were realised using the Stratasys QSR proprietary material. The GrabCAD Print software by Stratasys (Version 1.22) was used to slice the STL models of the components and generate the deposition paths. Two different layer thicknesses of 0.178 mm and 0.330 mm were selected. Once chosen, the thickness was fixed and kept constant for all the layers. According to the GrabCAD Print software, three different infill strategies (i.e., the so-called "solid", S, "sparse high-density", HD, and "sparse low-density", LD were chosen. The "S" strategy provides the highest density (with infill lines that touch each other). It is generally used for structural components and implies high material consumption. On the other hand, in the "LD" strategy the infill lines are widely spaced (about 2 mm) to allow material savings and shorter printing times. The "HD" strategy provides an intermediate result between the previous ones (Figure 37). A subset of experimental tests was identified to achieve a wide variation in the average Deposition Rate (which was preliminarily simulated by means of the GrabCAD Print software), with the aim to investigate its effects on the SEC and SPE parameters. The (a) layer thickness (0.178mm or 0.330 mm), the (b) infill strategy ("S", "HD" or "LD") and the (c) component material (ABS or PC-ABS) were the three considered factors.

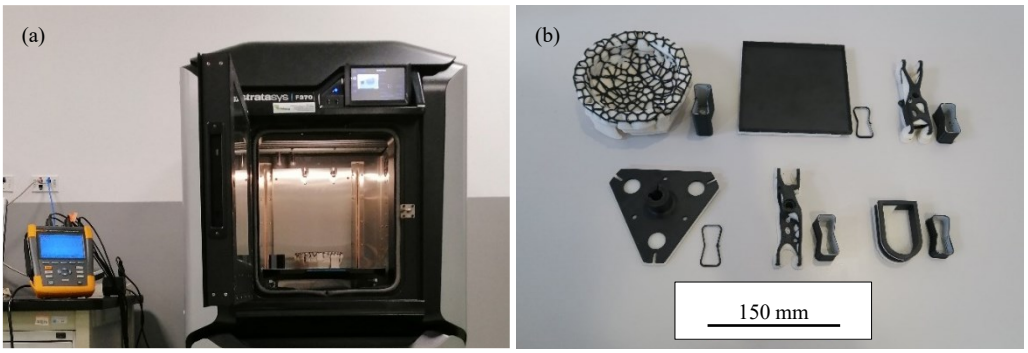

Figure 36. Experimental setup (a) and additively manufactured components (b) on the Stratasys F370.

In addition, to better highlight the correlation between the process parameters and the measured outcomes, a full factorial plan was designed for the experiments concerning the "E" component. Among the other components, part "E" was chosen since the high number of layers with large areas allows the GrabCAD Print software to significantly diversify the extrusion path while changing the process parameters. All the tests were performed under the "eco-mode" setting for

the FDM machine, in which the temperature of the build chamber is cooled down to the room temperature at the end of the JOB. The JOBs were randomly located onto the build plate, and a purge part was produced in each JOB to guarantee the cleaning of the extruders and, therefore, the quality of manufactured JOBs. The "last swap" option was chosen to reduce the material consumption due to the purge part. Under this configuration, the height of the purge part corresponds to the height of the last layer in which there is an alternate deposition of materials of which component and support structures are made of. The main material properties are listed in Table 8. The build chamber needs to be heated up to 90 °C and 95 °C respectively for ABS and PC-ABS. The extrusion temperature of PC-ABS was 30 °C higher than that of ABS, due to the different rheological properties of the two materials. A slight difference in the specific gravity of PCABS and ABS was found in the datasheet of the build materials [78]. The soluble QSR material by Stratasys for support structures was extruded at 265 °C during printing and kept at 170 °C when the extruder was not in use. The QSR material was then dissolved by immersing the printed JOB in a solution of 600 g of sodium hydroxide in 40 L of water at 70 °C for 8 h. Table 9 summarises all the performed experiments.

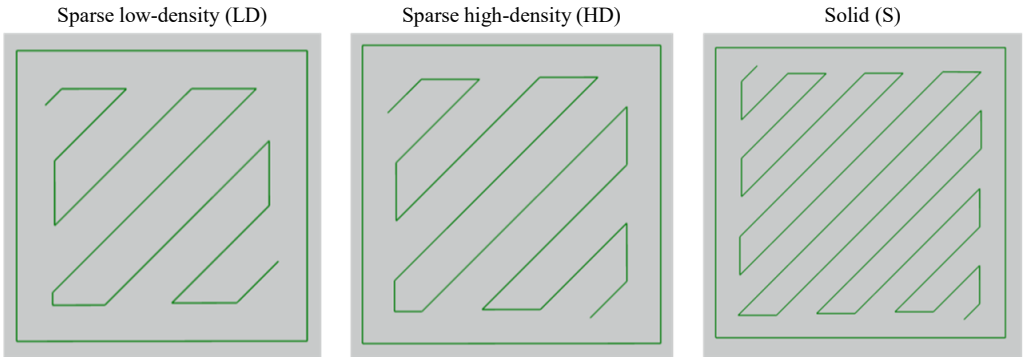

Figure 37. Different infill strategies within the GrabCAD Print software for a simple cube.

According to the description given in Chapter 1, five main subphases can be distinguished: (1) switch-on, (2) idle #1, (3) heating and calibration, (4) printing and (5) idle #2. A decomposition of the machine architecture into its main subunits is carried out as follows: (i) base system of the machine, (ii) chamber heaters and (iii) extruder heaters and axes. Machine subunit (i) is powered during the entire process at the same level. During the process subphase (4), the subunit (ii) is powered in order to keep the process temperature of the build chamber (dependent from the material). On the other hand, during the process subphase

(5), the machine subunit (ii) is powered in order to keep the idle temperature of the build chamber. A calibration of the machine subunit (iii) is present during the process subphase (3), however, it is mainly powered during the printing phase.

Parameter	Stratasys ABSplus-P430	Stratasys PC-ABS
Chamber temperature [°C]	90	95
Extrusion temperature [°C]	255 (Printing); 190 (Not in use)	285 (Printing); 190 (Not in use)
Specific gravity (ASTM D792)	1.04	1.10
Tensile strength (ASTM D638) [MPa]	33	41
Tensile modulus (ASTM D638) [MPa]	2200	1900
Tensile elongation at break (ASTM D638) (%)	8	6
Heat Deflection Temperature (HDT) @ 66 psi (ASTM D648) [°C]	96	110
Heat Deflection Temperature (HDT) @ 264 psi (ASTM D648) [°C]	82	96
Vicat softening temperature [°C]	Not available	112
Glass transition temperature [°C]	108	125
Coefficient of thermal expansion [mm/mm/°C]	$8.82 \cdot 10^{-5}$	$7.38 \cdot 10^{-5}$

Table 8. Main characteristics for ABS and PC-ABS materials provided from Stratasys [78]**.**

The Stratasys F370 is powered by an AC single-phase system. The AC current clamps (one for the single AC phase and one for the neutral phase) and the voltage clamps were connected to the electricity supply wires on the FDM machine. The measuring instrument showed a power factor of ranging from 0.86 to 1 between the real power and the apparent power. The power demand of the (i) base system of the machine was measured evaluating the machine on its standby condition. The power profile during the printing phase was compared with that of subphase (5), to compute the power demand of subunit (iii). Since subphase (4) and (5) mainly differ for the powering of subunit (iii), the energy due to the power demand of subunit (i) and of subunit (iii) were subtracted to the overall measured energy for subphase (4) to compute the average power demand of subunit (ii) during the printing subphase.

JOB ID	Geometry ID	Material	Layer thickness [mm]	Infill strategy	Part volume [cm^3] *	Support volume [cm^3] *
1	A	ABS	0.18	LD	13562	103273

2	B	ABS	0.18	LD	12244	14825
3	C	ABS	0.18	LD	16100	23012
4	D	ABS	0.18	LD	13878	9664
5	D	ABS	0.18	S	18206	9664
6	E	ABS	0.18	LD	33842	14017
7	E	ABS	0.33	LD	39103	13779
8	E	ABS	0.18	HD	48835	14017
9	E	ABS	0.33	HD	44672	13779
10	E	ABS	0.18	S	56470	14017
11	E	ABS	0.33	S	49874	13779
12	F	ABS	0.18	LD	68607	51651
13	A	PC-ABS	0.18	LD	11706	101323
14	B	PC-ABS	0.18	LD	10417	14365
15	C	PC-ABS	0.18	LD	14130	22478
16	D	PC-ABS	0.18	LD	10831	9255
17	D	PC-ABS	0.18	S	17961	9255
18	E	PC-ABS	0.18	LD	29453	12796
19	E	PC-ABS	0.33	LD	37126	13790
20	E	PC-ABS	0.18	HD	41712	12796
21	E	PC-ABS	0.33	HD	49022	13790
22	E	PC-ABS	0.18	S	55392	12796
23	E	PC-ABS	0.33	S	51790	13790
24	F	PC-ABS	0.18	LD	68874	48820

Table 9. Samples manufactured on the Stratasys F370. * Software estimations.

On the other hand, the average power demand of subunit (ii) during subphase (5) was computed measuring the energy demand during this process window for a certain time range and subtracting the energy demand due to machine subunit (i). This methodology was applied due to the impossibility to disassemble the machine into its subunits and to power them one by one.

3.1.2 Electron Beam Melting

The effects of the part and process designs were described by means of six different JOBs (Figure 38), manufactured with the Standard Arcam Ti6Al4V powders [29] (Table 10). Each part was designed using Solidworks 2018.

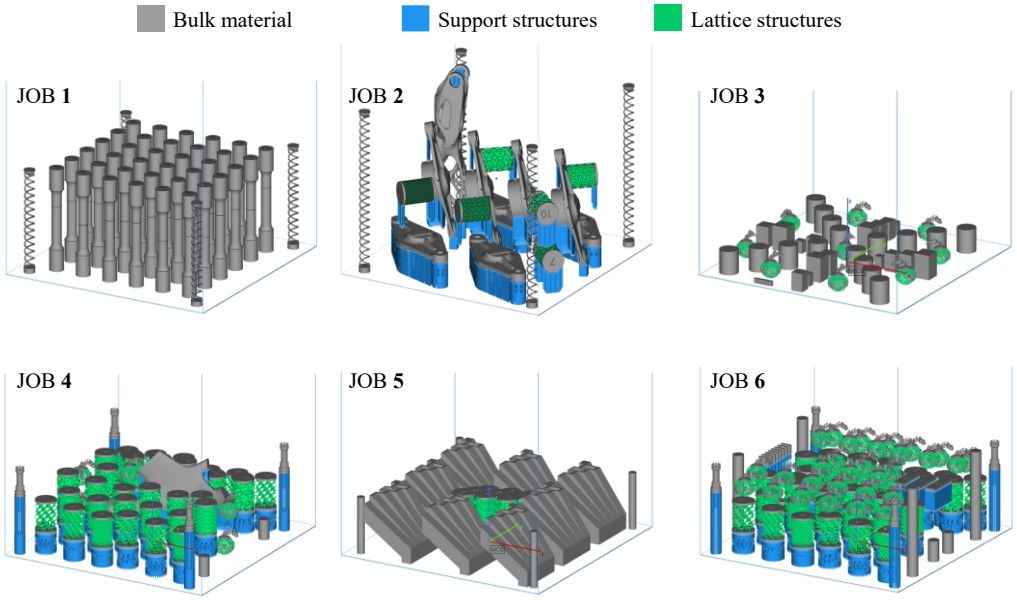

Figure 38. Designed JOB for the Arcam A2X.

JOB 1 shows only the melting of bulk material. JOB 3 was designed to study the presence of both bulk material and lattice structures. JOBs 2, 4, 5 and 6 were designed to analyse the effect of the presence of all the themes. Therefore, contrary to what has been done in the literature the bulk, support and lattice structures were all included. Considering JOB 2, it was designed to have the bulk and support materials only in the first part of the production. JOB 2 has replicas of the same component which were positioned in two different orientations. Replicas which were oriented at a certain angle with respect to the building direction are representative of a part that is orientated to reduce the support number and improve the chamber saturation. The horizontal position was chosen because it represents a component that is oriented in the worst orientation for the EBM process because a high number of supports needs to be included. Moreover, there is a great variation between the melted area and non-melted area (support) along the building direction. On the other hand, this orientation may be the best orientation from the dimensional and accuracy points of view. Table 11 shows the geometrical specifications of each JOB. The building height ranges between 26.82

mm (JOB 3) and 141.15 mm (JOB 2). The level of the used building volume was computed as the product between the start plate area and the height of the JOB. It tells about the overall amount of powder used during the process. The degree of saturation of the build volume (Table 11) is the ratio between the nominal volume (STL volume) and the total amount of powder provided during the JOB.

Parameter	Ti6Al4V
Yield Strength [MPa]	950
Ultimate Tensile Strength [MPa]	1020
Elongation (%)	14
Reduction of Area (%)	40
Modulus of Elasticity [GPa]	120
Density [g/cm^3]	4.43

Table 10. Main characteristics for Ti6Al4V powder provided from Arcam [29]**.**

The minimum degree of saturation considered in this study was about 4% for JOB 2 and the maximum was around 11% for JOB 3. Differences in the degree of saturation allow to analyse the effect of build height and nesting on the SEC values to be evaluated. Each JOB was prepared using Magics 21 and processed using Build Processor 2.0. The standard Arcam themes for Ti6Al4V were used. According to that, the layer thickness was set equal to 0.050 mm. The process parameters are summarised in Table 12. The average beam current was set to 30 mA. The beam current for the support is 5.5 mA. The JOB was produced on a standard start plate with 210×210 mm^2 dimensions.

Three main subphases can be distinguished according to the process description presented in Chapter 1: (1) vacuum generation, (2) the building phase and (3) the cooling phase. Process subphase (2) can be further subdivided into: (2.1) beam alignment, (2.2) start plate heating and (2.3) the printing phase. Arcam systems have a specific control that records all the outputs of all the sensors that are present in the machine and monitors the process. The outputs and their time history are saved in a log file. The log file and the Fluke acquisition were used to extract all the information about the times for the energy consumption calculation. Moreover, according to the electric scheme of Arcam EBM A2X, a decomposition of the machine architecture into its main subunits is carried out as follows: (i) base system of the machine, (ii) vacuum pumps, (iii) high voltage unit,

(iv) electron beam, and (v) rake and start plate. These units are incorporated in the EBM Arcam A2X machine, while a chiller unit is connected externally to the machine. The Arcam A2X EBM machine is powered by an AC three-phase system. The AC current clamps (one for each single AC phase and one for the neutral phase) and the voltage clamps were connected to the electricity supply wires on the EBM machine. The Arcam A2X EBM machine is powered by a current stabiliser, which cleans noises in the power grid and provides the current and voltage phasors with 120 degrees of mutual angular delay as well as a power factor of about 0.95 between the real power and the apparent power. The energy demand for each unit was obtained by the additional energy contribution required respect to a reference condition. In detail, the power demand of the base system of the machine was measured evaluating the machine on its standby condition.

JOB ID	JOB height [mm] *	Used building volume [cm^3]	Degree of saturation of the build chamber (%)	STL volume [cm^3] *	Bulk volume [cm^3] *	Support volume [cm^3] *	Lattice volume [cm^3] *
1	96.08	4237.3	7.75	328.6	328.6	0.0	0.0
2	141.15	6224.9	4.09	254.9	222.4	23.6	8.9
3	26.82	1182.7	11.26	133.2	132.5	0.0	0.7
4	83.27	3672.4	4.35	159.8	84.6	28.0	47.2
5	55.00	2425.5	8.50	206.2	189.7	4.9	11.6
6	87.04	3838.6	4.45	170.7	94.2	26.5	50.0

Table 11. Samples manufactured on the Arcam A2X. * Software estimations.

That measurement was also repeated during the cooling phase, which is characterised by only this machine subunit as well. Then the motor of the rake and the motor of the start plate were operated manually one per time. Their contributions were calculated by the differences between the total power demands and the one associated with the stand-by condition. After each JOB, these contributions were double-checked in the log file of the machine. The contributions were found to be constant along the building direction and throughout the JOBs. The total contribution due to the rake and the start plate motors was obtained by multiplying the obtained values for the number of the layers. To measure the contribution of the pumps, the pumps have been started up from the stand-by condition. The vacuum pumps contribution was quantified by

the difference between the overall energy demand during the vacuum generation phase and the one during the base system of the machine. Then, the high voltage unit was activated, and its contribution was calculated by the difference between the overall energy demand and the previously calculated. During the JOB, the remained energy demand quantity is the one associated with the electron beam.

Process parameter for the contour of the bulk						
Melting strategy	Scan speed [mm/s]	Focus Offset [mA]	Beam Current [mA]	Number of spots	Number of contours	Hatch contours [mm]
MultiBeam	850	6	5	70	3	0.29
Process parameter for the hatching for the bulk						
Melting strategy	Speed Function	Focus Offset [mA]	Beam Current Max [mA]	Reference Length [mm]	Reference Current [mA]	Line Offset [mm]
Continuous	45	25	20	45	12	0.2
Process parameter for the outer contour of the lattice						
Melting strategy	Scan speed [mm/s]	Focus Offset [mA]	Beam Current Max [mA]	Number of contours	Hatch contours	
Continuous	450	0	3	1	0.13	
Process parameter for the inner contour of the lattice						
Melting strategy	Scan speed [mm/s]	Focus Offset [mA]	Beam Current Max [mA]	Number of contours	Hatch contours	
Continuous	470	0	3	1	0.13	

Table 12. Process parameters for the melting phase of the EBM process.

3.1.3 Continuous Filament Fabrication

Table 13 lists the material properties of the investigated materials in this work, as provided from the technical datasheet by Markforged [84]. Four geometries were selected, respectively named as: “A” for the flange, “B” for the cube, “C” and “D” respectively for the first and the second tensile samples shown in Figure 39. Geometry “A” was chosen since it offers a high number of layers with large area, allowing a significant diversify for the extrusion path while changing the process parameters. Fixing all process parameters, the effect of the layer thickness was investigated, with a variation from 0.100 mm to 0.200 mm. Similarly, the effect of the perimeter number was investigated with geometry “A”, using 1, 2 and 4 concentric perimeters. The effect of the infill style and density was also studied with geometry “A”, since a rectangular solid fill was compared

with a hexagonal strategy (30% infill density). On the other hand, geometry "B" was selected to assess the effect of the part design, since it has a simpler geometry comparing with the others, allowing, for instance, a simpler extrusion path than that of geometry "A". All experiments conducted on "A" and "B" were produced with both PA6 and Onyx to study the effect of the matrix material. Geometry "C" was used to fully assess the effects of the infill strategy/density. More in detail, the three available infill styles on the Markforged Mark Two were considered (i.e., triangular, hexagonal and rectangular), while the infill density was varied from solid to 30%. As far as the experiments performed in this study are concerned, Table 14 summarises the investigated combinations of geometries and process parameters for the 3D printed not reinforced samples.

Parameter	PA6	Onyx	CF	Kevlar
Density [g/cm^3]	1.1	1.2	1.4	1.2
Tensile Modulus [GPa]	1.7 (ASTM D638)	1.4 (ASTM D638)	60 (ASTM D3039)	27 (ASTM D3039)
Tensile Stress at Yield [MPa]	51 (ASTM D638)	36 (ASTM D638)	-	-
Tensile Strain at Yield (%)	4.5 (ASTM D638)	25 (ASTM D638)	-	-
Tensile Stress at Break [MPa]	36 (ASTM D638)	30 (ASTM D638)	800 (ASTM D3039)	610 (ASTM D3039)
Tensile Strain at Break (%)	150 (ASTM D638)	58 (ASTM D638)	1.5 (ASTM D3039)	2.7 (ASTM D3039)
Heat Deflection Temp [°C]	41 (ASTM D648 B)	145 (ASTM D648 B)	105 (ASTM D648 B)	105 (ASTM D648 B)

Table 13. Main characteristics for the materials provided from Markforged [84]**.**

Specimens "D" were used to address the effects of fibre deposition in terms of energy and time demands. The "D" specimens were fabricated with a single reinforced layer which was designed to be in the central layer of the specimen. Additionally, to fully assess the energy requirements of the fibres deposited by the 3D printer Mark Two, the reinforcement filament was deposited in six orientation: (a) 0 degrees, (b) 15 degrees, (c) 30 degrees, (d) 45 degrees, (e) 60 degrees and (f) 90 degrees. According to the Markforged setting, the "D" samples reinforced with CF were printed with a layer thickness equal to 0.125 mm while it was set equal to 0.100 mm for those reinforced with Kevlar. The fibre path deposition was set to isotropic, a single perimeter and the solid infill were selected for the PA6 matrix (Table 15). Geometry "D" was also printed without the fibre layer, to have a reference for the energy demands of the reinforced samples (Table 14). Therefore,

a layer thickness of 0.125 mm was considered as reference for the CF samples, while 0.100 mm was used for the Kevlar ones. Table 14 and Table 15 list the volume estimations for the printed samples.

The CAD file of the selected geometries was processed by Markforged Eiger, the proprietary software. During the JOB preparation, the user can set the path deposition style for the fibre (isotropic or concentric), the reinforcement filaments, the fibre's orientation, the number of layers to be reinforced and where. Similarly, it is possible to decide the infill style (triangular, hexagonal and rectangular) and density for the matrix. The path deposition also includes the number of perimeters, which are printed concentric to each other and using the matrix filament.

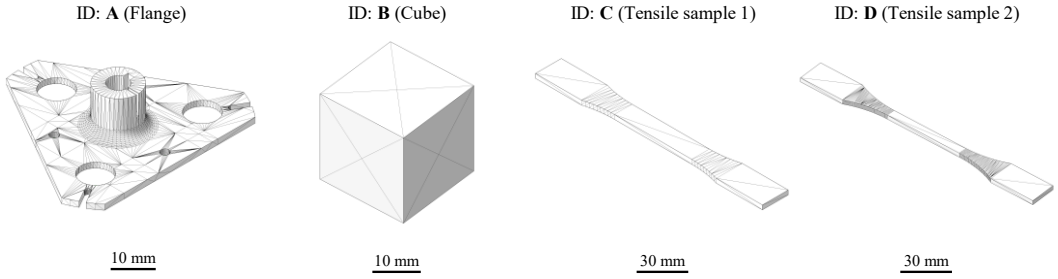

Figure 39. Selected geometries for the Markforged Mark Two.

JOB ID	Geometry ID	Infill strategy	Infill density	Perimeter number	Layer thickness [mm]	Matrix material	Matrix volume [cm^3] *
1	A	Rect.	Solid	1	0.200	PA6	5.48
2	A	Rect.	Solid	1	0.100	PA6	5.39
3	A	Rect.	Solid	4	0.100	PA6	4.87
4	A	Rect.	Solid	2	0.100	PA6	5.23
5	A	Hexagonal	30%	1	0.100	PA6	2.18
6	A	Rect.	Solid	1	0.200	Onyx	5.75
7	A	Rect.	Solid	1	0.100	Onyx	5.70
8	A	Rect.	Solid	4	0.100	Onyx	5.34
9	A	Rect.	Solid	2	0.100	Onyx	5.48
10	A	Hexagonal	30%	1	0.100	Onyx	2.27
11	B	Rect.	Solid	1	0.200	PA6	15.98

12	B	Rect.	Solid	1	0.200	Onyx	16.10
13	C	Rect.	Solid	2	0.125	Onyx	8.61
14	C	Rect.	80%	2	0.125	Onyx	7.82
15	C	Rect.	50%	2	0.125	Onyx	6.33
16	C	Rect.	30%	2	0.125	Onyx	5.37
17	C	Hexagonal	50%	2	0.125	Onyx	4.87
18	C	Hexagonal	30%	2	0.125	Onyx	4.61
19	C	Triangular	50%	2	0.125	Onyx	6.33
20	C	Triangular	30%	2	0.125	Onyx	5.41
21	D	Rect.	Solid	1	0.125	PA6	7.24
22	D	Rect.	Solid	1	0.100	PA6	7.13

Table 14. Not reinforced samples manufactured on the Markforged Mark Two. * Software estimations.

Geometry "D"	CF reinforced samples			Kevlar reinforced samples		
Fibre direction (degrees)	JOB ID	PA6 matrix volume [cm^3] *	Fibre volume [cm^3] *	JOB ID	PA6 matrix volume [cm^3] *	Fibre volume [cm^3] *
0	23	7.48	0.22	29	7.35	0.18
15	24	7.50	0.21	30	7.36	0.18
30	25	7.50	0.21	31	7.36	0.18
45	26	7.50	0.21	32	7.36	0.18
60	27	7.49	0.21	33	7.35	0.17
90	28	7.49	0.21	34	7.35	0.17

Table 15. Reinforced samples manufactured on the Markforged Mark Two. * Software estimations.

According to the process description given in Chapter 1, the CFF process can be divided in the same subphases highlighted of the FDM process: (1) switch-on, (2) idle #1, (3) heating and calibration, (4) printing and (5) idle #2. However, the Markforged Mark Two does not have a heated build chamber. Therefore, subphase (3) aims to heat the extruders and calibrate the axes. A decomposition of the machine architecture into its main subunits is possible as follows: (i) base system of the machine and (ii) extruder heaters and axes.

The energy analyser and the Mark Two machine are visible in Figure 40. The studied machine is powered by an AC single-phase system. The AC current

clamps (one for the single AC phase and one for the neutral phase) and the voltage clamps were connected to the electricity supply wires of the Markforged Mark Two. The power factor of about 0.97 between the real power and the apparent power was observed during the printing phase. The power demand of the base system of the machine was measured evaluating the machine on its standby condition. The computed power value of subunit (i) was subtracted to the average power demand of the printing subphase to obtain that of subunit (ii). This methodology was applied due to the impossibility to disassemble the machine into its subunits and to power them one by one.

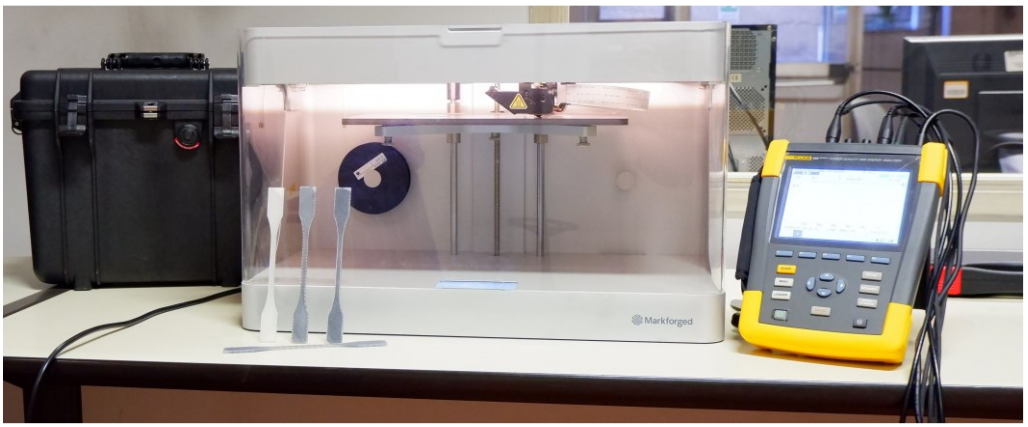

Figure 40. Experimental setup and additively manufactured components on the Markforged Mark Two.

3.2 Results

This paragraph presents the results of the conducted experiments on the three AM machines. First, for each machine a description of the process is given showing the acquisition of a significative experiment. The power acquisition is shown for the Arcam A2X. On the other hand, the current acquisition is shown for the Stratasys F370 and the Markforged Mark Two because their power profile does not highlight properly every detail (due to the low energy demand of the machine subunits). Then, the energy demand of every subphase is reported for all the 3D printed samples as well as the printed mass values and all the time windows.

3.2.1 Fused Deposition Modelling

Figure 41 plots an example of the current profile considering JOB 3 from the subphase (1) to the subphase (5). In Figure 41 the first variation in the current

profile is due to the switching on of the electronic parts. In the subphase (2) the machine waits for the upload of the file containing the information regarding the JOB path and the order of the operator to start the process. In this phase only the machine subunit (i) is powered, and a constant power demand of 30 W is observed. In the subphase (3) the machine heats the chamber up to the process temperature, which is related to the material being printed.

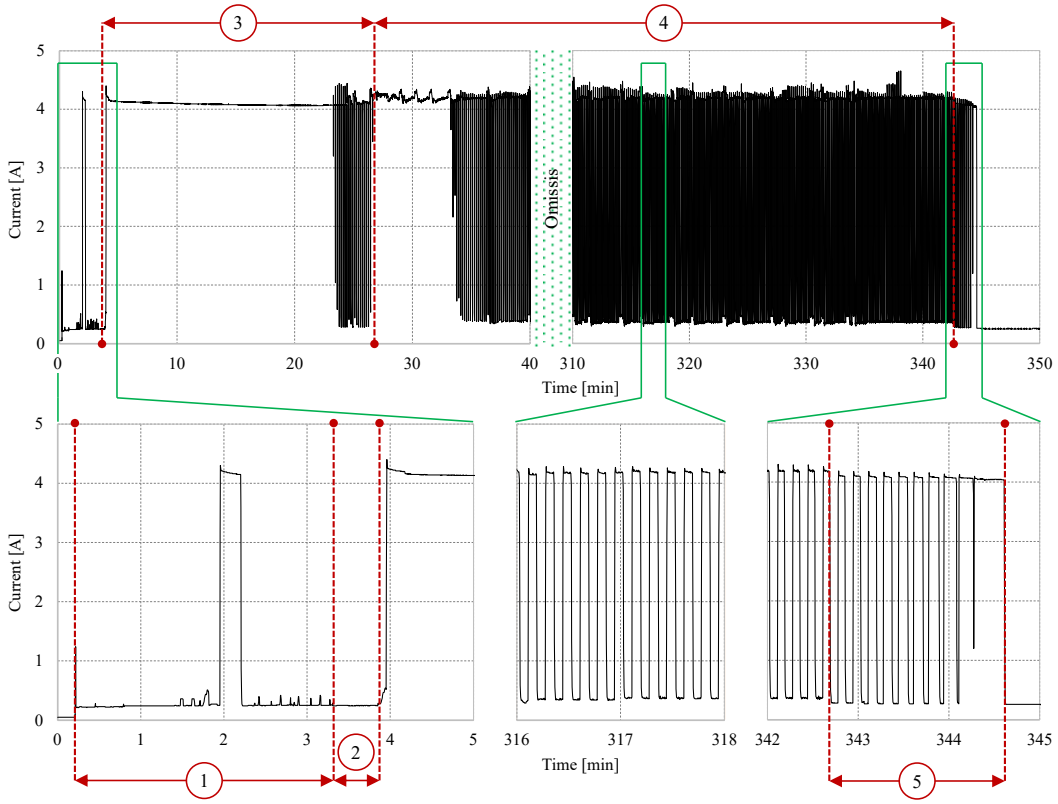

Figure 41. Data acquisition and identification of the main process subphases for the Stratasys F370 (JOB 3).

The power demand is almost constant during the entire phase to a value of 850 W for both materials. However, once the temperature of the build chamber is close to the target one for the given material, the heating system is powered with a duty cycle. At the same time, the calibration of the axes and extruders starts. In the subphase (4) the component and its support structures are deposited. Initially a base is created to attach the part to the start plate. As visible from Figure 41, in this earlier sub-phase, the heating system of the chamber is continuously powered. Then, almost the entire subphase (4) is characterised by a typical duty cycle, as detailed in Figure 41, and the energy consumption is mainly due to the chamber heating. The duration of the subphase (4) depends on the dimensions and on the

complexity of the JOB. The subphase (5) starts when the last layer of the build is completed. The build chamber is kept at the process temperature during subphase (5), until the machine receives a command from the operator who confirms that the JOB is removed from the table. An overall average power demand of 476 W is computed during this phase for both materials. This value is due to the constant power demand of machine subunit (i), which is 30 W, and to that of the subunit (ii), computable as difference between these two values. After that command, the machine returns into its stand-by mode (with the same power demand of the subphase (2)). The differences in the maximum and minimum values of the duty cycles of subphase (4) and (5), which are highlighted by a detailed view in Figure 41, also allow to quantify the contribution to the total power demand due to the machine subunits (ii) and (iii).

Sample characterisation

The process time and the energy consumption were quantified per each JOB and each process subphase. As visible in Table 16, the contributions due to the not productive subphases can be considered as constant.

Subphase		Process time [min]	Energy consumption [Wh]
(1) Switch-on		3.2	5.4
(2) Idle #1		1.5	0.9
(3) Heating and calibration	ABS	23.0	319.1
	PC-ABS	25.8	356.3
(5) Idle #2		1.5	11.9

Table 16 Time and energy demand for phases (1), (2), (3) and (5) for the Stratasys F370.

JOB ID	t_4 [min]	E_4 [Wh]	Part mass [g]	Support mass [g]
1	1380.9	10931.8	25.5	126.0
2	242.4	2045.0	13.5	16.7
3	315.7	2666.7	18.5	26.0
4	100.0	859.6	12.6	8.9
5	105.1	912.0	16.3	8.9

6	162.2	1399.0	31.2	13.5
7	69.6	630.3	42.5	15.6
8	170.0	1439.7	43.5	13.5
9	71.3	613.0	48.3	15.6
10	200.3	1658.8	50.6	13.5
11	71.6	613.6	53.3	15.6
12	383.8	3218.4	62.0	47.8
13	1403.1	11730.4	26.4	126.0
14	216.8	1914.5	12.6	16.7
15	284.8	2466.2	15.9	26.0
16	80.7	727.0	10.6	8.9
17	89.4	841.9	17.1	8.9
18	115.9	1025.0	27.4	13.5
19	68.4	634.0	41.3	15.6
20	139.8	1230.8	38.6	13.5
21	72.3	698.0	54.5	15.6
22	144.0	1272.4	51.3	13.5
23	72.1	670.9	57.1	15.6
24	365.4	3202.3	65.7	47.8

Table 17. Printing phase: energy, time and mass results for samples manufactured on the Stratasys F370.

The duration and the energy demand of subphase (3) are a function of the printed material, due to the different operating temperature of the build chamber (as detailed in Table 8). Moreover, the subphases (2) and (5) rely on the operator, who has to provide a manual command to the FDM machine to proceed. In this work, a constant time of 1.5 min was considered for both phases, based on the experimental evidence. The only subphase which is dependent on the component being manufactured is the printing subphase, as visible from Table 17. The measured masses of each produced JOB are also reported in Table 17. The results are presented by separating the contributions of the component material and the support material to the total mass, including the amount due to the purge part. As

visible from Table 17, the mass of the support structures (a) does not vary if the deposited material or the infill strategy are changed, (b) is affected by the layer thickness, (c) increases while increasing the geometrical complexity of the component and its plan projection. Component "A" requires structures to support the branched geometry for more than 80% of the total JOB weight. On the other hand, component "F", despite its reduced complexity, needs a significant amount of support material (higher than 40% of the total weight) to create the large base. The masses of the ABS components are not always lower than those of the PC-ABS ones (as shown in Table 17), even when adopting the same infill strategy and layer thickness to produce the same geometry. Such differences can be traced back to the deposition path of the extruders.

For the sake of clarity, Figure 42 compares (for both the ABS and PC-ABS materials) some deposition paths for component "B".

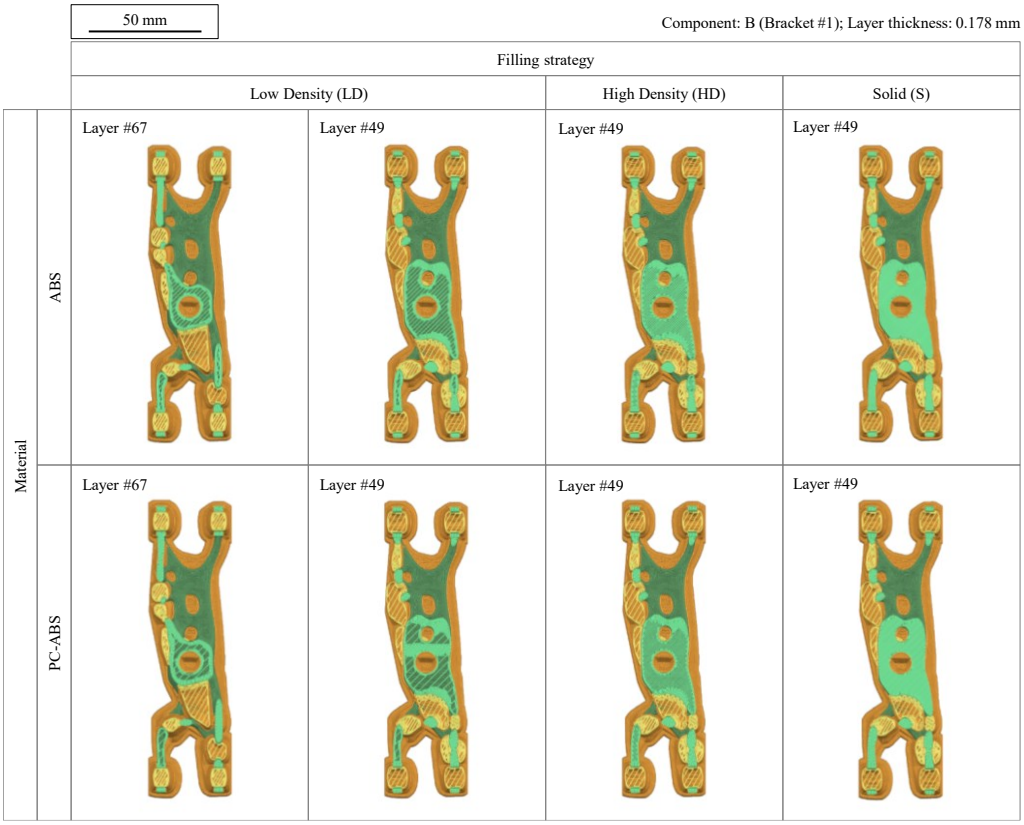

Figure 42. Infill strategies as a function of the component material computed with the GrabCAD Print software.

The deposition paths for the QSR material (drawn in yellow colour) do not change while varying the process parameters. On the other hand, once the (LD,

HD or S) infill strategy is chosen, the GrabCAD Print software computes, for the same layer, different paths for ABS or PC-ABS (drawn in green colour). This difference is more evident for the "LD" infill strategy, while the extruders' paths become comparable when a denser infill strategy is selected. As far as the results for component "E" are concerned (Table 17): (a) when the "S" infill strategy is selected, the mass of the ABS part is lower than that of the PC-ABS one, for both the layer thicknesses, according to the slight differences in the specific material densities; (b) when the "LD" infill strategy is used, the mass of the ABS parts is higher for both the layer thicknesses, due to the tightened deposition path elaborated by the software. In general, the final mass of a printed component is influenced from the extruders' paths, which in turn are influenced by the layer thickness, infill strategy and kind of deposited material.

3.2.2 Electron Beam Melting

The power profile of JOB 1 is shown in Figure 43.

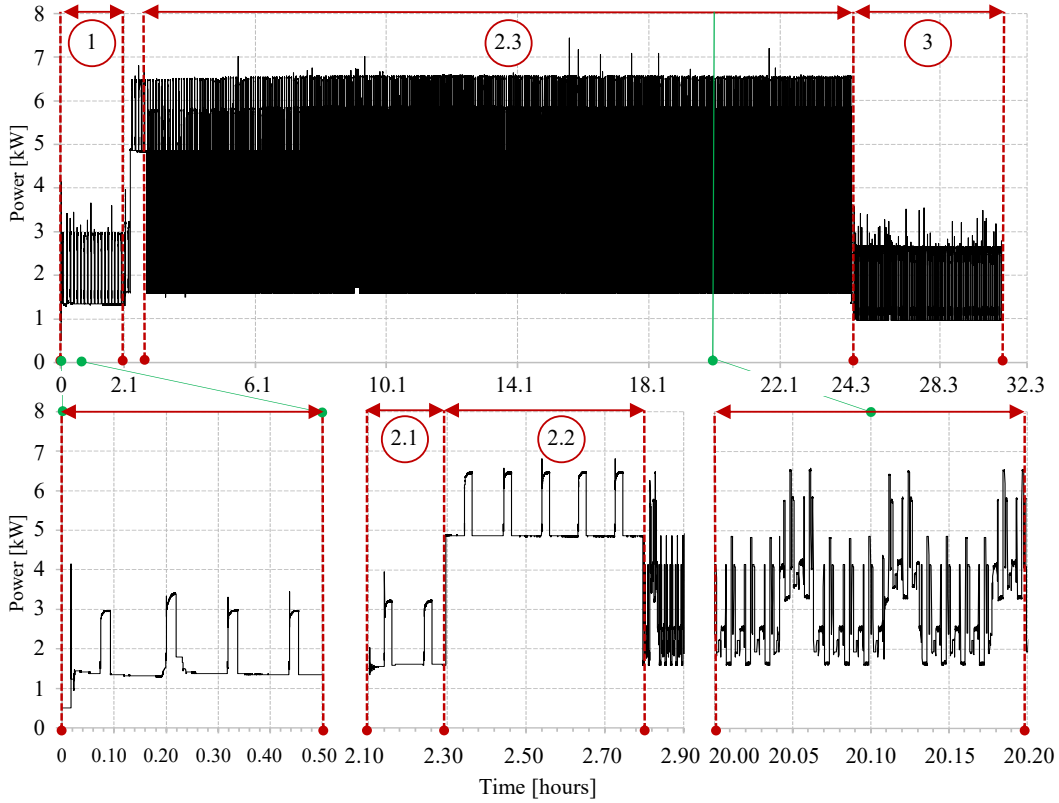

Figure 43. Data acquisition and identification of the main process subphases for the Arcam A2X (JOB 1).

In Figure 43, the chiller unit acquisition was added to that of the EBM machine for the entire process, from subphase (1) to subphase (3). The chiller is characterised by a duty cycle that ranges from 0.45 kW to 2 kW. The duration of the lower and upper power levels depends on the machine condition. Therefore, the average power was computed for each process subphase. The measured average chiller power demand for process subphase (1) was 720 W, while a value of 1000 kW was computed for process subphase (2) due to the higher heat flow produced during the melting procedures. A slight lower power (920 W) was registered during the cooling subphase.

Process subphase (1): Vacuum generation

The vacuum generation subphase starts with the machine set to the idle condition. The relative machine power demand due to the base systems of the machine (i) is 510 W. The operator then begins the vacuum generation procedure, which needs to be manually started. Figure 43 shows a rise in the power demand after about one minute, which is due to the power initialisation of the two vacuum pumps. After their transitory phase, the power demand of machine subunit (ii) stabilises at 390 W. Table 18 displays the time and the overall energy (i.e., also considering the chiller system) needed to reach a vacuum condition that is suitable to switch on the EB.

The differences in time can mainly be attributed to the amount of powder in the hoppers for the JOB that has to be manufactured and the amount of residual powder in the hoppers from the previous JOB.

JOB ID	Process time [h]	Energy demand [MJ]
1	2.1	12.2
2	1.3	7.3
3	1.7	9.9
4	1.1	6.2
5	1.6	9.1
6	1.0	5.9

Table 18. Process time and energy demand results for the vacuum generation process of the Arcam A2X.

Process subphase (2): Build process

Once the machine reaches the vacuum pressure, the power demand is around 900 W, which is given by the sum of machine subunits (i) and (ii). A value of 720 W needs to be added due to the chiller. The electron beam needs a manual procedure to be switched on and this is carried out during process subphase (2.1). The machine activates the high voltage unit (iii) which requires a delta power of 230 W, as shown in Figure 43. Once beam alignment is achieved, process subphase (2.2) can start. Moreover, the electron beam subunit (iv) is activated during subphases (2.1) and (2.2) with a power demand that depends on the specific action of the moment. For instance, during process subphase (2.2), the electron beam is powered up to 3.3 kW to provide the necessary heat to the build table. Table 19 reports the time and energy demand of process subphases (2.1) and (2.2), considering the contribution of the chiller. These phases are not influenced by the JOB being manufactured since they are related to the internal procedures of the EBM Arcam A2X machine and control system.

Subphase	Process time [min]	Energy consumption [MJ]
(2.1) Beam alignment	12.1	1.6
(2.2) Start plate heating	30.0	9.7

Table 19. Process time and energy consumption of the subphases (2.1) and (2.2) of the Arcam A2X.

The lower central area of Figure 43 shows details of process subphase (2.3) for the realisation of several layers together with the duty cycle of the chiller. On the other hand, Figure 44 shows the machine power demand during the printing phase for JOB 3 during the manufacturing of three subsequent layers without the presence of the chiller. The orange, blue and yellow line respectively depicts the power demand of machine subunit (i), (ii) and (iii). As described above, their power demand is constant. The power profile for the electron beam (iv) (green line) depends on the specific action. The rake and start plate profiles are depicted in red and purple, respectively. The first peak indicates the start plate movement. The three subsequent hills that indicate the three rake movements from one side to the other side to distribute the correct amount of powder onto the previous layer can be seen between each layer. The time necessary to distribute the powder is about 11 seconds for each layer. The rake and start plate power demands are negligible, compared with those of the other machine subunits. However, an

overall energy demand of 0.97 kJ was considered in this work regarding the machine subunit (v) for each layer. The energy demand for the single movement of the start plate is around 30% of that of the rake. Machine subunits (iv) and (v) are powered alternatively when the beam is melting and during the powder distribution. The trend of the electron beam machine subunit can be further specified by evaluating each melting step, considering JOB 3 in Figure 45. As mentioned in Chapter 1, the following steps can be observed for each layer during the EBM process: (a) first preheating, (b) second preheating, (c) contouring, (d) melting, (e) support melting and (f) postheating/cooling.

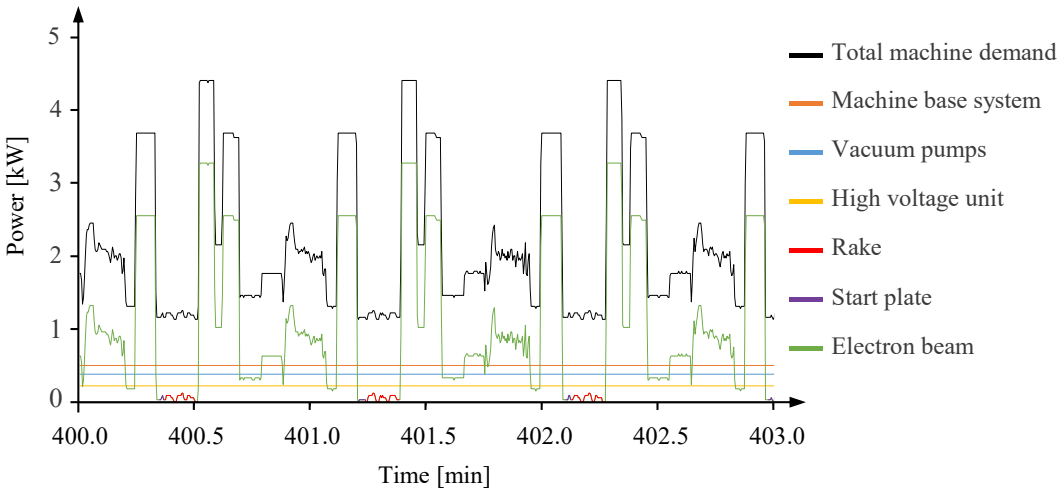

Figure 44. Printing phase: data acquisition and identification of the different machine subunits for the Arcam A2X (JOB 3).

During phase (a), a large amount of power is required to heat the preheating area. As in process subphase (2.2), the electron beam is highly defocused and a high amount of power of about 3.3 kW is required. However, a low amount of specific energy is involved in the process because only the sintering of the powder is performed. Phase (b) requires a power demand of 2.5 kW, but only for selected areas on the layer. The duration of this phase appears to depend on the dimension of the subsequent melted area. The necessary specific melting energy is given during phases (c)-(e). The contour consists of two different contours that are melted with the MB strategy. The power demands generally required for the first and second contour strategies can be assumed constant and equal to 0.34 kW and 0.64 kW, respectively (Figure 45). The duration of phase (c) depends on the total length of the perimeters. The melting phase (d) consists of the melting of the bulk area or lattice structures according to the CAD file. The power demand for phase

(d) ranges from 0.6 to1.4 kW for the bulk theme. The Arcam A2X control system adjusts the power in order to provide a constant average amount of heat to each layer section being melted. The constant power demand of 0.19 kW is required for the lattice structure, as can be seen in Figure 45. The duration of phase (d) depends on the extension of the overall melted layer area. The support structures are melted during phase (e), with a constant power of 0.37 kW (not shown in Figure 45). The duration of this phase is related to the number of supports in the layer. Finally, the post heating or cooling balances the total heat amount provided for each layer. Therefore, the time and power demand of this phase depend to a great extent on the design of the part and the JOB (orientation and number of supports). Table 20 reports the time and energy (including the chiller consumption) demand due to subphase (2.3).

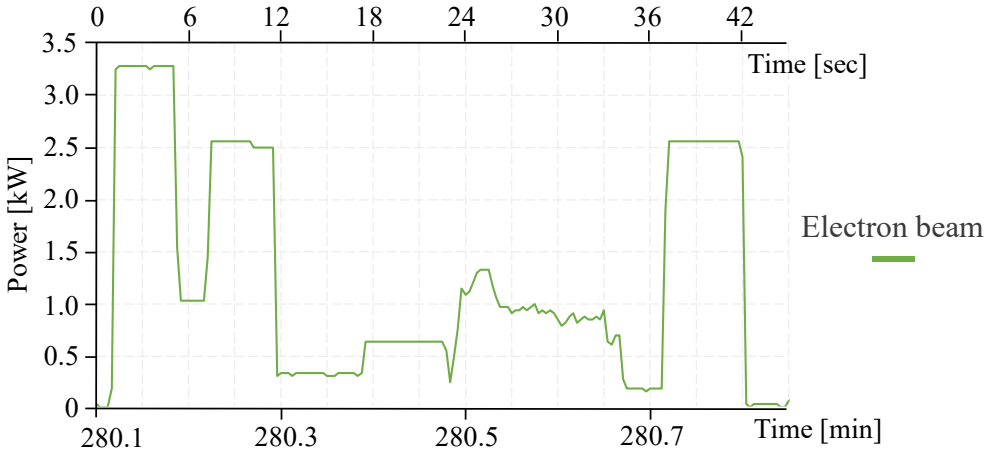

Figure 45. Printing phase: data acquisition of the electron beam and identification of the layer production subphases (JOB 3).

JOB ID	Process time [h]	Energy demand [MJ]
1	21.6	248.0
2	29.5	332.4
3	7.6	87.7
4	23.8	277.2
5	18.2	210.6
6	25.0	290.5

Table 20. Process time and energy demand results for the printing phase of the Arcam A2X.

Process subphase (3): Cooling

As can be seen in Figure 43, once the JOB is completed, the power demands drop because the electron beam, the rake and start plate unit and the vacuum pumps are no longer powered. Only the energy consumption for the machine electronics and the chiller can be observed in this subphase. Table 21 presents the time and the energy needed for each JOB to reach a temperature of 80 °C, which is the target temperature necessary to unload the built JOB. Table 21 shows that the energy demand mainly depends on the part and manufacturing designs. In detail, the most relevant factor is the JOB height. However, JOB 1 and JOB 2 have the same cooling time but different build heights. This difference can be explained considering the total amount of melted material, which is higher for JOB 2 and may, therefore, lead to a higher temperature in the chamber and a longer cooling time.

JOB ID	Process time [h]	Energy demand [MJ]
1	6.8	34.9
2	6.8	34.9
3	2.2	11.9
4	6.1	31.3
5	5.7	29.4
6	6.5	33.2

Table 21. Process time and energy demand for the cooling phase of the Arcam A2X.

3.2.3 Continuous Filament Fabrication

The realisation of the CF 15 degrees reinforced sample (JOB 24) is used as example in Figure 46 to report the current acquisition during the production cycle. For sake of clarity the acquisition during the subphases (1) and (2) is highlighted at the left bottom side of Figure 46. The initial peak is related to the first power on of the machine during subphase (1). After that, the machine starts its standby mode (2). A duration of 1.5 min is kept as reference for subphase (2) of all samples, based on the practical experience. Once the subphase (3) begins, the machine heats the matrix and fibre extruders to the process temperatures. At this stage, the power demand rises from about 10 W to 110 W. Once the temperature

of the extruders reaches the targets (green vertical line) the start plate rises until it reaches the extruder heads (blue vertical line). Then the matrix extruder deposits the purge tape along the major side of the start plate. The deposition of the first layer lasts longer than the others to help the adherence of the part on the start plate.

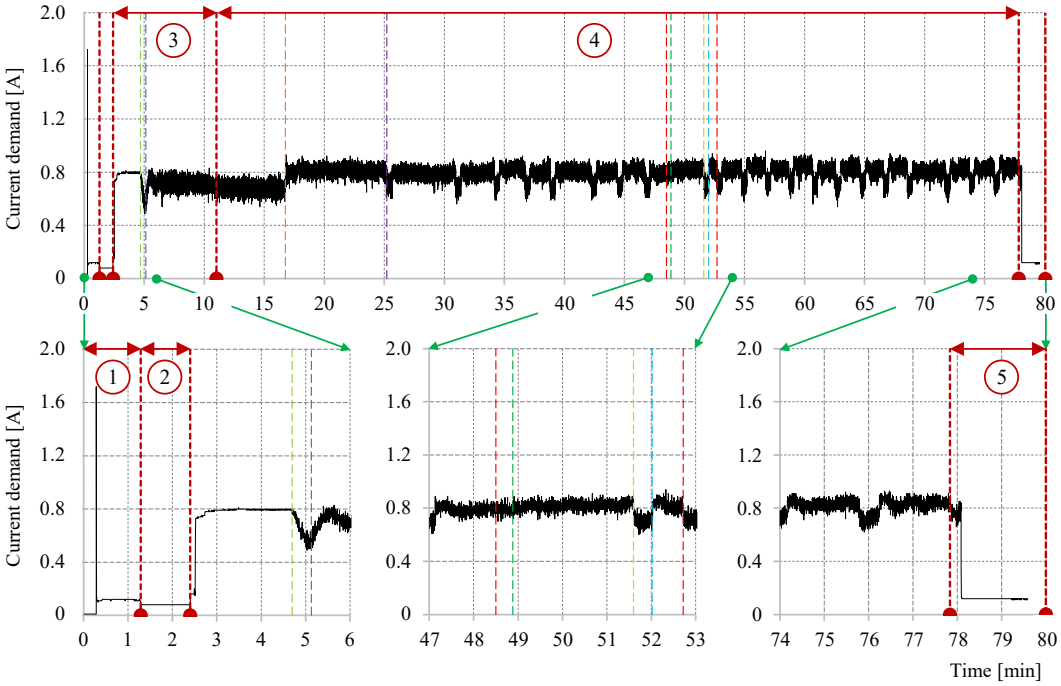

Figure 46. Data acquisition and identification of the main process subphases for the Markforged Mark Two (JOB 24).

On the other hand, the time needed to deposit layers 2, 3 and 4 occur between the orange and the purple vertical lines. This difference is due to the minor velocity of the extrusion system and of the axes during the first layer. This aspect it is also visible in the current profile as well as in that of the power. In fact, the range of 60-90 W is observed for the first layer, while a range of 90-120W is present during the layers 2, 3 and 4. The 5th layer starts after the purple vertical line. From this point, there is an alteration on the deposition velocities of perimeter and area and therefore a difference in the current demand is present. In fact, from Figure 46 it is clearly visible the alternation between the layers. The current demand for the reinforced layer is highlighted in the bottom central area of Figure 46. Initially the deposition of the corner purge layer occurs, with an average duration of 14 sec (until the green vertical line). Then, the fibre is deposited (between the green and the yellow vertical lines). Finally, the deposition

of PA6 occurs, first along the perimeter (between the yellow and the cyan vertical lines) and then in the gaps (from the cyan vertical line until the red one). A higher current demand is visible for the deposition of the corner purge part, as well as for that of the fibre and for the PA6 filling. After the fibre layer a quick alternation between perimeter and area deposition occurs, due to the end of the corner purge part (see Figure 46). The details of the idle time II (5) are visible in the right bottom side of Figure 46. When the print of the sample ends, the start plate reaches the stand-by position in about 10 sec. At this point the extrusion system stops to be powered and the machines remains is this idle condition until the next order. A reference value of 1.5 minutes was used for subphase (5), which are needed from the operator to remove the 3D printed part and to clean the start plate from the initial glue stick. The production cycle of the Kevlar-reinforced samples follows the same profile highlighted in Figure 46 for the CF case.

Sample characterisation

Once the material being printed is fixed, the process windows (1), (2), (3) and (5) show the same time and energy demands for each experiment since these phases are characterised from repetitive operations with equal power profile. Table 22 reports these values for the different studied materials. On the other hand, the results for the printing subphase vary for each experiment. The results for the samples additively manufactured by using the matrix materials only summarised in Table 14 are reported in Table 23 in terms of printing time (t_{Matrix}), printing energy (E_{Matrix}) and printed mass (m_{Matrix}). Considering the reinforced samples (as shown in Table 15), the time to print the entire matrix material (t_{Matrix}) (i.e., the matrix of the sample and that of the purge corner part) and the time to deposit the fibre (respectively t_{CF} for the CF and t_K for the Kevlar reinforcement) are reported in Table 24.

The relative energy demands are reported in Table 24 as well, considering E_{Matrix} as the energy to print the entire matrix material (i.e., the matrix of the sample and that of the purge corner part), and E_{CF} and E_K respectively for the energy needed to deposit the CF and the Kevlar reinforcement. The sum of the two time contributes (i.e., t_{Matrix} and $t_{CF(K)}$) gives the total printing time (t_4). Similarly, the sum of the two energy contributes (i.e., E_{Matrix} and $E_{CF(K)}$) gives the total printing energy demand (E_4). The contribution of the reinforcement in term of mass ($m_{CF(K)}$) is computed using the nominal density provided by the

Markforged's datasheet and volume estimated by Markforged Eiger (see Table 13 and Table 15).

Sample		Time [min]	Energy Demand [Wh]
(1) Switch-on		1.0	0.0 *
(2) Idle #1		1.5	0.3
(3) Heating and calibration	Only PA6	8.4	13.5
	Only Onyx	8.4	14.0
	Fibre reinforced	8.6	14.2
(5) Idle #2		1.5	0.3

Table 22. Time and energy demand for phases (1), (2), (3) and (5) for the Markforged Mark Two. * This value was computed equal to 0.01 Wh, however, only the significant digits were reported.

JOB ID	t_{Matrix} [min]	E_{Matrix} [Wh]	m_{Matrix} [g]
1	37.6	62.1	5.2
2	66.3	109.2	4.9
3	71.7	113.1	5.1
4	68.7	111.1	4.8
5	41.0	65.3	2.1
6	38.4	67.9	5.3
7	67.4	118.4	5.3
8	74.3	124.1	5.3
9	70.5	121.6	5.2
10	41.7	70.3	2.3
11	70.7	119.7	16.1
12	71.6	128.5	15.9

13	71.0	112.0	9.1
14	65.5	102.5	8.3
15	55.2	86.5	6.8
16	48.8	77.0	5.7
17	49.8	77.9	5.2
18	45.5	72.4	4.9
19	55.8	87.2	6.7
20	49.4	77.1	5.8
21	61.0	102.3	7.4
22	72.8	121.2	7.4

Table 23. Printing energy, time and mass for not reinforced samples manufactured on the Markforged Mark Two.

Fibre direction (degrees)	CF reinforced samples					Kevlar reinforced samples				
	JOB ID	t_{CF} [sec]	E_{CF} [Wh]	t_{Matrix} [min]	E_{Matrix} [Wh]	JOB ID	t_{K} [sec]	E_{K} [Wh]	t_{Matrix} [min]	E_{Matrix} [Wh]
0	23	163	5.3	62.9	115.7	29	161	5.1	75.5	137.5
15	24	163	5.2	63.0	113.6	30	163	5.2	75.6	140.3
30	25	175	5.5	63.0	112.3	31	179	5.8	75.6	139.4
45	26	190	6.1	63.0	116.4	32	190	6.0	75.6	138.5
60	27	199	6.0	63.0	111.0	33	200	6.4	75.6	139.7
90	28	208	6.7	63.0	116.2	34	209	6.6	75.6	138.8

Table 24. Printing energy and time for reinforced samples manufactured on the Markforged Mark Two.

Fibre direction (degrees)	CF reinforced samples				Kevlar reinforced samples			
	JOB ID	m_{Sample} [g]	m_{Matrix} [g]	m_{CF} [g]	JOB ID	m_{Sample} [g]	m_{Matrix} [g]	m_{K} [g]
0	23	7.6	7.5	0.3	29	6.9	6.9	0.2
15	24	7.7	7.6	0.3	30	7.2	7.2	0.2
30	25	7.6	7.5	0.3	31	7.3	7.3	0.2
45	26	7.6	7.5	0.3	32	7.4	7.4	0.2
60	27	7.6	7.5	0.3	33	7.5	7.5	0.2
90	28	7.6	7.5	0.3	34	7.6	7.6	0.2

Table 25. Printing mass results for reinforced samples manufactured on the Markforged Mark Two.

The mass of the total printed matrix for the reinforced samples (m_{Matrix}) takes into account not only the matrix of the reinforced sample itself, but also the mass of the corner purge tape (m_{Corner}). The latter value is equal to 0.2 g for all the Jobs detailed in Table 15. On the other hand, the mass of the reinforced samples

(m_{Sample}) is given by the sum of the matrix of the reinforced sample itself and that of the relative reinforcement (i.e., m_{CF} or m_K), as reported in Table 25.

The total printed mass is here and after defined as "m_{JOB}". This value is computed by the sum of "m_{Matrix}", "m_{Corner}" and "m_{CF}" (or m_K) for the reinforced samples. On the other hand, it corresponds to "m_{Matrix}" and "m_{Sample}" for the samples additively manufactured by using the matrix materials only.

Figure 47 shows the deposition path in the CF reinforced layer of geometry "D" at different orientation extracted from Markforged Eiger. The white line represents the deposition of the matrix filament, while the blue line is the CF reinforcement filament. The number of head inversions during the deposition of the reinforcement depends on the fibre orientation. Since the fibre is deposited in continuous, the empty areas are filled subsequently with PA6. The deposition path is independent from the fibre material. Therefore, the same paths are found for the Kevlar reinforced layer of geometry "D".

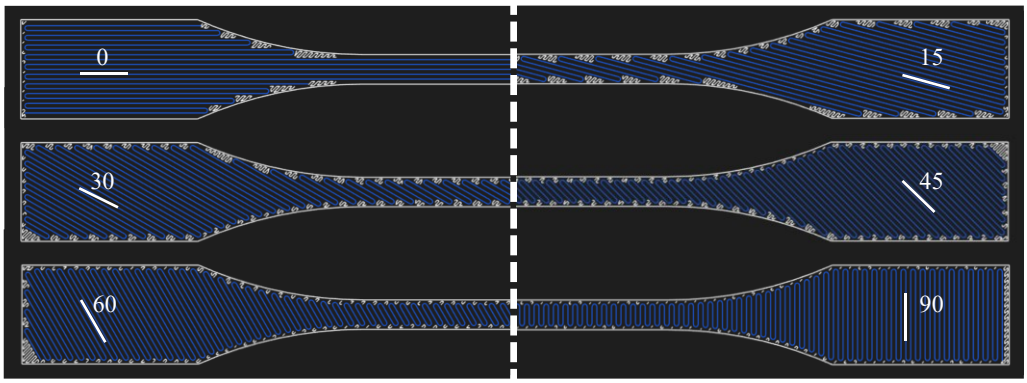

Figure 47. Extruder path for the CF layers of geometry "D" for the different inclinations.

3.3 Discussion

This paragraph presents models to predict the energy demands of AM machines. The three investigated technologies are used as case studies. The different studied processes were initially decomposed into substeps and a bottom-up approach is adopted to provide models for the energy evaluation of each subphase of the process as well as for a characterisation of the unit process level energy. An innovative empirical model for the assessment of the time and energy efficiency of the AM technology is developed. Finally, the main subunits of the different AM machines are isolated, and the relative energy demand is computed.

3.3.1 Fused Deposition Modelling

The printing phase depends on the component being printed and on the process parameters. All the experimental results highlight a linear correlation between the energy demand for the printing phase (in MJ) and the printing time (in min), as shown in Figure 48. As visible in Figure 41, the power profile versus the printing time shows a typical duty cycle. It can be approximated by means of constant average power demand. Therefore, the higher the printing time is, the higher the energy consumption. Overall, the total energy consumption of the FDM process (E_{FDM}, in MJ) can be computed according to Eq. 4. The values of the "a" coefficient were calculated by means of MATLAB R2019a software and are listed in Table 26. The coefficient value for PC-ABS is slightly higher than that for ABS, and this is due to the different extrusion temperatures (declared in Table 8).

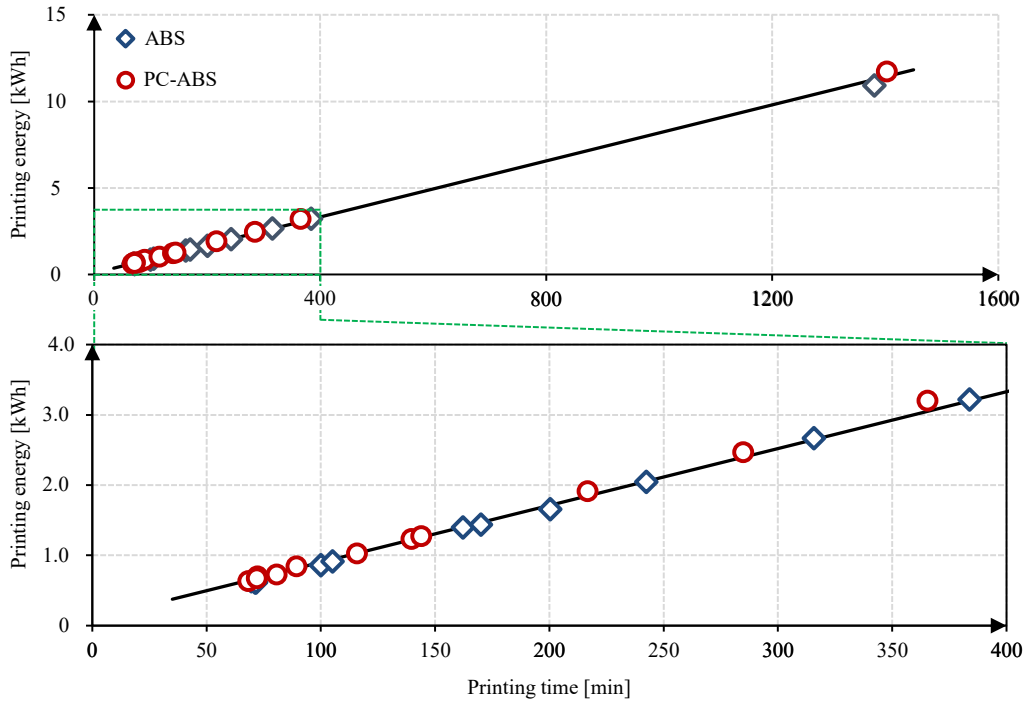

Figure 48. Printing phase: correlation between energy and time for the Stratasys F370.

Figure 49 shows the printing energy demand and the total mass of the deposited materials (i.e., including component, support structures and purged filaments) connected to the information regarding the process parameters (see Table 9). As far as the power demand of the process subphase (4) is concerned, negligible differences can be noticed for the deposition of the component or of the

QSR material. Therefore, the total deposited mass (m_{tot}) is considered in the following discussion. The supports cover from the 83% of the total printed mass in case of component "A" to the 21% in case of component "E".

$$\textbf{Eq. 4} \qquad \mathbf{E_{FDM} = E_1 + E_2 + E_3 + E_4 + E_5 = E_{constant} + a \cdot t_4}$$

Set of data	a [MJ/min] [95% confidence bounds]	R^2
ABS	$2.89 \cdot 10^{-2}$ [$2.84 \cdot 10^{-2}$, $2.94 \cdot 10^{-2}$]	0.99
PC-ABS	$3.03 \cdot 10^{-2}$ [$2.99 \cdot 10^{-2}$, $3.08 \cdot 10^{-2}$]	0.99
All data	$2.96 \cdot 10^{-2}$ [$2.92 \cdot 10^{-2}$, $3.00 \cdot 10^{-2}$]	0.99

Table 26. Values of the "a" coefficient in Eq. 4 for the Stratasys F370.

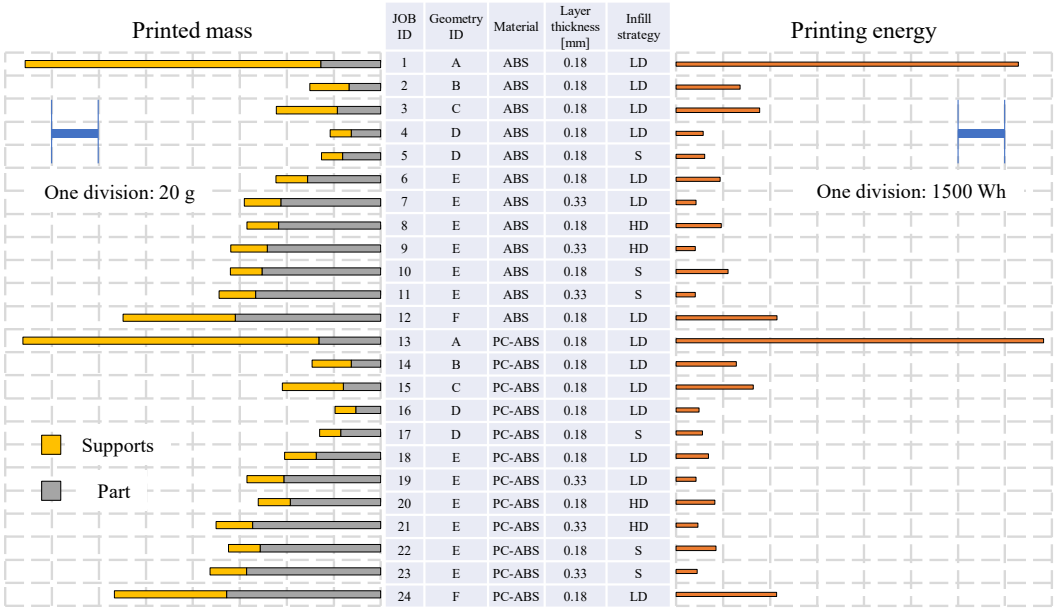

Figure 49. Printing phase: energy and mass results for samples manufactured on the Stratasys F370.

It is possible to notice that not in all cases the same trend is kept between the printed mass and the printing energy. Therefore, a variation of the ratio between the printing energy demand and the printed mass is expected. Considering JOB 1, JOB 11 and JOB 12 (all made of ABS), JOB 12 has a percentage variation of the printing energy and of the printed mass respectively equal to +425% and +59% referring to the relative values for JOB 11. On the other hand, JOB 1 has a percentage variation of the printing energy and of the printed mass respectively equal to +1682% and +120% referring to the relative values for JOB 11. This phenomenon implies that the variation of the energy efficiency is influenced more

from the process parameters and from the geometry features than from the deposited mass.

Focusing on geometry "E", Figure 50 analyses the variation of energy and time as a function of the total mass of the deposited materials (m_{tot}). For a fixed layer thickness, the printing time and the energy increase when a denser infill strategy is chosen (i.e., moving from a "low density" to a "solid dense" component). Such differences are less significant for the layer thickness of 0.330 mm, as the overall number of layers decreases. A reduction in time and energy demand for the components made of PCABS can be noticed for a layer thickness of 0.178 mm respect to those made of ABS, despite the higher process temperatures which are requested by the material (Table 8), while the results for a lower number of layers (i.e., for a layer thickness of 0.330 mm) are comparable. A thinner layer thickness means a greater number of layers to be deposited. Therefore, as the number of layers increases, the total length of the extruder path increases. Consequently, the time for the printing phase increases, together with the related energy consumption. On the other hand, the total length of the path also depends on the infill strategy. "LD" corresponds to a shorter path. Therefore, lower energy and time are required for the printing. The analysis of material effect confirms that the machine software differently manages the two materials (as shown in Figure 42).

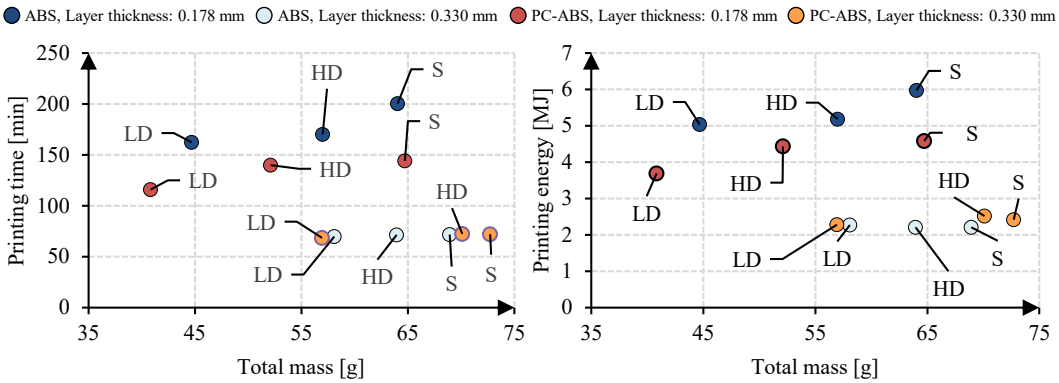

Figure 50. Effect of process parameters on the printing time and the energy demand of the Stratasys F370.

Empirical models for energy consumption

All the experimental results showing the correlation between the SPE and the DR_{aprint} variables are plotted in Figure 51. The SPE values decrease when the DR_{aprint} increases. For a given mass of material to be deposited, the higher the

DR_{aprint} is, the lower the deposition time. The DR_{aprint} for the Stratasys F370 FDM machine represents a holistic measure of the complexity of the deposition path, which in turn depends on the chosen process parameters, the material to be deposited and the component shape. In fact, with respect to the results concerning the component "E" (i.e., JOBs 6-11 and JOBs 18-23), the DR_{aprint} has experimentally proved to increase (a) when increasing the layer thickness, (b) when choosing an infill strategy towards a "solid dense" part, (c) when using PC-ABS instead of ABS. An analysis performed by means of MATLAB R2019a revealed that a hyperbolic curve provides the best fit of the results plotted in Figure 51, according to the empirical model proposed in Eq. 5.

$$\textbf{Eq. 5} \qquad \mathbf{SPE} = \mathbf{C_0} + \frac{\mathbf{C_1}}{\mathbf{DR_a}}$$

The "C_0" and "C_1" coefficients are listed in Table 27, while considering different sets of data. The constant "C_0" (in MJ/kg) is representative of a fixed specific energy that has to be included independently from the value of the time efficiency. The energy consumption due to the "C_0" term increases linearly when the mass to be deposited increases. On the other hand, "C_1" (in MJ/min) quantifies the constant power rate due to the energy consumption of equipment such as the machine subunits (i) and (ii). Therefore, "C_1" is mainly linked to the architecture of the machine. The model proposed in Eq. 5 can be applied to characterise the FDM machine independently from the actual material being printed, since the R^2 value of the model regarding all the experimental data is higher than 0.99. Overall, the total energy consumption of the FDM process (E_{FDM}, in MJ) can also be computed according to Eq. 6. Where "m_{tot}" (in kg) is the total mass of material (i.e., the component, support structures and purge part) to be deposited.

$$\textbf{Eq. 6} \qquad \mathbf{E_{FDM}} = \mathbf{E_{constant}} + \mathbf{SPE} \cdot \mathbf{m_{tot}} = \mathbf{E_{constant}} + \left(\mathbf{C_0} + \frac{\mathbf{C_1}}{\mathbf{DR_a}}\right) \cdot \mathbf{m_{tot}}$$

The modelling approach performed for the printing subphase can also be extended to the entire FDM unit process (i.e., including both productive and not productive phases), as shown in Figure 51 according to Eq. 7. The "C_2" and "C_3" coefficients are listed in Table 28, while considering different sets of data.

$$\textbf{Eq. 7} \qquad \mathbf{SEC} = \mathbf{C_2} + \frac{\mathbf{C_3}}{\mathbf{DR_a}}$$

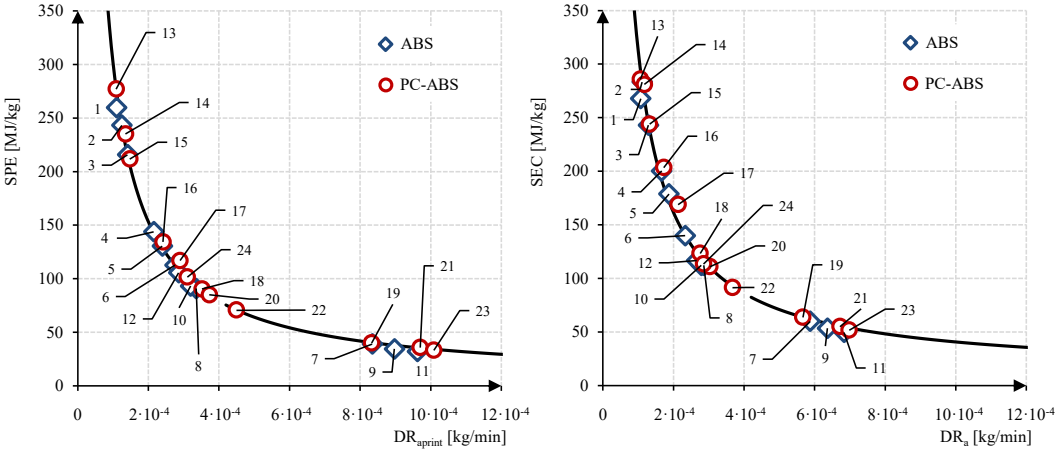

Figure 51. Empirical approach applied to the printing phase of the Stratasys F370.

Set of data	C_0 [MJ/kg] [95% confidence bounds]	C_1 [MJ/min] [95% confidence bounds]	R^2
ABS	4.18 [0.00, 9.64]	$2.92 \cdot 10^{-2}$ [2.81, 3.04]$\cdot 10^{-2}$	0.99
PC-ABS	5.07 [0.69, 9.44]	$3.04 \cdot 10^{-2}$ [2.94, 3.13]$\cdot 10^{-2}$	0.99
All data	4.81 [0.90, 8.73]	$2.97 \cdot 10^{-2}$ [2.89, 3.06]$\cdot 10^{-2}$	0.99

Table 27. Values of the "C_i" coefficients in Eq. 5, expressed in MJ/min, for the Stratasys F370.

Set of data	C_2 [MJ/kg] [95% confidence bounds]	C_3 [MJ/min] [95% confidence bounds]	R^2
ABS	9.69 [0.00, 21.06]	$2.97 \cdot 10^{-2}$ [2.76, 3.17]$\cdot 10^{-2}$	0.99
PC-ABS	10.84 [0.00, 21.99]	$3.09 \cdot 10^{-2}$ [2.87, 3.31]$\cdot 10^{-2}$	0.99
All data	10.53 [2.68, 18.38]	$3.02 \cdot 10^{-2}$ [2.87, 3.17]$\cdot 10^{-2}$	0.99

Table 28. Values of the "C_i" coefficients in Eq. 7 for the Stratasys F370.

Model validation

In order to validate the above-proposed models, the same amounts of material characterising JOB 13 were deposited by producing, in the same JOB, two cubes made of PCABS and QSR having respectively dimensions of 29.2 × 29.2 × 29.2 mm^3 and 48.9 × 48.9 × 48.9 mm^3 (Figure 52). The total deposited mass (m_{tot}) was 149.5 g. The process time and the energy consumption were measured, and the results are summarised in Figure 52. The printing time was 301.4 min, coherently with the expected time of 311 min obtained by means of a simulation preliminarily performed by the GrabCAD Print software. On the other hand, the

printing energy was 2625.3 Wh. The experimental DR_{aprint} was computed to be $4.96 \cdot 10^{-4}$ kg/min and the experimental SPE was equal to 63.2 MJ/kg.

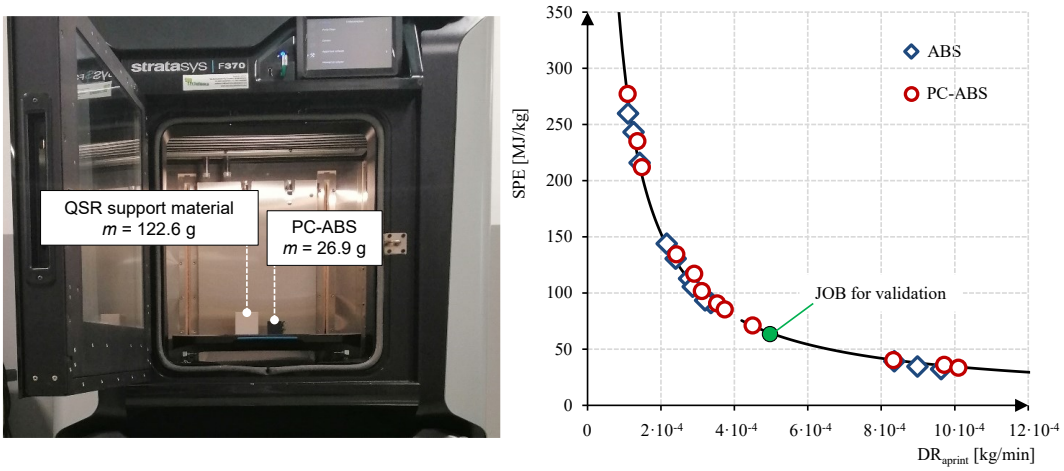

Figure 52. Experimental test for model validation of the Stratasys F370.

The SPE of the deposition phase can be quantified from Eq. 5 using the DR_{aprint}. If the average coefficients "C_0" and "C_1" for PCABS (Table 27) are applied, the predicted SPE of 66.3 MJ/kg lays in the hyperbolic curve (Figure 52). Moreover, a value of 2536.5 Wh is obtained for E_4, using the "a" constant for PC-ABS (Table 26). This value is the 3.4% lower than that found experimentally. Satisfactorily comparable results can be achieved by using the "a", "C_0" and "C_1" coefficients regarding the entire set of the experimental data, regardless of the kind of component material.

In addition, the printing time for the component "A" was 23.4 h. The time to print the same mass of materials in the simpler shape chosen to validate the model was reduced to approximately one fifth. Also, the energy consumption was proportionally lower. This experimental evidence confirms that the complexity in the deposition path directly affects the deposition and the energy efficiency of the FDM technology.

3.3.2 Electron Beam Melting

The vacuum generation subphase is characterised by the presence of machine subunits (i) base system of the machine, (ii) vacuum pumps and by the energy consumption related to the chiller. Machine subunits (i) and (ii) show a constant power with respect to time. The chiller energy consumption can be modelled in

the same way. Therefore, a linear model such as that proposed in Eq. 8 can be used, where "a" is the sum of the power of the three powered units.

$$\textbf{Eq. 8} \qquad \mathbf{E_{vacuum} = a \cdot t_{vacuum}}$$

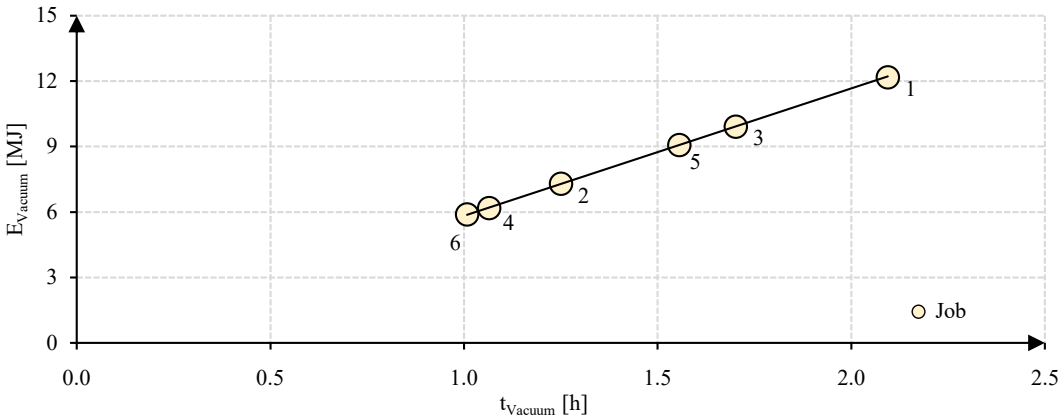

Figure 53. Experimental analysis between energy and time for the vacuum generation phase of the Arcam A2X.

Considering the process time in hours and the energy demand in MJ, the constant "a" is equal to 5.83 MJ/h. This equation is obtained by interpolating the experimental results reported in Figure 53, which connect the overall measured energy during subphase (1) with the relative process time (see Table 18). A linear regression of the experimental data is carried out using MATLAB R2019a, which provides a value of constant "a" equal to 5.83 MJ/h with the confidence interval equal to 95% (5.81-5.85 MJ/h, R^2=0.99).

Subphase (2.3) is characterised by the presence of all the machine subunits. As described from Eq. 9, a linear regression between the experimental time and energy results (Table 20) can be computed by means of MATLAB R2019a and fixing a confidence interval equal to 95%, as shown in Figure 54. The constant "b" is equal to 11.51 MJ/h (11.33-11.69 MJ/h, R^2=0.99).

$$\textbf{Eq. 9} \qquad \mathbf{E_{print} = b \cdot t_{print}}$$

The energy demand of the machine subunits (i) base system of the machine, (ii) vacuum pumps and (iii) high voltage unit, as well as the chiller, are linearly dependent on the time. Even though the machine subunits (iv) electron beam, and (v) rake and start plate do not have a constant power profile with respect to time, Figure 54 shows that a linear model is able to fit the experimental results for subphase (2.3). This trend can be explained as an effect of the adjustment on the beam power made by the EBM control to achieve a constant average amount of

heat to each layer section being melted. The contribution from the rake and start plate are constant as well.

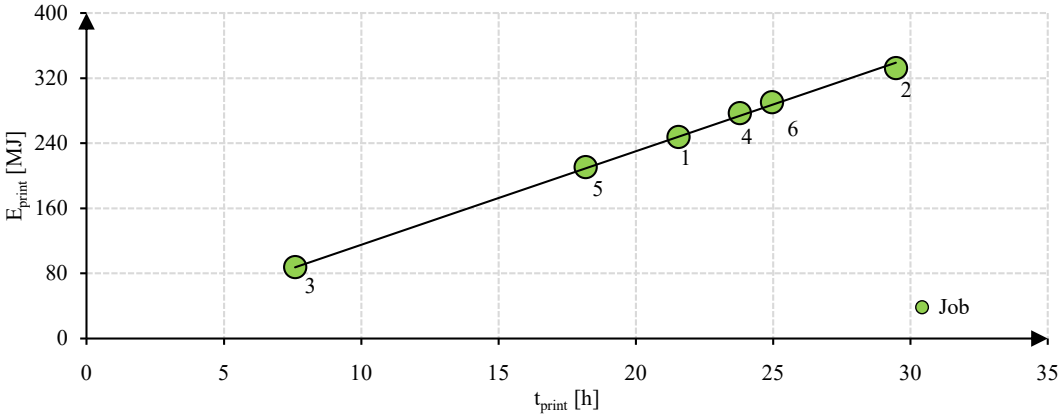

Figure 54. Experimental analysis between energy and time for the printing phase of the Arcam A2X.

Subphase (3) is characterised by the presence of machine subunit (i) and the energy consumption related to the chiller. The same approach adopted for process subphase (1) can be applied here, as reported from Eq. 10.

$$\textbf{Eq. 10} \qquad E_{cooling} = c \cdot t_{cooling}$$

where "c" is the sum of the power of the two powered units. Considering the process time in hours and the energy demand in MJ, the modelled value of constant "c" is 5.15 MJ/h. In the same way, as for subphase (1), a linear regression was obtained between the experimental time and energy results by means of MATLAB R2019a, fixing interval confidence equal to 95% (Figure 55), and using the results reported in Table 21. The experimental value of constant "c" is equal to 5.14 MJ/h (5.10-5.19 MJ/h, R^2=0.99).

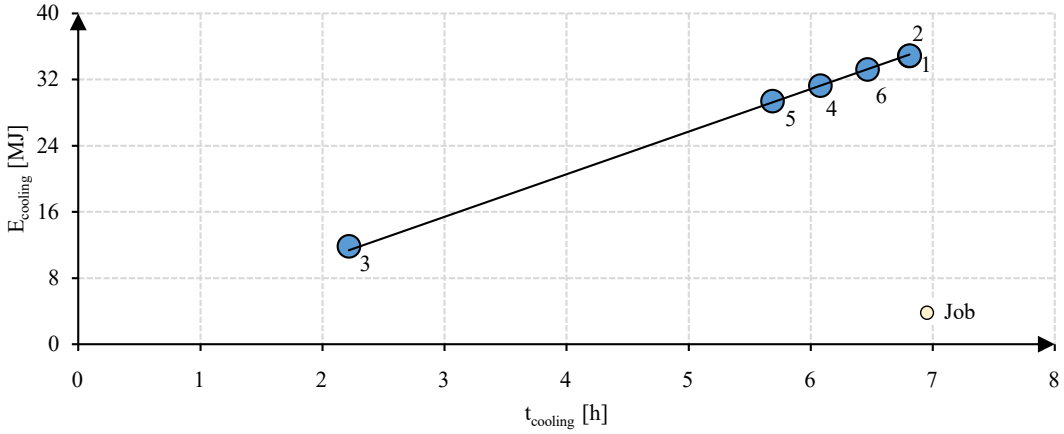

Figure 55. Experimental analysis between energy and time for the cooling phase of the Arcam A2X.

The energy demand of the entire EBM process can be predicted with Eq. 11. All the energy demand contributions for the powder bed set up (E_{bed}) or for build chamber cleaning ($E_{cleaning}$), respectively, can be assessed at the beginning and at the end of the EBM process, as having a power demand of 1230 W (which considers machine subunit (i) plus the chiller power demand in its standby condition). The energy demand of process subphase (1) (E_{vacuum}) and process subphase (3) ($E_{cooling}$) can be assessed as reported in Eq. 8 and Eq. 10, respectively. The energy involved in process subphase (2) is computed as in Eq. 12, which also includes Eq. 9 for the process subphase (2.3). The energy demands for beam alignment ($E_{alignment}$) and start plate heating (E_{table}) are assumed to be constant, according to Table 19.

$$\textbf{Eq. 11} \qquad E_{EBM} = E_{bed} + E_{vacuum} + E_{build} + E_{cooling} + E_{cleaning}$$

$$\textbf{Eq. 12} \qquad E_{build} = E_{alignment} + E_{table} + b \cdot t_{print}$$

Figure 56 and Figure 57 show the process subphase times and energy as percentages of the total demands, respectively.

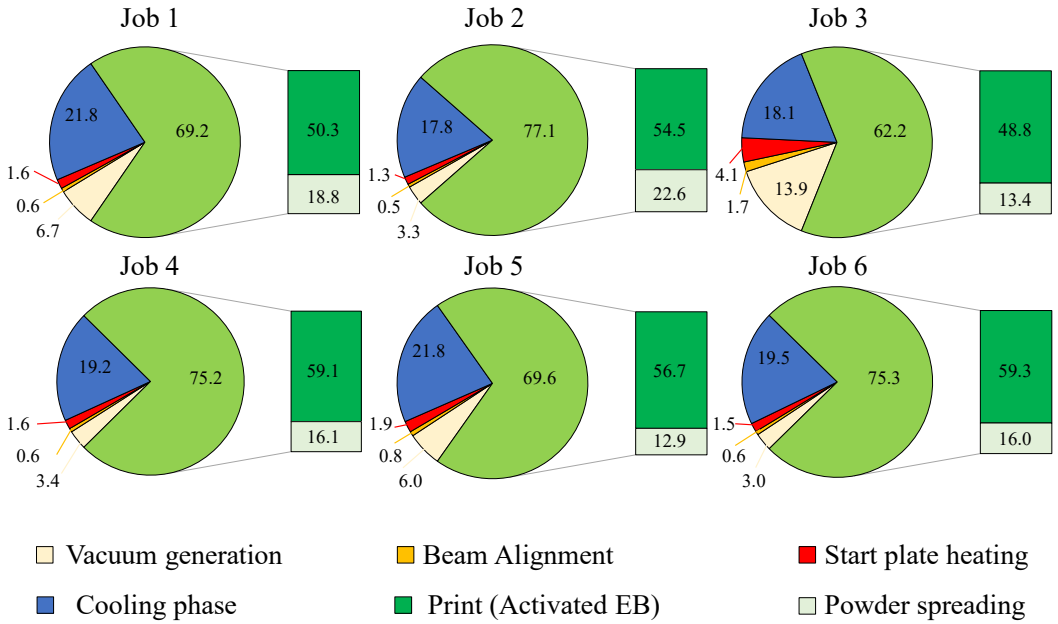

Figure 56. Process subphase times as percentages of the total demand of the Arcam A2X.

Moreover, process subphase (2.3) is decomposed into the contributions related to the spread of the powder layer (Powder spreading) and that of the

melting procedure (Activated EB). The vacuum generation procedure affects the time and energy demands respectively by 3-7% and 2-4% on average. When a small JOB is considered (e.g., JOB 3), the weight of process subphase (1) can reach 14% and 8% of the total time and energy demand, respectively. The beam alignment step and the heating of the start plate have constant duration is negligible. However, due to the power demand of machine subunit (iv), their energy impacts can be compared with that of the vacuum generation subphase.

Figure 57. Process subphase energies as percentages of the total demand of the Arcam A2X.

The printing window accounts for over 60% of the process time in all the cases, with a maximum of 77% for JOB 2. The energy impact of this phase on the overall demand is even higher (between 72% and 86%), since subphase (2.3) is mainly characterised by the presence of machine subunit (iv). The entities of the powder spreading time and energy depend on the JOB height (Table 11). As far as the results of this work are concerned, the cumulative time and energy of the coating represent 13-22% and 10-18% of the total time and energy, respectively. Only the base system of the machine and the chiller are powered during the cooling phase. Therefore, even though this phase can last a long time, its weight on the total energy demand is at least half of that of the total time demand.

Empirical models for energy consumption

As far as the SPE is concerned, further considerations can be made on the energy efficiency of the EBM technology by focusing on process subphase (2.3). A statistical analysis, performed by means of MATLAB R2019a, highlighted a hyperbolic law (Figure 58) with an R^2 value equal to 0.99. This result is related to the linear relationship that exists between the printing energy and the printing time. As mentioned above, the power demand of all machine subunits is or can be approximated as constant. In fact, if both terms of Eq. 9 are divided by the mass and expressed as a function of DR_{aprint}, the hyperbolic relationship is obtained as expressed in Eq. 13. "C_{print}" is a constant (in MJ/h) and quantifies the average constant power rate resulting from the energy consumption of the different machine subunits which are powered during process subphase (2.3). Its value and the relative 95% confidence interval (Table 29) are in fact close to those of constant "b" modelled in Eq. 9.

$$\textbf{Eq. 13} \qquad \mathbf{SPE} = \frac{\mathbf{C_{print}}}{\mathbf{DR_{aprint}}}$$

Considering Figure 38, it is possible to notice how JOBs characterised by the presence of lattice structures and supports (4 and 6) slow down the deposition efficiency. The JOBs that are mainly composed of melted volumes (1 and 3) show the highest deposition efficiency. If only the effect of the bulk material theme is considered, JOBs with greater height (such as JOB 2) have a lower DR_{aprint} than shorter JOBs (such as JOB 3) since powder spreading is a not an active phase. If the deposited mass change (meaning a change in the JOB design), the new SPE and DR_{aprint} values will still belong to the same curve. At the unit process level, the SEC parameter and the overall DR_a can be considered. As before, the experimental analysis showed a hyperbolic law between these two variables with an R^2 value equal to 0.99 (see Figure 58 and Eq. 14).

$$\textbf{Eq. 14} \qquad \mathbf{SEC} = \frac{\mathbf{C_{EBM}}}{\mathbf{DR_a}}$$

Process window	C_i [MJ/h] [95% confidence bounds]	R^2
C_{print}	11.56 [11.40, 11.72]	0.99
C_{EBM}	10.16 [9.97, 10.36]	0.99

Table 29. Values of the "C_i" coefficient in Eq. 13 and Eq. 14, expressed in MJ/h, for the Arcam A2X.

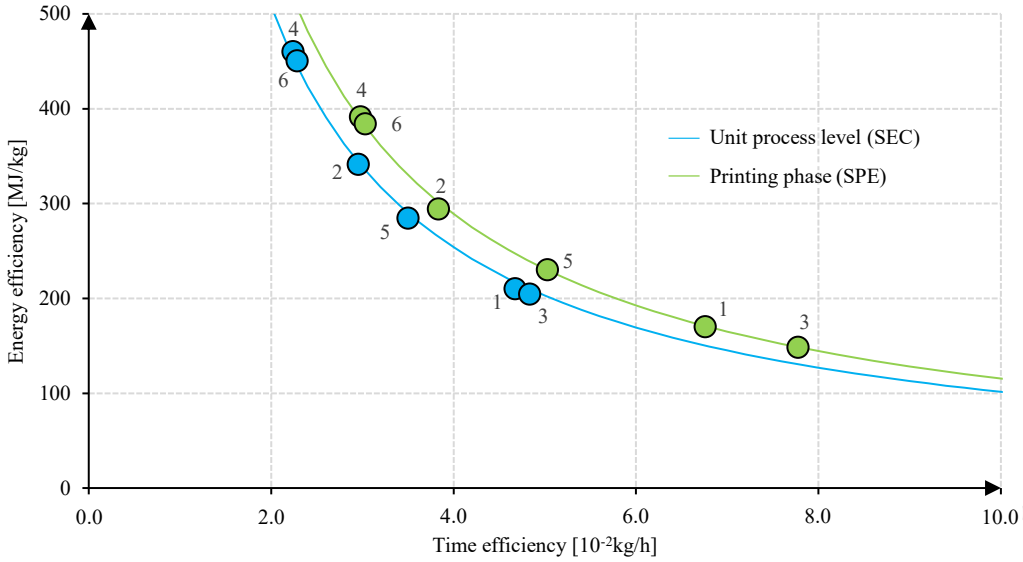

Figure 58. Empirical approach applied to the Arcam A2X at the unit process level and to the printing phase.

Where "C_{EBM}" is a constant expressed in MJ/h (Table 29). Significant increase of SEC can be observed for lower DR_a, while for the higher DR_a values, the SEC stabilises itself, reflecting relatively SEC reduction for higher DR_a values. The meaning of both "C_{print}" and "C_{EBM}" is thus connected closely to the process control and machine architecture. The value of "C_{Print}" is higher than that of "C_{EBM}" because the presence of non-printing phases lowers the energy consumption referred to a fixed time window. The SEC-DR_a curve is moved to a lower time and energy efficiency position, with respect to the SPE-DR_{aprint} curve. As previously mentioned, the print phase (2.3) dominates all the time and energy demands. A similar trend is in fact observed if the printing phase or the unit process level is taken into consideration. Both curves depend directly on the architecture of the machine and the process control. In fact, even when a wide variation of input parameters is considered, all the results lie on the same hyperbolic curve. Each input variable affects the time efficiency, which is holistically described by the DR_a. In this sense, as far as the energy efficiency characterisation of the EBM process is concerned, the complexity affects the SEC value, and a complex JOB has features that can slow down the DR_a (such as supports or small melting areas, as in the case of a lattice structure).

3.3.3 Continuous Filament Fabrication

As highlighted for the FDM and the EBM technologies, Figure 59 shows the experimental correlations between the overall printing energy (E_4) and the overall printing time (t_4). The linear law appears to be independent from the process parameters and component features. Moreover, it implies that an average power demand can be computed for the printing phase which is similar for all samples.

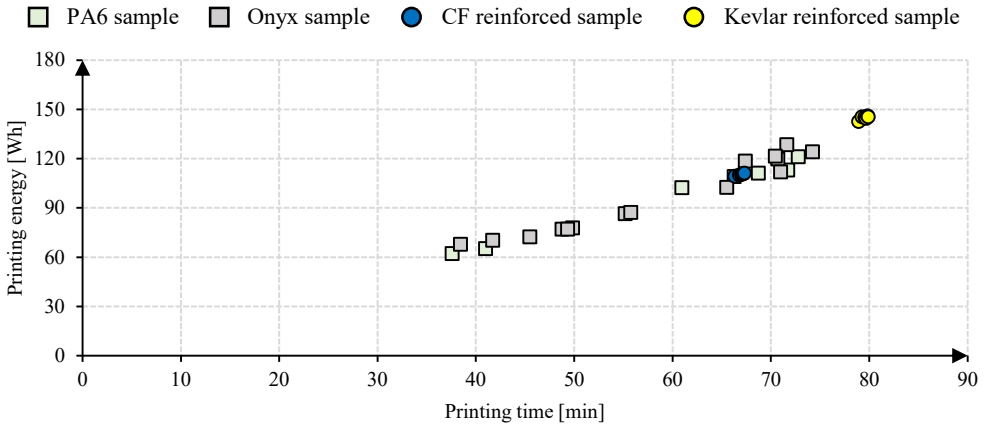

Figure 59. Printing phase: correlation between energy and time for the Markforged Mark Two.

Figure 60 shows the printing energy demand and the printed mass connected to the information regarding the process parameters (see Table 14) for the not reinforced samples manufactured on the Markforged Mark Two.

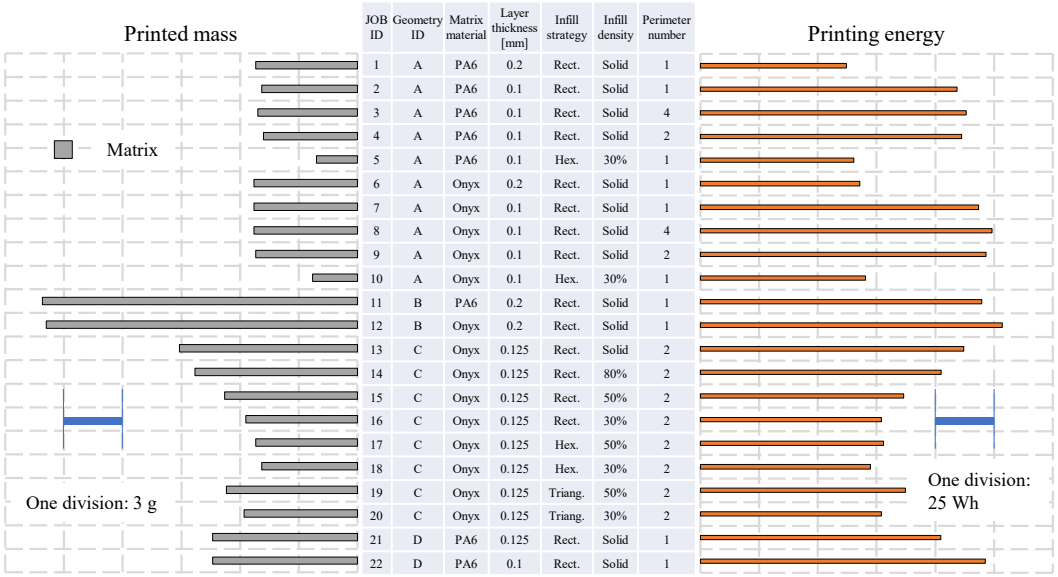

JOB ID	Geometry ID	Matrix material	Layer thickness [mm]	Infill strategy	Infill density	Perimeter number
1	A	PA6	0.2	Rect.	Solid	1
2	A	PA6	0.1	Rect.	Solid	1
3	A	PA6	0.1	Rect.	Solid	4
4	A	PA6	0.1	Rect.	Solid	2
5	A	PA6	0.1	Hex.	30%	1
6	A	Onyx	0.2	Rect.	Solid	1
7	A	Onyx	0.1	Rect.	Solid	1
8	A	Onyx	0.1	Rect.	Solid	4
9	A	Onyx	0.1	Rect.	Solid	2
10	A	Onyx	0.1	Hex.	30%	1
11	B	PA6	0.2	Rect.	Solid	1
12	B	Onyx	0.2	Rect.	Solid	1
13	C	Onyx	0.125	Rect.	Solid	2
14	C	Onyx	0.125	Rect.	80%	2
15	C	Onyx	0.125	Rect.	50%	2
16	C	Onyx	0.125	Rect.	30%	2
17	C	Onyx	0.125	Hex.	50%	2
18	C	Onyx	0.125	Hex.	30%	2
19	C	Onyx	0.125	Triang.	50%	2
20	C	Onyx	0.125	Triang.	30%	2
21	D	PA6	0.125	Rect.	Solid	1
22	D	PA6	0.1	Rect.	Solid	1

Figure 60. Printing energy and mass for not reinforced samples manufactured on the Markforged Mark Two.

Even for CFF it is noticeable that the variation of the energy efficiency is influenced more from the process parameters and from the geometry features than from the deposited mass. Considering the effect of the layer thickness for instance, JOB 2 practically shows the same mass of JOB 1 (i.e., a relative percentage variation of -6%). On the other hand, the corresponding variation on the printing energy is evident (i.e., a relative percentage variation of +76%). A similar consideration can be made regarding the geometry features: comparing to JOB 1, JOB 11 shows a relative percentage variation of +210% and of +93% respectively for the printed mass and the printing energy.

Figure 61 compares the trend of the fibre (t_{CF}, t_K), the perimeter ($t_{contour}$) and the gap depositions (t_{gap}) for the reinforces samples (JOBs 23-34). For both reinforcement filaments, Figure 61 highlights a dependence of "t_{CF}" and "t_K" from the fibre orientation. These terms rise moving from 0 degrees to 90 degrees. The extrusion paths explain how the rise of the inclination degree involves a higher number of inversions (see Figure 47). A more complicated path is affected from higher time losses because more acceleration and deceleration ramps occur.

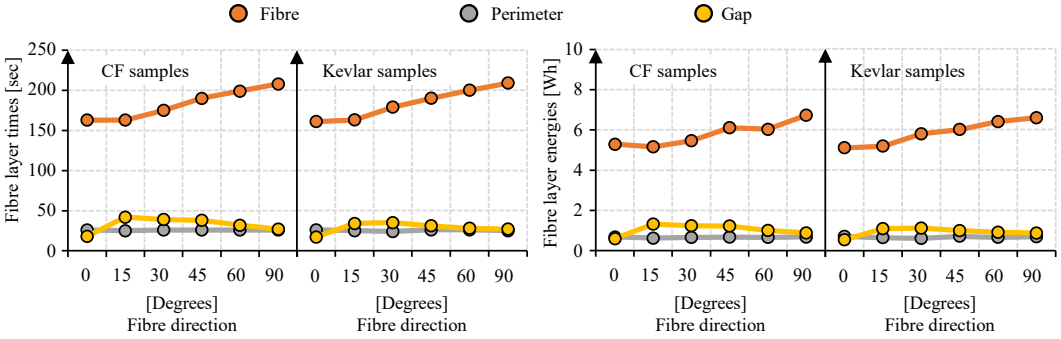

Figure 61. Time and energy demand for the reinforced samples (JOBs 23-34).

In fact, as typical for the FDM-based systems, for the Markforged Mark Two the deposition happens by means of mechanical movements of the axes and of the extruder feeders. The term "$t_{contour}$" has a value of about 26 sec for all the reinforced samples, because the external path is equal for each experimented condition (see Figure 47). On the other hand, "t_{gap}" is related to the fibre deposition time, since it is the time needed to fill the gaps between the perimeter and the reinforcement. For both reinforcements, "t_{gap}" increases moving from 0 degrees to 15 degrees, but then it reduces progressively moving to higher orientations. The time needed to deposit the CF and the Kevlar fibre are similar, as shown in Table 24. In fact, comparing CF and Kevlar reinforced samples, the difference on the overall printing time is mainly due to the PA6 matrix which is

characterised from a different layer number in the two cases (24 and 30 respectively for CF and Kevlar samples). Similar considerations can be done considering the energy demands for the fibre (E_{CF}, E_K), perimeter ($E_{contour}$) and gap (E_{gap}) depositions (Figure 61).

Empirical models for energy consumption

The Specific Printing Energy for the matrix deposition (SPE_{Matrix}) is computed as the ratio between "E_{Matrix}" and "m_{Matrix}". The average Deposition Rate referred to the matrix deposition window ($DR_{aprintMatrix}$) is calculated as the ratio between the deposited mass (m_{Matrix}) and the relative time window (t_{Matrix}). The Specific Printing Energy for the CF (or the Kevlar) deposition ($SPE_{CF(K)}$) is computed as the ratio between "$E_{CF(K)}$" and "$m_{CF(K)}$". The average Deposition Rate referred to the reinforcement deposition window ($DR_{aprintCF(K)}$) is calculated as the ratio between the deposited mass ($m_{CF(K)}$) and the relative time window ($t_{CF(K)}$). Figure 62 summarises the computed parameters. Both data for the CF and the Kevlar reinforced layers (i.e., from JOB 23 to JOB 34) lay in the same regression law, despite the change of reinforcement material and the variation of the fibre orientation. Considering the data for the matrix materials (i.e., from JOB 1 to JOB 22), all samples lay in the same curve as well even if a large variability of input process parameters was provided. As result of the linear trend discussed for Figure 59, both variables are connected from a hyperbolic law, as shown in Eq. 15. The regression law shown in Eq. 15 is evaluated by means of MATLAB R2019a, considering the set of data for the reinforced layers and that for the matrix materials. Table 30 reports the characteristic constant (C_{print}) for the two subsets with their 95% confidence bounds and the R^2 value.

$$\textbf{Eq. 15} \qquad \mathbf{SPE} = \frac{\mathbf{C_{print}}}{\mathbf{DR_{aprint}}}$$

Process window	C_i [MJ/min] [95% confidence bounds]	R^2
C_{Matrix}	$5.90 \cdot 10^{-3}$ [5.80, 6.00]$\cdot 10^{-3}$	0.99
C_{Fibre}	$6.86 \cdot 10^{-3}$ [6.78, 6.93]$\cdot 10^{-3}$	0.99

Table 30. Values of the "C_i" coefficients in Eq. 15 for the fibre and matrix curve, expressed in MJ/min.

In particular, "C_{print}" is a constant (in MJ/min) and quantifies the average constant power rate resulting from the energy consumption of the different machine subunits which are powered during the printing subphase, respectively of

the matrix (C_{Matrix}) and of the reinforcement (C_{Fibre}). Figure 62 presents a difference on the SPE values for the fibres and for the matrix depositions. This is due to the higher average current demand during the fibre deposition than that during the matrix one, as visible from the value of the regression constants in Table 30.

Considering the experiments for the matrixes, an increase of the layer thickness improves the deposition efficiency. JOB 1 and JOB 6 (both printed with a layer thickness of 0.200 mm) have a deposition efficiency which is about double that of JOB 2 and JOB 7 (both printed with a layer thickness of 0.100 mm). Fixing the layer thickness, considering JOB 2, JOB 3 and JOB 4, a similar deposition efficiency is visible even if the perimeter number was varied (respectively 1, 4 and 2 perimeters). The same consideration applies to JOB 7, JOB 8 and JOB 9 (having respectively 1, 4 and 2 perimeters) even if the matrix material was changed. JOB 5 and JOB 10 (both printed with a hexagonal infill style and 30% as infill density) demonstrate that an infill style and density which provide a more complex extrusion path also give a lower energy efficiency. On the other hand, JOB 11 and JOB 12 show the highest energy efficiency since the simplest tool path was designed: a rectangular infill style and a solid infill density were selected. Moreover, the layers of geometry “B” offer a simpler deposition path than those of the other geometries and the 0.200 mm layer thickness used for JOB 11 and JOB 12 further pushes up their deposition efficiency. Considering all JOBs from JOB 1 to JOB 12, it is possible to evaluate the effect of the matrix material. All JOBs made of Onyx lay on the upper side of the regression curve for the matrix material. Instead, all JOBs made of PA6 lay on the lower side, due to a slightly higher current demand of Onyx comparing with PA6. JOBs 13-20 carry out a full assessment of the infill style and density. More in detail, the triangular and hexagonal infill style normally report the lowest deposition efficiency, as well as infill density below 80%. JOBs 13-20 were printed with 2 perimeters and a high layer thickness (0.125 mm) which reduces the overall number of filled areas. The presence of two perimeters in these samples slightly move their data on the lower side of the regression law if compared with other samples made by Onyx. However, the effect of a different number of perimeters has a low significance as highlighted from the data referred to the geometry “A”. Therefore, the main effect can be attributed to the inner area, as proved by the higher average current demand required respect to the contour (Figure 46). Moreover, this phenomenon

is increased from the smaller layer thickness (0.100 mm) of geometry “A”, which increases the overall number of filled areas.

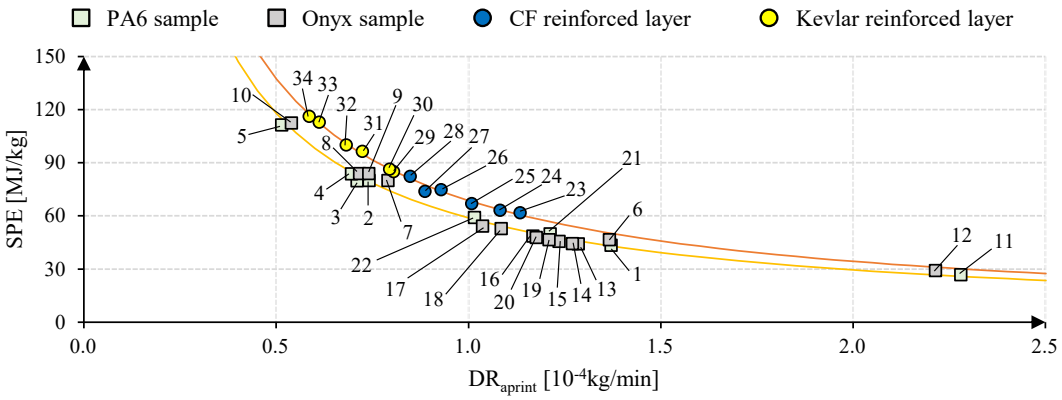

Figure 62. Empirical approach applied to the Markforged Mark Two for the matrix and fibre deposition.

Considering the reinforced layers (belonging to JOBs 23-34), two different areas can be notices in Figure 62: the points referred to the Kevlar layers lay in the higher part of the curve, while the points for the CF layers cover the lower part. Once the fibre orientation and the layer geometry are fixed, the Markforged Eiger software produces a unique extrusion paths for any fibre reinforcement, despite the different layer thickness. The deposition times and energies are comparable for the CF and the Kevlar reinforced layers (see Table 24), but the deposited masses for CF are higher than those for Kevlar (see Table 25), for the superior material density (see Table 13). This explains why a higher time efficiency is gained from CF respect to Kevlar for a fixed extrusion path. Finally, Figure 62 highlights a connection between the fibre orientation degree and its position on the regression curve due to the different number of inversions (see Figure 47).

Computing the SPE_{Matrix} and $DR_{aprintMatrix}$ parameters for JOBs 23-34, a variation is not expected among the reinforced samples with a different fibre orientation once the fibre material is fixed. Considering what exposed above, this is due to the lack of variation on the process and part designs for the matrixes. On the other hand, a difference can be noticed comparing the matrixes of the CF samples with those of the Kevlar ones, because of the different layer thickness. Therefore, once the fibre material is fixed a common value can be assumed for the SPE_{Matrix} and $DR_{aprintMatrix}$. A standard deviation of 1.07 MJ/kg for an average SPE_{Matrix} equal to 54.85 MJ/kg is found for CF samples (JOBs 23-28). For Kevlar samples (JOBs 29-34) a standard deviation of 2.28 MJ/kg for an average SPE_{Matrix} equal to 69.01 MJ/kg is computed. Similarly, a standard deviation of 4.26E-07

kg/min is calculated for an average $DR_{aprintMatrix}$ equal to 1.17E-04 kg/min for CF samples (JOBs 23-28). For Kevlar samples (JOBs 29-34) a standard deviation of 3.25E-06 kg/min is computed for an average $DR_{aprintMatrix}$ equal to 9.49E-05 kg/min. Regarding JOB 21 and JOB 22, the SPE_{Matrix} and $DR_{aprintMatrix}$ values are respectively equal to 49.81 MJ/kg and 1.21E-04 kg/min for a layer thickness of 0.125 mm and respectively equal to 59.06 MJ/kg and 1.02E-04 kg/min for a layer thickness of 0.100 mm. A reduction on the time efficiency can be seen for the PA6 deposited for the reinforced samples (JOBs 23-34), comparing with that of JOB 21 and JOB 22. Even if for the reinforced samples there is the presence of "m_{Corner}", its deposition requires more movements of the extrusion head towards the corner side of the start plate and back to the printing area, which globally slows down the time efficiency of the PA6 deposition.

Model validation

In this section the validation of the two hyperbolic curves reported in Figure 62 is carried out.

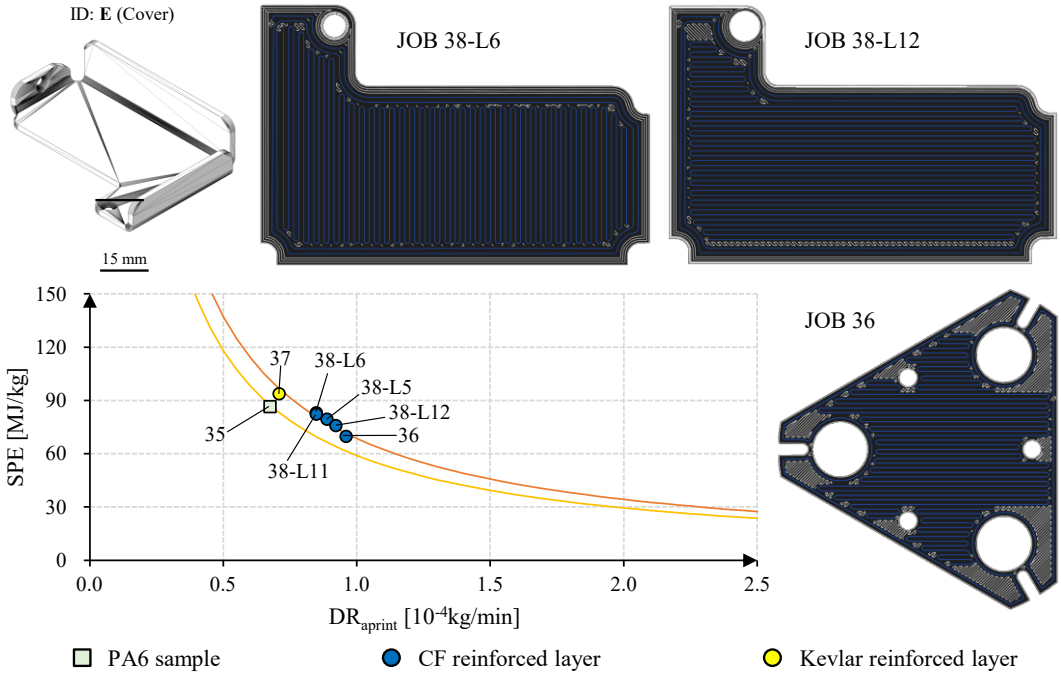

Figure 63. Experimental tests for model validation of the Markforged Mark Two.

The geometry "E" is introduced as shown in Figure 63 to validate the matrix regression curve. Geometry "E" is a cover which was customised for the user

thank to the design freedom offered from the AM technology. JOB 35 was thought using geometry "E", PA6 as material and the following process parameters: 4 perimeters, hexagonal infill style and an infill density of 62%. The 9th layer of geometry "D" was reinforced to validate the fibre regression curve, using PA6 as matrix material, an isotropic fibre path and CF in a first experiment (giving JOB 36) and Kevlar in a second case (giving JOB 37). As prescribed from Markforged Eiger, the layer thickness of JOB 36 must be 0.125 mm, while that of JOB 37 must be 0.100 mm. Finally, geometry "E" was also selected to validate the fibre regression curve. The layers 5, 6, 11 and 12 were reinforced with CF using an isotropic fibre path in all cases and PA6 as matrix. The fibre inclination was set to 0 degrees for the layers 5 and 12, while it was set to 90 degrees for the layers 6 and 11. All results for the validation JOBs are reported in Table 31. As visible from Figure 63, all experiments lay in the relative regression laws. JOB 35 shows a low deposition and energy efficiency since its process parameters create a tool path with several inversions due to the hexagonal infill style and low infill density. Focusing on the reinforced layers, the JOB 37 lays in the upper level of the regression law respect to JOB 36, due to the deposition of the Kevlar fibre instead of CF. Considering JOB 38, the layers with an inclination equal to 90 degrees show a higher number of inversion respect to those with an inclination equal to 0 degrees (see Figure 63).

JOB ID	t_{Matrix} [min]	$t_{CF(K)}$ [sec]	E_{Matrix} [Wh]	$E_{CF(K)}$ [Wh]	m_{Matrix} [g]	$m_{CF(K)}$ [g]
35	108.7	-	176.3	-	7.3	-
36	56.5	140	98.5	4.3	4.8	0.2
37	68.5	142	121.0	4.4	4.5	0.2
38-L5	82.2	171	138.5	5.6	7.3	0.3
38-L6		179		5.8		0.3
38-L11		179		5.8		0.3
38-L12		172		5.6		0.3

Table 31. Results of the JOBs used to validate the regression laws of the Markforged Mark Two.

Energy prediction of 3D printed composites via CFF

Focusing on the printing phase, Eq. 16 shows how to combine the two SPE contributes (i.e., that of the reinforcement and that of the matrix) to evaluate that of the JOB being printed (SPE_{JOB}). The SPE_{JOB} factor is computed by the ratio between the energy demand of the printing phase (4), (E_4), and the printed mass (i.e., m_{JOB}). By means of Eq. 16, SPE_{JOB} can be computed as weighted average of SPE_{Matrix} and $SPE_{CF(K)}$.

$$\textbf{Eq. 16} \qquad \mathbf{SPE_{JOB}} = \frac{\mathbf{E_4}}{\mathbf{m_{JOB}}} = \frac{\mathbf{E_{CF(K)} + E_{Matrix}}}{\mathbf{m_{JOB}}} = \frac{\mathbf{E_{CF(K)}}}{\mathbf{m_{CF(K)}}} \cdot \frac{\mathbf{m_{CF(K)}}}{\mathbf{m_{JOB}}} + \frac{\mathbf{E_{Matrix}}}{\mathbf{m_{Matrix}}} \cdot \frac{\mathbf{m_{Matrix}}}{\mathbf{m_{JOB}}} = \mathbf{SPE_{CF(K)}} * \frac{\mathbf{m_{CF(K)}}}{\mathbf{m_{JOB}}} + \mathbf{SPE_{Matrix}} * \frac{\mathbf{m_{Matrix}}}{\mathbf{m_{JOB}}}$$

$$\textbf{Eq. 17} \qquad \mathbf{E_4 = m_{JOB} \cdot SPE_{JOB}}$$

The term "E_4" is then estimated as in Eq. 17 by the product between "m_{JOB}" and the modelled SPE_{JOB}. Using Eq. 16 and Eq. 17, it is possible to use the two regression laws reported in Figure 62 to assess the energy demand of 3D printed composites via CFF. Table 32 lists the "E_4" values experimentally measured for all the reinforced JOBs assessed in this study (JOBs 23-34, JOBs 36-38). Moreover, the modelled "E_4" evaluated by means of Eq. 16 and Eq. 17 are also shown in Table 32 together with the relative percentage errors. All percentage errors are low enough to make this method a valid tool to predict the energy demand of 3D printed composites via CFF.

However, a further improvement can be achieved considering the energy contribute needed to deposit the purge corner part, which is present until the last reinforced layer. In fact, this contribute is not evaluated in the regression law for the matrix material reported in Figure 62. Considering the energy to print one layer of the corner purge part (e_{Corner}, equal to 0.42 Wh) and the number of layers cumulated until the last reinforced one (n), Eq. 18 can be used to better estimate "E_4". Table 32 lists the modelled "E_4" values computed with Eq. 18 with the relative percentage errors, which are lower than those computed without the correction for the purge corner part.

Finally, the energy demand of the entire CFF process can be evaluated with Eq. 19, including the contributes of the not productive phases.

$$\textbf{Eq. 18} \qquad \mathbf{E_4 = m_{Job} \cdot SPE_{Job} + n \cdot e_{Corner}}$$

$$\textbf{Eq. 19} \qquad \mathbf{E_{CFF} = E_1 + E_2 + E_3 + E_4 + E_5}$$

JOB ID	m_{JOB} [g]	Measured E_4 [Wh]	SPE_{JOB} [MJ/kg] - Eq. 16	E_4 [Wh] - Eq. 17	E_4 Error (%) - Eq. 17	n	E_4 [Wh] - Eq. 18	E_4 Error (%) - Eq. 18
23	7.8	121.0	50.8	109.5	-9.5	13	114.9	-5.0
24	7.8	118.8	50.6	110.2	-7.2	13	115.7	-2.6
25	7.8	117.7	51.3	110.6	-6.0	13	116.1	-1.4

26	7.8	122.5	51.2	111.0	-9.4	13	116.5	-5.0
27	7.8	117.0	51.5	111.1	-5.1	13	116.6	-0.4
28	7.8	122.9	51.3	111.3	-9.5	13	116.7	-5.0
29	7.1	142.6	66.5	130.1	-8.8	16	136.8	-4.0
30	7.4	145.4	63.8	130.7	-10.1	16	137.4	-5.5
31	7.4	145.2	63.6	131.2	-9.6	16	137.9	-5.0
32	7.6	144.5	62.5	131.5	-9.0	16	138.2	-4.4
33	7.7	146.1	61.9	131.8	-9.8	16	138.5	-5.2
34	7.7	145.4	61.4	131.9	-9.3	16	138.6	-4.6
36	5.0	102.8	69.5	97.0	-5.6	9	100.8	-1.9
37	4.6	125.4	90.9	116.9	-6.8	9	120.6	-3.8
38	8.4	161.3	67.6	157.0	-2.7	12	162.0	0.4

Table 32. Results of the model for the energy prediction of 3D printed composites with the Markforged Mark Two.

Considering the reinforced samples manufactured in this study *and a conversation factor equal to 0.38 according to the European average* [67], the range found for the SEC of the CFF technology is 161-287 MJ/kg (Oil equivalent). This range is higher in general than that found for the reviewed technologies in Figure 6. Due to the low productivity rates of AM techniques the SEC parameter increases because power has to be supplied for longer time. However, higher values were found for the autoclave process with reference to low production rate [129] and aeronautic application [130].

3.3.4 Final considerations

This section provides final consideration on the work performed in this Chapter. It is articulated in four subparagraph which discuss about: (a) the weight of the energy to melt the material respect to the overall printing energy, (b) a comparison between the energy and the deposition efficiency of the investigated AM processes, (c) the implications of this research respect to the rules of design for AM and (d) interconnections with quality criteria.

Melting energy and overall energy demand: the weight of the machine subunits

Considering the unit process level, Table 33 shows the average values of the energy demand of each subunit of the AM machines studied in this work as percentage of the total energy demand and the relative standard deviation. The interesting result is that similar proportions are maintained from the different subunits for each JOB. In fact, the results of the standard variations do not affect the magnitude of the average values. Considering the Stratasys F370, the energy demand of the base system of the machine is below 6% for both materials. The heaters of the build chamber characterise almost the maximum overall energy demand (around 90%). On the other hand, the energy demand to melt the plastic wire is below the 5% for both materials. Considering the Arcam A2X, the energy demand of the rake and start plate is negligible, because it is related to 0.52% of the total energy demand. The chiller system is the highest energy consumption unit, with a value of 34.64%. This unit is followed by the electron beam (29.28%). Then, the base system of the machine, the vacuum pumps and the high voltage unit follow with 18.27%, 11.21% and 6.08%, respectively. A further reflection can be made considering that only 29.28% of the total energy demand is needed for the Arcam EBM A2X machine for the melting procedure. Instead, 70.72% of the total energy demand is needed to make the melting procedure possible. As effect of the simple machine architecture of the Markforged Mark Two, the energy demand share of the extruder heaters and axes is around the 90% of the total. The results exposed for the three AM technologies tell that the optimisation of the energy efficiency of an AM system requires not only the optimisation of the additive process itself, but also that of the different machine subunits.

Machine subunit	Average in percentage	Standard deviation in percentage
Stratasys F370 - ABS		
Base system of the machine	5.81	0.20
Chamber heaters	89.53	0.95
Extruder heaters and axes	4.66	0.77
Stratasys F370 - PC-ABS		
Base system of the machine	5.53	0.21

Chamber heaters	90.21	0.98
Extruder heaters and axes	4.26	0.79
Arcam A2X		
Base system of the machine	18.27	0.38
Vacuum pumps	11.21	0.28
High voltage unit	6.08	0.27
Electron beam	29.28	0.91
Rake and start plate	0.52	0.11
Chiller	34.64	0.46
Markforged Mark Two - PA6		
Base system of the machine	10.60	0.26
Extruder heaters and axes	89.40	0.26
Markforged Mark Two - Onyx		
Base system of the machine	10.08	0.28
Extruder heaters and axes	89.92	0.28
Markforged Mark Two - Onyx (2 perimeters)		
Base system of the machine	10.99	0.07
Extruder heaters and axes	89.01	0.07
Markforged Mark Two - CF reinforced samples		
Base system of the machine	9.81	0.20
Extruder heaters and axes	90.19	0.20
Markforged Mark Two - Kevlar reinforced samples		
Base system of the machine	9.57	0.12
Extruder heaters and axes	90.43	0.12

Table 33. Energy demand share of each machine subunit as a percentage of the total energy demand for the AM machines investigated in this work.

Comparison between AM technologies: FDM, EBM and CFF

The reviewed data in Chapter 1 for FDM (Table 1) and for EBM (Table 2) are included in the comparison considering the SEC-DR_a relationships in Figure 64. The legend of Figure 64 was thought in order to distinguish the different AM technologies present in this study by means of the shape of the marker.

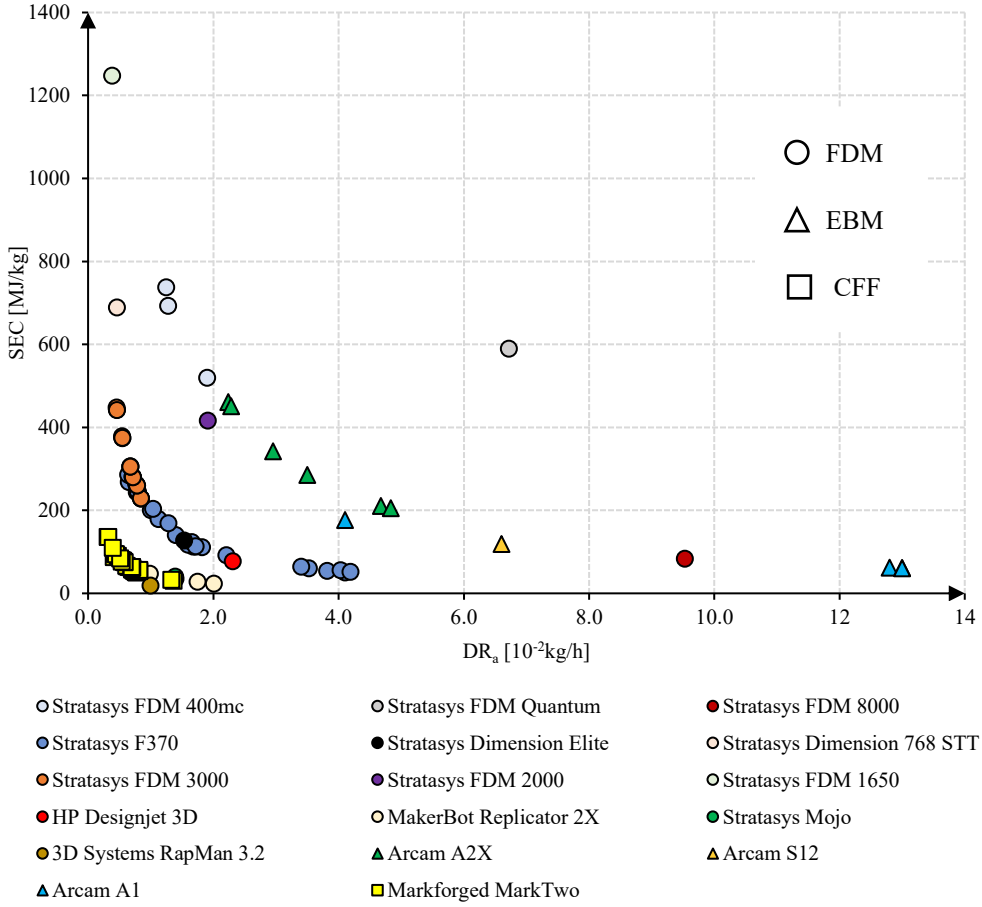

Figure 64. Comparison between SEC and DR_a data from literature and from this study.

Considering the FDM machines (circle marker), they show different build chamber capacities as well as applications from the semi-professional to the industrial context. MakerBot Replicator 2X, Stratasys Mojo, 3D System RapMan 3.2 have the lowest SEC values, the lowest build chamber size and the simplest architecture. For instance, MakerBot Replicator 2X and 3D System RapMan 3.2 do not have the chamber or the start plate heated. On the other hand, Stratasys FDM 400mc, Stratasys FDM Quantum and Stratasys FDM 8000 are machines for

industrial uses and they show the highest build chamber capacity and high SEC. The other FDM machines reviewed in Table 1, belong to the middle range size. However, Stratasys FDM 1650 and Stratasys FDM 2000 report similar DR_a to other machines of their size but higher SEC. This can be explained considering that Stratasys FDM 1650 and Stratasys FDM 2000 belong to the first generation of the FDM machines and therefore an optimisation of the energy consumption was not present yet. As the most recent of the middle range size, the Stratasys F370 reports the highest DR_a and the lowest SEC for its range. Considering the EBM machines (triangle marker), the data available in literature and the experiments performed in this study seem to lay in the same hyperbolic regression curve. However, the Arcam A2X shows higher SEC due to the higher power of its electron beam subunit, comparing with the other EBM machines. Moreover, the data available for the Arcam A1 showed the highest deposition efficiency for the EBM technology, which is much higher than that attainable from the FDM and CFF techniques (square marker).

Sustainability and design for AM (DfAM)

As visible from Figure 64, the high SEC values found for the AM technologies investigated in this research agree with the variation ranges available in the literature. It is possible to assess that the manufacturing step plays a key role when realising a product by means of AM due to the magnitude of the SEC parameter. In fact, the evaluation of practical case studies showed that the manufacturing phase can count for around 30-55% of the CED for the production of one titanium lifting bracket for a jet aircraft engine manufactured with EBM [66]. A higher predominance (85-95%) of the manufacturing share on the CED was shown for a L-PBF technique applied to produce one airplane bearing bracket, due to the low energy efficiency of the laser source [67]. One of the outcomes of this Chapter is the possibility to include environmental constrains (such as the energy demand, costs and CO_2 emissions) in the design for AM (DfAM), as shown in [165], thanks to an evaluation of the SEC and DR_a parameter which are directly connected to the precise studied design. For instance, considering the FDM and the CFF technology, the slicing software could include the option to apply an infill style which aims to reduce the acceleration and decelerations ramps. With the same aim, the position of a component in the build chamber could be considered in order to minimise the support structures for EBM.

Interdependencies with quality criteria

In general, it is possible to assess that the process parameters define the DR_a as well as the quality of the 3D printed component, both at the aesthetic level and at the functional level. However, it is worth to precise that, although counterintuitive, a higher deposition efficiency is not necessary connected to a lower surface finishing. It is true, for instance, that a higher layer thickness speeds up the productivity of a generic AM process (due the faster achievement of the final height) and increases the surface roughness due the staircase effect. However, considering the FDM technology, the geometry "A" (see Figure 35) which was produced in the JOB 1 and JOB 13 gave the lowest DR_a. Their finishing surfaces were the worst obtained among the components produced by means of the Stratasys F370 in this study, due to the quick changes in the direction of the extrusion path. Considering EBM, the work performed in this Chapter shows that what reduces the deposition efficiency for this technology is the presence of particular subphases, such as those to manufacture support structures and lattice parts. However, lattice and support structures are manufactured with other process parameters respect to those for the bulk material (see Table 12), therefore, it is not possible to make an association between the surface quality and the deposition efficiency a priori.

Conclusions and outlooks

In the following, the results of this work are summarised, and their limits and possible future improvements are discussed.

Chapter 2:

Chapter 2 aimed to compare the environmental impact of the CE strategies with that of the linear economy model. In particular, the advantages and disadvantages deriving from the application of the remanufacturing strategy by means of additive techniques are addressed. The works available in the state-of-the-art literature only focus on the single production of the product and do not pursue the comparison for the further lives the product may have thanks to the application of CE. Moreover, the implications of the reliability property on the iterated products represent a central topic to address, which was not taken into account from the available literature. These topics open important questions on how to assess the remaining useful lifetime of products and on how to extend the existing LCA methodologies to a function-oriented analysis. Chapter 2 takes into account the implications of reliability distinguishing between products that were used under the prescribed working conditions and those that were not used under the prescribed working conditions during their previous "i" life. A reduction in the physical lifetime was modelled for the next "i+1" life of the second group. Chapter 2 uses a Markovian approach to model the changes in the numbers of these two types of products along the time window required from the iterations of the analysis. Moreover, Chapter 2 proposes a Markovian modelling of the remanufacturing process. In particular, Chapter 2 brings new concepts into the LCA analysis, such as (a) the introduction of products which last for a lower physical lifetime (L_B) than others (L_A), (b) the presence of scraps which require to be replaced with brand-new products, (c) a not linear evaluation of the remanufacturing process which may require multiple internal iterations and (d) a distribution of the products (i.e., those belonging to Group A and Group B) which changes during the time window of the analysis. Thanks to these characteristics, Chapter 2 highlights a different breakeven value for the performed function-oriented analysis respect to a simple comparison between two technologies (such

as that described from Figure 19). This proves that appropriate tools are needed for not conventional LCA studies to take into account the higher complexity of the actions of the circular economy. Considering the entire time range of the analysis, some more considerations are given for the baseline scenario to show where the efficiency losses and possible fields of action are for improvement (see Figure 20). Moreover, the proposed sensitivity analysis (see the discussion section of Chapter 2) helps to better understand the potentialities of the developed LCA methodology, investigating the variation of the main variables that characterise the studied scenarios.

Finally, it is useful to discuss the limits of the performed analysis in Chapter 2 and its future improvements. First of all, the study evaluated two extreme conditions which are the remanufacturing logic and the brand-new manufacturing one. On the other hand, a better strategy could take into account both approaches in order to perform an optimisation of the overall target function (F_P). In fact, in some cases the overall target function was largely overcome from the final iteration because the second-last one could not reach "F_P" for few shares (e.g., Figure 27, Figure 30). Moreover, a combined approach could decide the proper route as consequence of the remanufactured needed material from a given product. Second, the study focused on a product which holds a market share equal to one. Further studies could focus on a product with a lower market share in order to model the implications of its substitution (Figure 8), in terms of CED metric for instance. Third, the analysis of Chapter 2 does not take into account the cumulative effect of the working conditions of all the past lives in the term "L_B". On the other hand, it only considers the effect of the previous "i" life in the next "i+1" one. Fourth, once the manufacturing and remanufacturing technologies are selected, their energy requirements should be investigated according to the model proposed in Chapter 3 in order to compute the right SEC parameter for the precise remanufacturing or manufacturing condition. Fifth, the energy demands due to the reverse and the distribution logistics are not taken into account.

These considerations would create an increase of the computational effort because the analysis should take into account the path of the single product. On the other hand, they are treated in aggregate form in this study. Finally, it is worth to remember that the analysis should be completed including the concept of "Absolute Sustainability", discussed in Chapter 1. Therefore, the IPAT equation should be used to assess the overall environmental impact according to the product of the human population (P), the human affluence (A) and the technology

factor (T). The resultant value should be then compared with the absolute boundaries posed by the Earth's Life Support System.

Chapter 3:

The experimental campaigns of Chapter 3 aimed to identify the effects of the main parameters and of the part designs on the process time and energy consumption of AM techniques. Fused Deposition Modelling (FDM), Electron Beam Melting (EBM) and Continuous Filament Fabrication (CFF) were selected as case study for this analysis. SEC is a well-known parameter that has been used in literature to assess the energy efficiency of different technologies at the unit process level, while DR_a can be used to evaluate the time efficiency of additive processes. In Chapter 3, the relationship between these two factors has been investigated. As far as the printing phase is concerned, a linear correlation between time and energy demand for printing is highlighted for the three technologies. The main finding of the study is the identification of a hyperbolic variation law between time efficiency and energy efficiency. This law is closely correlated with the architecture of the machine and the process control. In fact, even if wide variations of input parameters were provided, fixing the AM machine, all the results lie on the same hyperbolic curve, which can be computed at the unit process level or for the printing window. Each input variable affects the time efficiency, which is holistically described by the DR_a. Regarding the FDM and the CFF systems, the DR_a is influenced from the deposition path. Regarding the EBM system, the DR_a can be represented by the design complexity, which includes the use of supports or small melting areas, as in the case of a lattice structure. These results represent (a) a step forward in the energy characterisation of AM technologies, (b) open the way to a wide application of the presented methodology to characterise other AM machines, (c) help to obtain a better understanding of the dispersion of SEC values currently available in the literature (see Chapter 1) and (d) offer a practical methodology to be applied at industrial level for the energy characterisation of the AM systems with the requirement of low time and cost.

Finally, it is worth to consider the similarities with other conventional technologies and the applicability of the proposed methodology to other systems. An empirical methodology to define SEC is reported in [73,166] for injection moulding, where this parameter was hyperbolically correlated to the throughput provided from the machine. Further studies on injection moulding were made in

[167,168]. Subtractive unit-processes were characterised in [72,168–170] connecting SEC to the Material Removal Rate (MRR). The energy efficiency of not conventional technologies as Electrical Discharge Machining and Friction Stir Extrusion was similarly characterised respectively correlating SEC to the MRR [171] and to the Extrusion Rate [172]. These studies have in common a hyperbolic law between the energy efficiency and a characteristic variable of the technology which holistically evaluates its time efficiency. This result is typical of processes dominated from a constant power demand which does not change (or which can be approximated not to change) with the process parameters or part designs, as discussed in [173].

Sustainable manufacturing alternatives: AM and other processes:

This work focalised on AM processes to develop an LCA methodology which can suit properly the constraints that a circular economy system requires. However, this methodology and the hypothesis reported in Table 3 can be extended to other manufacturing techniques. This work does not go into the details of the selection of the proper manufacturing process for a product in a CE system. However, this consideration opens the important topic of what should be the *"design for circular economy"* of a product and indirectly which should be the relative production technique. For instance, Figure 65 reports a cable holder support (a) manufactured with conventional processes and (b) manufactured (and redesigned) by means of an AM technique (SLS by EOS [24]) with a strong reduction of the component number. Its original modularity suits better CE actions closer to the user, such as repairing in case component breakage, giving a better sustainable alternative due to "the power of inner circle" and "the value of circling longer", discussed in Chapter 1 [41]. On other hand, its redesign for AM leaves recycling as most likely action to be activated in case of breakage, since it becomes a monolithic product. The case study of Chapter 2 makes more evident that AM by means of the DED process can be an interesting choice to perform the remanufacturing of the product respect to conventional technologies, such as GTAW and PTA [63]. Therefore, the selection of the proper manufacturing process for a product in a CE system brings further complexities comparing with those present in a linear economy system. Moreover, the logistic effort (which is higher in a CE system) also represents another complexity and can affect the manufacturing technique to be chosen. This thesis does not explore this topic due to the urgent need to focus first on the development of LCA methodologies to be

applied to a CE scenario. However, they can be used for such goal, once developed and finished.

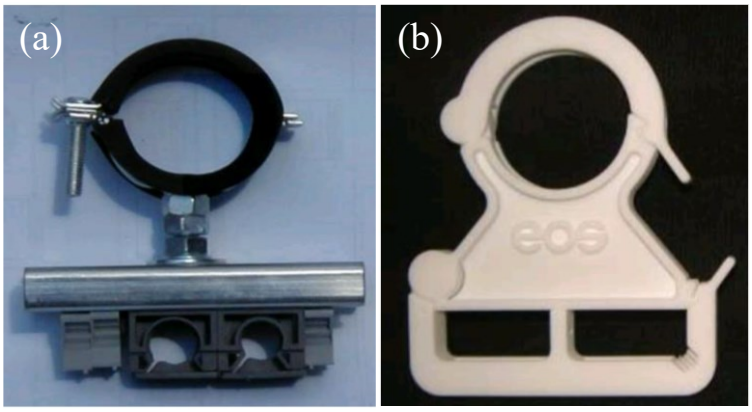

Figure 65. Example of a product (a) produced with conventional processes and (b) relative redesigned for AM.

Studies on the selection of a sustainable manufacturing alternative have been already proposed by the author of this thesis in [165], for an economy scenario which only considers recycling and the production of an unique product. The work in [165] performs a LCA comparing the manufacturing of a product batch by means of machining or AM (plus finishing) under cradle-to-gate boundaries (i.e., neglecting the use phase) and using the LCA methodology reported in [37,65,66,70]. Moreover, it uses the methodology proposed in Chapter 3 for EBM [74] and that applied in [72] for machining to include into the analysis the benefits deriving from a proper evaluation of the unit process energy efficiency. The paper shows breakeven surfaces for the CED, cost and CO_2 emission metrics. The inclusion into the LCA of the SEC models provided a variation on the shapes of the breakeven surfaces for those metrics respect to those computed with a constant SEC value for the two manufacturing techniques. It numerically highlighted that the increase of the time efficiency is a crucial driver for the environmental and economic sustainability of EBM and enlarged the competitiveness of EBM for a higher portion of the investigated domain. Finally, the presented methodology in [165] gives the opportunity to compare the goodness of different design rules for AM that can be chosen for a product and better defines the sustainability borders between the two manufacturing approaches.

Interactions between Chapter 2 and Chapter 3:

Finally, it is necessary to discuss about the interactions between the LCA methodology for a CE scenario reported in Chapter 2 and the study on the energy

efficiency at the unit process level of additive techniques performed in Chapter 3. As shown in Figure 1, which highlights the conceptual framework of this thesis, the two methodologies were performed independently. However, they apparently investigate two different dimensions of sustainability. Even if the nowadays world asks for studies at a higher level which can handle the circular economy actions, the investigation of the unit process level still holds an importance. In fact, it should be considered as propaedeutic to the goodness of the obtainable results with more complex LCA methodologies. This consideration applies not only to AM, but also to other manufacturing techniques and therefore, to the relative methodologies for their energy efficiency quantification reported in [72,73,166–173]. As discussed above, the work in [165] improved the existing LCA methodologies giving greater degrees of freedom to the study. Similar outcomes can be obtained for LCA methodologies which approach the circular economy actions. However, it is important to remark that the contribute of a higher transparency on the energy efficiency of the unit process level is higher if circular economy actions closer to the product manufacturing stage are considered, such as remanufacturing (Figure 20). On the other hand, the overall predictability of CE concepts reduces if circular actions closer to the user are taken into account, such as maintenance, repairing and product reuse (see Figure 4).

Appendix A: MATLAB code to compute the Markovian steps of the market evolution for each life

```
% This code aims to compute the number of user A and of user B for each
% iteration of the market evolution

P=82; %Product number;

U1=[0.1 0.9]; %Initial distribution of the Market;
MU=[0.8 0.2;
  0.5 0.5]; %“Probability matrix” of the market evolution;

p=10^2; %Max iteration number;

nA=linspace(0,0,p); %Initialisation of the vector for the A users
nB=linspace(0,0,p); %Initialisation of the vector for the B users

for i=1:p %Cycle to compute the distribution of the Market for each new life (the iteration is conducted for a conventional number of times "p");

   Ui=U1*MU^i;
   Ui(1)=ceil(P*Ui(1));
   Ui(2)=P-Ui(1);

   nA(i)=Ui(1);
   nB(i)=Ui(2);

end

nA(2:end)=nA(1:end-1);
nB(2:end)=nB(1:end-1);
nA(1)=floor(P*U1(1));
```

```
nB(1)=P-floor(P*U1(1));

% PAST DATA OF THE FIRST STEP ON EXCEL FILE

filename = 'Filescrittura.xlsx';
writematrix(nA,filename,'Sheet',2,'Range','B6:Z6')
writematrix(nB,filename,'Sheet',2,'Range','B7:Z7')
```

Appendix B: MATLAB code to compute the Markovian steps of the remanufacturing process for each life

```
% This code aims to compute, for each iteration of the market evolution,
% the internal flows of the markov chain-based remanufacturing process

m=7; %Iteration number for the Markovian remanufacturing process (this number is up to the structure of the modelled Markov chain, i.e., to the internal connections and number of Nodes;

NODE1=zeros(m,p);
NODE2=zeros(m,p);
NODE3=zeros(m,p);
NODE4=zeros(m,p);
NODE5=zeros(m,p);
NODE6=zeros(m,p);
NODE7=zeros(m,p);
NODE8=zeros(m,p);
NODE9=zeros(m,p);
```

```
for i=1:p %Cycle to compute the number of products for each Node of the remanufacturing process and for each life;

R0=[P 0 0 0 0 0 0 0 0]; %Initial distribution of the Nodes of the remanufacturing process;
Nodes=9;
B=zeros(m,Nodes);


Zi=(nA(1,i))/(P); %computation of the "state transition probabilities" that change for each life (due to the market evolution)
Noto=Zi;
NonNoto=1-Noto;
p12=1*NonNoto;
p13=0.95*Noto;

p19=1-p12-p13; %computation of the "state transition probabilities" that do not change for each life
p23=0.8;
p29=1-p23;
p45=0.05;
p48=1-p45;
p56=0.95;
p59=1-p56;
p78=0.95;
p79=1-p78;

MR=[0 p12 p13 0 0 0 0 0 p19; %“Probability matrix” of the remanufacuturing process;
  0 0 p23 0 0 0 0 0 p29;
  0 0 0 1 0 0 0 0 0;
  0 0 0 0 p45 0 0 p48 0;
  0 0 0 0 0 p56 0 0 p59;
  0 0 0 0 0 0 1 0 0;
  0 0 0 0 0 0 0 p78 p79;
  0 0 0 0 0 0 0 1 0;
  0 0 0 0 0 0 0 0 1];

for k=1:m

Ri=R0*(MR^k);
```

```
B(k,1:end)=Ri;

end

S1=B(1:end,1);
S2=B(1:end,2);
S3=B(1:end,3);
S4=B(1:end,4);
S5=B(1:end,5);
S6=B(1:end,6);
S7=B(1:end,7);
S8=B(1:end,8);
S9=B(1:end,9);

NODE1(1:end,i)=S1;
NODE2(1:end,i)=S2;
NODE3(1:end,i)=S3;
NODE4(1:end,i)=S4;
NODE5(1:end,i)=S5;
NODE6(1:end,i)=S6;
NODE7(1:end,i)=S7;
NODE8(1:end,i)=S8;
NODE9(1:end,i)=S9;

end

% PAST DATA OF THE SECOND STEP ON EXCEL FILE

filename = 'Filescrittura.xlsx';
writematrix(NODE1,filename,'Sheet',1,'Range','B2:Z8')
writematrix(NODE2,filename,'Sheet',1,'Range','B11:Z17')
writematrix(NODE3,filename,'Sheet',1,'Range','B20:Z26')
writematrix(NODE4,filename,'Sheet',1,'Range','B29:Z35')
writematrix(NODE5,filename,'Sheet',1,'Range','B38:Z44')
writematrix(NODE6,filename,'Sheet',1,'Range','B47:Z53')
writematrix(NODE7,filename,'Sheet',1,'Range','B56:Z62')
writematrix(NODE8,filename,'Sheet',1,'Range','B65:Z71')
writematrix(NODE9,filename,'Sheet',1,'Range','B74:Z80')
```

References

[1] W. Steffen, W. Broadgate, L. Deutsch, O. Gaffney, C. Ludwig, The trajectory of the Anthropocene: The Great Acceleration, The Anthropocene Review. 2 (2015) 81–98. https://doi.org/10.1177/2053019614564785.

[2] J. Rockström, Bounding the Planetary Future: Why We Need a Great Transition, (2015).

[3] W. Steffen, K. Richardson, J. Rockstrom, S.E. Cornell, I. Fetzer, E.M. Bennett, R. Biggs, S.R. Carpenter, W. de Vries, C.A. de Wit, C. Folke, D. Gerten, J. Heinke, G.M. Mace, L.M. Persson, V. Ramanathan, B. Reyers, S. Sorlin, Planetary boundaries: Guiding human development on a changing planet, Science. 347 (2015) 1259855–1259855. https://doi.org/10.1126/science.1259855.

[4] M.Z. Hauschild, S. Kara, I. Røpke, Absolute sustainability: Challenges to life cycle engineering, CIRP Annals. 69 (2020) 533–553. https://doi.org/10.1016/j.cirp.2020.05.004.

[5] P.R. Ehrlich, J.P. Holdren, Impact of Population Growth, Science. 171 (1971) 1212–1217. https://doi.org/10.1126/science.171.3977.1212.

[6] B. Commoner, The environmental cost of economic growth, Population, Resources and the Environment. 339–363.

[7] G7, G7 Summit Declaration, (n.d.). www.consilium.europa.eu/en/meetings/international-summit/2015/06/07-08/.

[8] Ellen MacArthur Foundation, Growth within: a circular economy vision for a competitive europe, (2015). https://www.ellenmacarthurfoundation.org/assets/downloads/publications/EllenMacArthurFoundation_Growth-Within_July15.pdf.

[9] D. Chen, S. Heyer, S. Ibbotson, K. Salonitis, J.G. Steingrímsson, S. Thiede, Direct digital manufacturing: definition, evolution, and sustainability implications, Journal of Cleaner Production. 107 (2015) 615–625. https://doi.org/10.1016/j.jclepro.2015.05.009.

[10] I. Gibson, D.W. Rosen, B. Stucker, Additive Manufacturing Technologies, Springer US, Boston, MA, 2010. https://doi.org/10.1007/978-1-4419-1120-9.

[11] M. Matsumoto, S. Yang, K. Martinsen, Y. Kainuma, Trends and research challenges in remanufacturing, International Journal of Precision Engineering and Manufacturing-Green Technology. 3 (2016) 129–142.

https://doi.org/10.1007/s40684-016-0016-4.
[12] M. Leino, J. Pekkarinen, R. Soukka, The Role of Laser Additive Manufacturing Methods of Metals in Repair, Refurbishment and Remanufacturing – Enabling Circular Economy, Physics Procedia. 83 (2016) 752–760. https://doi.org/10.1016/j.phpro.2016.08.077.
[13] K. Kellens, R. Mertens, D. Paraskevas, W. Dewulf, J.R. Duflou, Environmental Impact of Additive Manufacturing Processes: Does AM Contribute to a More Sustainable Way of Part Manufacturing?, in: Procedia CIRP, The Author(s), 2017: pp. 582–587. https://doi.org/10.1016/j.procir.2016.11.153.
[14] K. Kellens, M. Baumers, T.G. Gutowski, W. Flanagan, R. Lifset, J.R. Duflou, Environmental Dimensions of Additive Manufacturing: Mapping Application Domains and Their Environmental Implications, Journal of Industrial Ecology. 21 (2017) S49–S68. https://doi.org/10.1111/jiec.12629.
[15] H.-S. Yoon, J.-Y. Lee, H.-S. Kim, M.-S. Kim, E.-S. Kim, Y.-J. Shin, W.-S. Chu, S.-H. Ahn, A comparison of energy consumption in bulk forming, subtractive, and additive processes: Review and case study, International Journal of Precision Engineering and Manufacturing-Green Technology. 1 (2014) 261–279. https://doi.org/10.1007/s40684-014-0033-0.
[16] S. Junk, S. Côté, A practical approach to comparing energy effectiveness of rapid prototyping technologies, Proceedings of AEPR'12, 17th European Forum on Rapid Prototyping and Manufacturing. (2012).
[17] European Commission, Closing the loop - An EU action plan for the Circular Economy, (n.d.). https://eur-lex.europa.eu/legal-content/EN/TXT/?uri=CELEX:52015DC0614.
[18] B. Su, A. Heshmati, Y. Geng, X. Yu, A review of the circular economy in China: moving from rhetoric to implementation, Journal of Cleaner Production. 42 (2013) 215–227. https://doi.org/10.1016/j.jclepro.2012.11.020.
[19] H. Wu, Y. Shi, Q. Xia, W. Zhu, Effectiveness of the policy of circular economy in China: A DEA-based analysis for the period of 11th five-year-plan, Resources, Conservation and Recycling. 83 (2014) 163–175. https://doi.org/10.1016/j.resconrec.2013.10.003.
[20] ISO/ASTM 52900:2015, Standard Terminology for Additive Manufacturing Technologies, Committee F42 on Additive Manufacturing Technologies. (2015).
[21] D.L.M. Nascimento, V. Alencastro, O.L.G. Quelhas, R.G.G. Caiado, J.A. Garza-Reyes, L. Rocha-Lona, G. Tortorella, Exploring Industry 4.0 technologies to enable circular economy practices in a manufacturing context, Journal of Manufacturing Technology Management. 30 (2019) 607–627. https://doi.org/10.1108/JMTM-03-2018-0071.
[22] P. Reeves, C. Tuck, R. Hague, Additive Manufacturing for Mass

Customization, in: 2011: pp. 275–289. https://doi.org/10.1007/978-1-84996-489-0_13.
[23] Renishaw, Last time accessed on October 21 2020, (n.d.). https://www.renishaw.com/en/renishaw-enhancing-efficiency-in-manufacturing-and-healthcare--1030.
[24] EOS, Last time accessed on October 21 2020, (n.d.). https://www.eos.info/en.
[25] Dall'Ava, Hothi, Di Laura, Henckel, Hart, 3D Printed Acetabular Cups for Total Hip Arthroplasty: A Review Article, Metals. 9 (2019) 729. https://doi.org/10.3390/met9070729.
[26] A. Salmi, F. Calignano, M. Galati, E. Atzeni, An integrated design methodology for components produced by laser powder bed fusion (L-PBF) process, Virtual and Physical Prototyping. 13 (2018) 191–202. https://doi.org/10.1080/17452759.2018.1442229.
[27] E. Atzeni, L. Iuliano, G. Marchiandi, P. Minetola, A. Salmi, E. Bassoli, L. Denti, A. Gatto, Additive manufacturing as a cost-effective way to produce metal parts, in: High Value Manufacturing: Advanced Research in Virtual and Rapid Prototyping, CRC Press, 2013: pp. 3–8. https://doi.org/10.1201/b15961-3.
[28] W. Davis, V. Lunetto, P.C. Priarone, D. Centea, L. Settineri, An appraisal on the sustainability payback of additively manufactured molds with conformal cooling, in: Procedia CIRP, 2020: pp. 516–521. https://doi.org/10.1016/j.procir.2020.01.064.
[29] General Electric, Last time accessed on October 21 2020, (n.d.). https://www.ge.com/.
[30] Avio Aero, Last time accessed on October 21 2020, (n.d.). https://arevo.com/.
[31] FASTRADIUS, Last time accessed on October 21 2020, (n.d.). https://www.fastradius.com/.
[32] 3D Print Canal House, Last time accessed on October 21 2020, (n.d.). https://doi.org/https://3dprintcanalhouse.com/.
[33] P.J. Crutzen, E.F. Stoermer, The "Anthropocene". Global change News Letter. The International Geosphere–Biosphere Programme (IGBP): A Study of Global Change of the International Council for Science (ICSU), (2000).
[34] M.Z. Hauschild, C. Herrmann, S. Kara, An Integrated Framework for Life Cycle Engineering, in: Procedia CIRP, 2017: pp. 2–9. https://doi.org/10.1016/j.procir.2016.11.257.
[35] B.V. Field CB, Barros VR, Mastrandrea MD, Mach KJ, Abdrabo MK, Adger N, Anokhin YA, Anisimov OA, Arent DJ, Burnett J, Summary for policymakers. Climate change 2014: Impacts, adaptation, and vulnerability. Part A: global and sectoral aspects, Contribution of Working Group II to

the Fifth Assessment Report of the Intergovernmental Panel on Climate Change. (2014) 1–32.
[36] United Nationes, The World Population Prospects: 2015 Revision, (2015). https://www.un.org/en/development/desa/publications/world-population-prospects-2015-revision.html.
[37] P.C. Priarone, G. Ingarao, Towards criteria for sustainable process selection: On the modelling of pure subtractive versus additive/subtractive integrated manufacturing approaches, Journal of Cleaner Production. 144 (2017) 57–68. https://doi.org/10.1016/j.jclepro.2016.12.165.
[38] Mckinsey, Resource revolution: Tracking global commodity markets, (2013). https://www.mckinsey.com/business-functions/sustainability/our-insights/resource-revolution-tracking-global-commodity-markets#.
[39] United Nations, The Sustainable Development Goals, (n.d.). https://www.un.org/sustainabledevelopment/.
[40] I.S. Jawahir, R. Bradley, Technological Elements of Circular Economy and the Principles of 6R-Based Closed-loop Material Flow in Sustainable Manufacturing, in: Procedia CIRP, Elsevier B.V., 2016: pp. 103–108. https://doi.org/10.1016/j.procir.2016.01.067.
[41] T. Tolio, A. Bernard, M. Colledani, S. Kara, G. Seliger, J. Duflou, O. Battaia, S. Takata, Design, management and control of demanufacturing and remanufacturing systems, CIRP Annals. 66 (2017) 585–609. https://doi.org/10.1016/j.cirp.2017.05.001.
[42] J.T. Lyle, Regenerative Design for Sustainable Development, 1996.
[43] W.R. Stahel, G. Reday-Mulvey, Jobs for tomorrow : the potential for substituting manpower for energy, 1981.
[44] M. Braungart, W. McDonough, Cradle to Cradle: Remaking the Way We Make Things, North Point Press, 2002.
[45] R. Frosch, Nicholas Gallopoulos, Strategies for Manufacturing, Scientific American. 261 (1989) 144–152.
[46] Gunter Pauli, Blue Economy-10 Years, 100 Innovations, 100 Million Jobs, Paradigm Publications, 2010.
[47] Ellen MacArthur Foundation, Towards the Circular Economy: Opportunities for the Consumer Goods Sector, 2013.
[48] A.D. Jayal, F. Badurdeen, O.W. Dillon, I.S. Jawahir, Sustainable manufacturing: Modeling and optimization challenges at the product, process and system levels, CIRP Journal of Manufacturing Science and Technology. 2 (2010) 144–152. https://doi.org/10.1016/j.cirpj.2010.03.006.
[49] I. s. Jawahir, O.W. Dillon, Sustainable manufacturing processes: New challenges for developing predictive models and optimization techniques, in: International Conference on Sustainable Manufacturing, 2007.
[50] J.R. Duflou, G. Seliger, S. Kara, Y. Umeda, A. Ometto, B. Willems, Efficiency and feasibility of product disassembly: A case-based study,

CIRP Annals. 57 (2008) 583–600. https://doi.org/10.1016/j.cirp.2008.09.009.
[51] M. Matsumoto, Y. Umeda, An analysis of remanufacturing practices in Japan, Journal of Remanufacturing. 1 (2011) 2. https://doi.org/10.1186/2210-4690-1-2.
[52] M. Colledani, G. Copani, T. Tolio, De-manufacturing Systems, Procedia CIRP. 17 (2014) 14–19. https://doi.org/10.1016/j.procir.2014.04.075.
[53] M. Colledani, T. Tolio, Integrated process and system modelling for the design of material recycling systems, CIRP Annals. 62 (2013) 447–452. https://doi.org/10.1016/j.cirp.2013.03.046.
[54] Y. Umeda, N. Miyaji, Y. Shiraishi, S. Fukushige, Proposal of a design method for semi-destructive disassembly with split lines, CIRP Annals. 64 (2015) 29–32. https://doi.org/10.1016/j.cirp.2015.04.045.
[55] S. Vongbunyong, S. Kara, M. Pagnucco, Application of cognitive robotics in disassembly of products, CIRP Annals. 62 (2013) 31–34. https://doi.org/10.1016/j.cirp.2013.03.037.
[56] M. Despeisse, M. Baumers, P. Brown, F. Charnley, S.J. Ford, A. Garmulewicz, S. Knowles, T.H.W. Minshall, L. Mortara, F.P. Reed-Tsochas, J. Rowley, Unlocking value for a circular economy through 3D printing: A research agenda, Technological Forecasting and Social Change. 115 (2017) 75–84. https://doi.org/10.1016/j.techfore.2016.09.021.
[57] C.M. Angioletti, F.G. Sisca, R. Luglietti, M. Taisch, R. Rocca, Additive Manufacturing as an opportunity for supporting sustainability through implementation of circular economies, in: Proceedings of the Summer School Francesco Turco, 2016: pp. 25–30.
[58] A. Garmulewicz, M. Holweg, H. Veldhuis, A. Yang, Disruptive Technology as an Enabler of the Circular Economy: What Potential Does 3D Printing Hold?, California Management Review. 60 (2018) 112–132. https://doi.org/10.1177/0008125617752695.
[59] M. Morsidi, P.T. Mativenga, M. Fahad, Fused Deposition Modelling Filament with Recyclate Fibre Reinforcement, in: Procedia CIRP, Elsevier B.V., 2019: pp. 353–358. https://doi.org/10.1016/j.procir.2019.09.026.
[60] A. Saboori, A. Aversa, G. Marchese, S. Biamino, M. Lombardi, P. Fino, Application of Directed Energy Deposition-Based Additive Manufacturing in Repair, Applied Sciences. 9 (2019) 3316. https://doi.org/10.3390/app9163316.
[61] J. Wang, S. Prakash, Y. Joshi, F. Liou, Laser Aided Part Repair-A Review, in: 13th Annual Solid Freeform Fabrication Symposium, 2002: pp. 57–64.
[62] B. Graf, A. Gumenyuk, M. Rethmeier, Laser Metal Deposition as Repair Technology for Stainless Steel and Titanium Alloys, Physics Procedia. 39 (2012) 376–381. https://doi.org/10.1016/j.phpro.2012.10.051.
[63] J.M. Wilson, C. Piya, Y.C. Shin, F. Zhao, K. Ramani, Remanufacturing of

turbine blades by laser direct deposition with its energy and environmental impact analysis, Journal of Cleaner Production. 80 (2014) 170–178. https://doi.org/10.1016/j.jclepro.2014.05.084.

[64] O. Yilmaz, N. Gindy, J. Gao, A repair and overhaul methodology for aeroengine components, Robotics and Computer-Integrated Manufacturing. 26 (2010) 190–201. https://doi.org/10.1016/j.rcim.2009.07.001.

[65] G. Ingarao, P.C. Priarone, A comparative assessment of energy demand and life cycle costs for additive- and subtractive-based manufacturing approaches, Journal of Manufacturing Processes. 56 (2020) 1219–1229. https://doi.org/10.1016/j.jmapro.2020.06.009.

[66] P.C. Priarone, G. Ingarao, V. Lunetto, R. Di Lorenzo, L. Settineri, The Role of re-design for Additive Manufacturing on the Process Environmental Performance, Procedia CIRP. 69 (2018) 124–129. https://doi.org/10.1016/j.procir.2017.11.047.

[67] P.C. Priarone, V. Lunetto, E. Atzeni, A. Salmi, Laser powder bed fusion (L-PBF) additive manufacturing: On the correlation between design choices and process sustainability, in: Procedia CIRP, Elsevier B.V., 2018: pp. 85–90. https://doi.org/10.1016/j.procir.2018.09.058.

[68] V. Lunetto, A.R. Catalano, P.C. Priarone, A. Salmi, E. Atzeni, S. Moos, L. Iuliano, L. Settineri, Additive Manufacturing for an urban vehicle prototype : Re-design and sustainability implications (In press), in: Procedia CIRP, 2021.

[69] P.C. Priarone, E. Pagone, F. Martina, A.R. Catalano, L. Settineri, Multi-criteria environmental and economic impact assessment of wire arc additive manufacturing, CIRP Annals. 69 (2020) 37–40. https://doi.org/10.1016/j.cirp.2020.04.010.

[70] P.C. Priarone, G. Campatelli, F. Montevecchi, G. Venturini, L. Settineri, A modelling framework for comparing the environmental and economic performance of WAAM-based integrated manufacturing and machining, CIRP Annals. 68 (2019) 37–40. https://doi.org/10.1016/j.cirp.2019.04.005.

[71] F. Walachowicz, I. Bernsdorf, U. Papenfuss, C. Zeller, A. Graichen, V. Navrotsky, N. Rajvanshi, C. Kiener, Comparative Energy, Resource and Recycling Lifecycle Analysis of the Industrial Repair Process of Gas Turbine Burners Using Conventional Machining and Additive Manufacturing, Journal of Industrial Ecology. 21 (2017) S203–S215. https://doi.org/10.1111/jiec.12637.

[72] S. Kara, W. Li, Unit process energy consumption models for material removal processes, CIRP Annals. 60 (2011) 37–40. https://doi.org/10.1016/j.cirp.2011.03.018.

[73] A. Thiriez, An Environmental Analysis of Injection Molding, IEEE, 2004.

[74] V. Lunetto, M. Galati, L. Settineri, L. Iuliano, Unit process energy consumption analysis and models for Electron Beam Melting (EBM):

Effects of process and part designs, Additive Manufacturing. 33 (2020) 101115. https://doi.org/10.1016/j.addma.2020.101115.
[75] V. Lunetto, P.C. Priarone, M. Galati, P. Minetola, On the correlation between process parameters and specific energy consumption in fused deposition modelling, Journal of Manufacturing Processes. 56 (2020) 1039–1049. https://doi.org/10.1016/j.jmapro.2020.06.002.
[76] M.D. Monzón, Z. Ortega, A. Martínez, F. Ortega, Standardization in additive manufacturing: activities carried out by international organizations and projects, The International Journal of Advanced Manufacturing Technology. 76 (2015) 1111–1121. https://doi.org/10.1007/s00170-014-6334-1.
[77] 3D Systems, Last time accessed on October 21 2020, (n.d.).
[78] Stratasys, Last time accessed on October 21 2020, (n.d.). www.stratasys.com.
[79] HP, Last time accessed on October 21 2020, (n.d.). https://www8.hp.com/us/en/printers/3d-printers.html.
[80] Prima Industrie, Last time accessed on October 21 2020, (n.d.). https://www.primaindustrie.com/it/.
[81] Optomec, Last time accessed on October 21 2020, (n.d.). https://optomec.com/.
[82] Sciaky Inc, Last time accessed on October 21 2020, (n.d.). https://www.sciaky.com/additive-manufacturing/electron-beam-additive-manufacturing-technology.
[83] Mcor Technologies, Last time accessed on October 21 2020, (n.d.). https://cleangreen3d.com/.
[84] Markforged, Last time accessed on October 21 2020, (n.d.). https://markforged.com/.
[85] G.D. Goh, Y.L. Yap, S. Agarwala, W.Y. Yeong, Recent Progress in Additive Manufacturing of Fiber Reinforced Polymer Composite, Advanced Materials Technologies. 4 (2019) 1800271. https://doi.org/10.1002/admt.201800271.
[86] X. Wang, M. Jiang, Z. Zhou, J. Gou, D. Hui, 3D printing of polymer matrix composites: A review and prospective, Composites Part B: Engineering. 110 (2017) 442–458. https://doi.org/10.1016/j.compositesb.2016.11.034.
[87] H.K. Sezer, O. Eren, FDM 3D printing of MWCNT re-inforced ABS nano-composite parts with enhanced mechanical and electrical properties, Journal of Manufacturing Processes. 37 (2019) 339–347. https://doi.org/10.1016/j.jmapro.2018.12.004.
[88] P. Geng, J. Zhao, W. Wu, W. Ye, Y. Wang, S. Wang, S. Zhang, Effects of extrusion speed and printing speed on the 3D printing stability of extruded PEEK filament, Journal of Manufacturing Processes. 37 (2019) 266–273. https://doi.org/10.1016/j.jmapro.2018.11.023.

[89] N. Hopkinson, P. Dicknes, Analysis of rapid manufacturing—using layer manufacturing processes for production, Proceedings of the Institution of Mechanical Engineers, Part C: Journal of Mechanical Engineering Science. 217 (2003) 31–39. https://doi.org/10.1243/095440603762554596.
[90] D. Sahebrao Ingole, A. Madhusudan Kuthe, S.B. Thakare, A.S. Talankar, Rapid prototyping – a technology transfer approach for development of rapid tooling, Rapid Prototyping Journal. 15 (2009) 280–290. https://doi.org/10.1108/13552540910979794.
[91] M. Dawoud, I. Taha, S.J. Ebeid, Mechanical behaviour of ABS: An experimental study using FDM and injection moulding techniques, Journal of Manufacturing Processes. 21 (2016) 39–45. https://doi.org/10.1016/j.jmapro.2015.11.002.
[92] Yanchun Luo, Zhiming Ji, M.C. Leu, R. Caudill, Environmental performance analysis of solid freedom fabrication processes, in: Proceedings of the 1999 IEEE International Symposium on Electronics and the Environment (Cat. No.99CH36357), IEEE, 1999: pp. 1–6. https://doi.org/10.1109/ISEE.1999.765837.
[93] F. Le Bourhis, O. Kerbrat, J.-Y. Hascoet, P. Mognol, Sustainable manufacturing: evaluation and modeling of environmental impacts in additive manufacturing, The International Journal of Advanced Manufacturing Technology. 69 (2013) 1927–1939. https://doi.org/10.1007/s00170-013-5151-2.
[94] M. Yosofi, O. Kerbrat, P. Mognol, Energy and material flow modelling of additive manufacturing processes, Virtual and Physical Prototyping. 13 (2018) 83–96. https://doi.org/10.1080/17452759.2017.1418900.
[95] P. Mognol, D. Lepicart, N. Perry, Rapid prototyping: energy and environment in the spotlight, Rapid Prototyping Journal. 12 (2006) 26–34. https://doi.org/10.1108/13552540610637246.
[96] M. Baumers, C. Tuck, R. Wildman, I. Ashcroft, R. Hague, Energy inputs to additive manufacturing: does capacity utilization matter?, in: 22nd Annual International Solid Freeform Fabrication Symposium - An Additive Manufacturing Conference, SFF 2011, 2011: pp. 30–40.
[97] M. Baumers, Economic Aspects of Additive Manufacturing : Benefits , Costs and Energy Consumption, 2012.
[98] V.A. Balogun, N. Kirkwood, P.T. Mativenga, Energy consumption and carbon footprint analysis of Fused Deposition Modelling: A case study of RP Stratasys Dimension SST FDM, International Journal of Scientific and Engineering Research. 6 (2015) 442–447.
[99] M. Yosofi, O. Kerbrat, P. Mognol, Additive manufacturing processes from an environmental point of view: a new methodology for combining technical, economic, and environmental predictive models, The International Journal of Advanced Manufacturing Technology. 102 (2019)

4073–4085. https://doi.org/10.1007/s00170-019-03446-2.
[100] M. Baumers, C. Tuck, D.L. Bourell, R. Sreenivasan, R. Hague, Sustainability of additive manufacturing: measuring the energy consumption of the laser sintering process, Proceedings of the Institution of Mechanical Engineers, Part B: Journal of Engineering Manufacture. 225 (2011) 2228–2239. https://doi.org/10.1177/0954405411406044.
[101] R. Huang, M. Riddle, D. Graziano, J. Warren, S. Das, S. Nimbalkar, J. Cresko, E. Masanet, Energy and emissions saving potential of additive manufacturing: the case of lightweight aircraft components, Journal of Cleaner Production. 135 (2016) 1559–1570. https://doi.org/10.1016/j.jclepro.2015.04.109.
[102] M. Galati, L. Iuliano, A literature review of powder-based electron beam melting focusing on numerical simulations, Additive Manufacturing. 19 (2018) 1–20. https://doi.org/10.1016/j.addma.2017.11.001.
[103] H. Paris, H. Mokhtarian, E. Coatanéa, M. Museau, I.F. Ituarte, Comparative environmental impacts of additive and subtractive manufacturing technologies, CIRP Annals. 65 (2016) 29–32. https://doi.org/10.1016/j.cirp.2016.04.036.
[104] M. Larsson, U. Lindhe, O. Harrysson, Rapid Manufacturing with Electron Beam Melting (EBM) - A Manufacturing Revolution?, in: International Solid Freeform Fabrication Symposium, 2003.
[105] H. Weiwei, J. Wenpeng, L. Haiyan, T. Huiping, K. Xinting, H. Yu, Research on Preheating of Titanium Alloy Powder in Electron Beam Melting Technology, Rare Metal Materials and Engineering. 40 (2011) 2072–2075. https://doi.org/10.1016/S1875-5372(12)60014-9.
[106] M. Galati, L. Iuliano, A. Snis, Experimental validation of a numerical thermal numerical model of EBM process for Ti6Al4V, in: Simulation for Additive Manufacturing, International Center for Numerical Methods in Engineering, 2017: pp. 33–34.
[107] J. Karlsson, T. Sjögren, A. Snis, H. Engqvist, J. Lausmaa, Digital image correlation analysis of local strain fields on Ti6Al4V manufactured by electron beam melting, Materials Science and Engineering: A. 618 (2014) 456–461. https://doi.org/10.1016/j.msea.2014.09.022.
[108] T.R. Mahale, Electron Beam Melting of Advanced Materials and Structures, mass customization, mass personalization, 2009.
[109] M. Galati, A. Snis, L. Iuliano, Powder bed properties modelling and 3D thermo-mechanical simulation of the additive manufacturing Electron Beam Melting process, Additive Manufacturing. 30 (2019) 100897. https://doi.org/10.1016/j.addma.2019.100897.
[110] E. Attar, Simulation of Selective Electron Beam Melting Processes, 2011.
[111] M. Galati, P. Minetola, G. Rizza, Surface Roughness Characterisation and Analysis of the Electron Beam Melting (EBM) Process, Materials. 12

(2019) 2211. https://doi.org/10.3390/ma12132211.
[112] M. Baumers, C. Tuck, R. Hague, I. Ashcroft, R. Wildman, A comparative study of metallic additive manufacturing power consumption, in: 21st Annual International Solid Freeform Fabrication Symposium - An Additive Manufacturing Conference, SFF 2010, 2010: pp. 278–288.
[113] M. Baumers, P. Dickens, C. Tuck, R. Hague, The cost of additive manufacturing: machine productivity, economies of scale and technology-push, Technological Forecasting and Social Change. 102 (2016) 193–201. https://doi.org/10.1016/j.techfore.2015.02.015.
[114] M. Baumers, C. Tuck, R. Wildman, I. Ashcroft, R. Hague, Shape Complexity and Process Energy Consumption in Electron Beam Melting: A Case of Something for Nothing in Additive Manufacturing?, Journal of Industrial Ecology. 21 (2017) S157–S167. https://doi.org/10.1111/jiec.12397.
[115] M. Baumers, C. Tuck, R. Wildman, I. Ashcroft, E. Rosamond, R. Hague, Transparency Built-in, Journal of Industrial Ecology. 17 (2013) 418–431. https://doi.org/10.1111/j.1530-9290.2012.00512.x.
[116] O. Kerbrat, F. Le Bourhis, P. Mognol, J.-Y. Hascoët, Environmental Impact Assessment Studies in Additive Manufacturing, in: 2016: pp. 31–63. https://doi.org/10.1007/978-981-10-0606-7_2.
[117] C. Herrmann, W. Dewulf, M. Hauschild, A. Kaluza, S. Kara, S. Skerlos, Life cycle engineering of lightweight structures, CIRP Annals. 67 (2018) 651–672. https://doi.org/10.1016/j.cirp.2018.05.008.
[118] Office of Energy Efficiency & Renewable Energy, Bandwidth Study on Energy Use and Potential Energy Saving Opportunities in U.S. Carbon Fiber Reinforced Polymer Manufacturing, (2017) 63.
[119] Office of Energy Efficiency & Renewable Energy, Bandwidth Study on Energy Use and Potential Energy Saving Opportunities in U.S. Glass Fiber Reinforced Polymer Manufacturing, (2017) 64.
[120] Lucintel, Composites Market Report: Trends, Forecast and Competitive Analysis, 2020.
[121] S. Singh, S. Ramakrishna, F. Berto, 3D Printing of polymer composites: A short review, Material Design & Processing Communications. 2 (2020). https://doi.org/10.1002/mdp2.97.
[122] P. Parandoush, D. Lin, A review on additive manufacturing of polymer-fiber composites, Composite Structures. 182 (2017) 36–53. https://doi.org/10.1016/j.compstruct.2017.08.088.
[123] M. Ashby, Materials and the Environment, second ed., Elsevier, 2013. https://doi.org/10.1016/C2010-0-66554-0.
[124] Y.S. Song, J.R. Youn, T.G. Gutowski, Life cycle energy analysis of fiber-reinforced composites, Composites Part A: Applied Science and Manufacturing. 40 (2009) 1257–1265.

https://doi.org/10.1016/j.compositesa.2009.05.020.
[125] Granta Design Limited, CES Selector Software 2017, (n.d.). https://www.grantadesign.com/industry/products/ces-selector/.
[126] J. Howarth, S.S.R. Mareddy, P.T. Mativenga, Energy intensity and environmental analysis of mechanical recycling of carbon fibre composite, Journal of Cleaner Production. 81 (2014) 46–50. https://doi.org/10.1016/j.jclepro.2014.06.023.
[127] C. V. Katsiropoulos, A. Loukopoulos, S.G. Pantelakis, Comparative Environmental and Cost Analysis of Alternative Production Scenarios Associated with a Helicopter's Canopy, Aerospace. 6 (2019) 3. https://doi.org/10.3390/aerospace6010003.
[128] G. Oliveux, L.O. Dandy, G.A. Leeke, Current status of recycling of fibre reinforced polymers: Review of technologies, reuse and resulting properties, Progress in Materials Science. 72 (2015) 61–99. https://doi.org/10.1016/j.pmatsci.2015.01.004.
[129] R.A. Witik, F. Gaille, R. Teuscher, H. Ringwald, V. Michaud, J.-A.E. Månson, Economic and environmental assessment of alternative production methods for composite aircraft components, Journal of Cleaner Production. 29–30 (2012) 91–102. https://doi.org/10.1016/j.jclepro.2012.02.028.
[130] T. Suzuki, J. Takahashi, Prediction of energy intensity of carbon fiber reinforced plastics for mass-produced passenger cars, in: Japan International SAMPE Symposium JISSE-9, 2005: pp. 14–19.
[131] A. Berejka, D. Montoney, D. Dispenza, L. Poveromo, R. Galloway, M. Cleland, M. Driscoll, Power Demands for Curing Carbon Fiber Composites for Automotive Components, SAE International Journal of Materials and Manufacturing. 9 (2016) 2016-01–0527. https://doi.org/10.4271/2016-01-0527.
[132] Y. Li, L. Cheng, J. Zhou, Curing multidirectional carbon fiber reinforced polymer composites with indirect microwave heating, The International Journal of Advanced Manufacturing Technology. 97 (2018) 1137–1147. https://doi.org/10.1007/s00170-018-1974-1.
[133] N. Li, Y. Li, J. Jelonnek, G. Link, J. Gao, A new process control method for microwave curing of carbon fibre reinforced composites in aerospace applications, Composites Part B: Engineering. 122 (2017) 61–70. https://doi.org/10.1016/j.compositesb.2017.04.009.
[134] J. Lee, X. Ni, F. Daso, X. Xiao, D. King, J.S. Gómez, T.B. Varela, S.S. Kessler, B.L. Wardle, Advanced carbon fiber composite out-of-autoclave laminate manufacture via nanostructured out-of-oven conductive curing, Composites Science and Technology. 166 (2018) 150–159. https://doi.org/10.1016/j.compscitech.2018.02.031.
[135] W.J.B. Grouve, Weld strength of laser-assisted tape-placed thermoplastic composites, University of Twente, 2012.

https://doi.org/10.3990/1.9789036533928.
[136] C. Brecher, R. Schmitt, F. Lindner, T. Peters, M. Emonts, M.G. Böckmann, Increasing Cost and Eco Efficiency for Selective Tape Placement and Forming by Adaptive Process Design, Procedia CIRP. 57 (2016) 769–774. https://doi.org/10.1016/j.procir.2016.11.133.
[137] G. Hammond, C. Jones, A BSRIA Guide. Embodied Carbon: The Inventory of Carbon and Energy., 2011.
[138] C. Chen, Y. Wang, H. Ou, Y. He, X. Tang, A review on remanufacture of dies and moulds, Journal of Cleaner Production. 64 (2014) 13–23. https://doi.org/10.1016/j.jclepro.2013.09.014.
[139] S. Kara, Assessing Remaining Useful Lifetime of Products, in: Wiley Encyclopedia of Operations Research and Management Science, John Wiley & Sons, Inc., Hoboken, NJ, USA, 2011. https://doi.org/10.1002/9780470400531.eorms0056.
[140] M.I. Mazhar, Lifetime Monitoring of Appliances for Reuse, The University of New South Wales School of Mechanical and Manufacturing Engineering, 2006.
[141] Rugrungruang F, An integrated methodology for assessing physical and technological life of products for reuse, The University of New South Wales, 2008.
[142] Y. Mizuno, N. Kintoki, Y. Kishita, S. Fukushige, Y. Umeda, A Study on Optimum Circulation Period of Products for Minimizing Lifecycle Energy Consumption, in: Procedia CIRP, Elsevier B.V., 2015: pp. 597–602. https://doi.org/10.1016/j.procir.2015.02.209.
[143] A. Singh, S. Adachi, Bathtub curves and pipe prioritization based on failure rate, Built Environment Project and Asset Management. 3 (2013) 105–122. https://doi.org/10.1108/BEPAM-11-2011-0027.
[144] A.Y. Alqahtani, S.M. Gupta, Evaluating two-dimensional warranty policies for remanufactured products, Journal of Remanufacturing. 7 (2017) 19–47. https://doi.org/10.1007/s13243-017-0032-8.
[145] W. Blischke, P. Murthy, Reliability: Modeling, Prediction, and Optimization, 2000.
[146] M. Colledani, T. Tolio, Performance evaluation of transfer lines with general repair times and multiple failure modes, Annals of Operations Research. 182 (2011) 31–65. https://doi.org/10.1007/s10479-009-0595-3.
[147] R. Assaf, M. Colledani, A. Matta, Analytical evaluation of the output variability in production systems with general Markovian structure, OR Spectrum. 36 (2014) 799–835. https://doi.org/10.1007/s00291-013-0343-6.
[148] M. Colledani, D. Gyulai, L. Monostori, M. Urgo, J. Unglert, F. Van Houten, Design and management of reconfigurable assembly lines in the automotive industry, CIRP Annals. 65 (2016) 441–446. https://doi.org/10.1016/j.cirp.2016.04.123.

[149] R.P. Davis, W.J. Kennedy, Markovian modelling of manufacturing systems, International Journal of Production Research. 25 (1987) 337–351. https://doi.org/10.1080/00207548708919845.
[150] K.-Y.C. Yu, D.L. Bricker, Analysis of a markov chain model of a multistage manufacturing system with inspection, rejection, and rework, IIE Transactions. 25 (1993) 109–112. https://doi.org/10.1080/07408179308964271.
[151] T. Jónás, N. Kalló, Z.E. Tóth, Application of Markov Chains for Modeling and Managing Industrial Electronic Repair Processes, Periodica Polytechnica Social and Management Sciences. 22 (2014) 87–98. https://doi.org/10.3311/PPso.7438.
[152] E. V. Zaretsky, J.S. Litt, R.C. Hendricks, S.M. Soditus, Determination of Turbine Blade Life from Engine Field Data, Journal of Propulsion and Power. 28 (2012) 1156–1167. https://doi.org/10.2514/1.B34375.
[153] H. Helms, U. Lambrecht, The potential contribution of light-weighting to reduce transport energy consumption, International Journal of LCA. (2006).
[154] M.R.M. Saade, A. Yahia, B. Amor, How has LCA been applied to 3D printing? A systematic literature review and recommendations for future studies, Journal of Cleaner Production. 244 (2020) 118803. https://doi.org/10.1016/j.jclepro.2019.118803.
[155] T. Kamps, M. Lutter-Guenther, C. Seidel, T. Gutowski, G. Reinhart, Cost- and energy-efficient manufacture of gears by laser beam melting, CIRP Journal of Manufacturing Science and Technology. 21 (2018) 47–60. https://doi.org/10.1016/j.cirpj.2018.01.002.
[156] F.R. Field, J.A. Isaacs, J.P. Clark, Life-cycle analysis of automobiles: A critical review of methodologies, JOM. 46 (1994) 12–16. https://doi.org/10.1007/BF03220667.
[157] Liemberger W, Miltner M, Harasek M, Efficient extraction of helium from natural gas by using hydrogen extraction technology, Chemical Engineering Transactions. 70 (2018) 865–870.
[158] E. Cook, The Helium Question, Science. 206 (1979) 1141–1147. https://doi.org/10.1126/science.206.4423.1141.
[159] M. Källén, Energy Efficiency Opportunities within the Heat Treatment Industry, Chalmers University of Technology, 2012.
[160] NIST: National Institute of Standards and Technology, Last time accessed on October 21 2020, (n.d.). https://www.nist.gov/.
[161] R.E. Laureijs, J.B. Roca, S.P. Narra, C. Montgomery, J.L. Beuth, E.R.H. Fuchs, Metal Additive Manufacturing: Cost Competitive Beyond Low Volumes, Journal of Manufacturing Science and Engineering. 139 (2017) 1–9. https://doi.org/10.1115/1.4035420.
[162] P.C. Priarone, M. Robiglio, L. Settineri, On the concurrent optimization of

environmental and economic targets for machining, Journal of Cleaner Production. 190 (2018) 630–644. https://doi.org/10.1016/j.jclepro.2018.04.163.
[163] J.B. Dahmus, T.G. Gutowski, An Environmental Analysis of Machining, in: Manufacturing Engineering and Materials Handling Engineering, ASMEDC, 2004: pp. 643–652. https://doi.org/10.1115/IMECE2004-62600.
[164] F. Pusavec, D. Kramar, P. Krajnik, J. Kopac, Transitioning to sustainable production – part II: evaluation of sustainable machining technologies, Journal of Cleaner Production. 18 (2010) 1211–1221. https://doi.org/10.1016/j.jclepro.2010.01.015.
[165] V. Lunetto, P.C. Priarone, S. Kara, L. Settineri, A comparative LCA method for environmentally friendly manufacturing: Additive manufacturing versus Machining case, in: Procedia CIRP, 2021.
[166] T. Gutowski, J. Dahmus, A. Thiriez, Electrical energy requirements for manufacturing processes, in: Proceedings of the 13th CIRP International Conference on Life Cycle Engineering, LCE 2006, 2006: pp. 623–628.
[167] W. Li, S. Kara, F. Qureshi, Characterising energy and eco-efficiency of injection moulding processes, International Journal of Sustainable Engineering. 8 (2015) 55–65. https://doi.org/10.1080/19397038.2014.895067.
[168] W. Li, Energy and eco-efficiency of manufacturing processes, School of Mechanical and Manufacturing Engineering The University of New South Wales Sydney, Australia, 2012.
[169] W. Li, S. Kara, An empirical model for predicting energy consumption of manufacturing processes: a case of turning process, Proceedings of the Institution of Mechanical Engineers, Part B: Journal of Engineering Manufacture. 225 (2011) 1636–1646. https://doi.org/10.1177/2041297511398541.
[170] W. Li, M. Winter, S. Kara, C. Herrmann, Eco-efficiency of manufacturing processes: A grinding case, CIRP Annals. 61 (2012) 59–62. https://doi.org/10.1016/j.cirp.2012.03.029.
[171] W. Li, S. Kara, Characterising Energy Efficiency of Electrical Discharge Machining (EDM) Processes, in: Procedia CIRP, Elsevier B.V., 2015: pp. 263–268. https://doi.org/10.1016/j.procir.2015.01.039.
[172] D. Baffari, A.P. Reynolds, A. Masnata, L. Fratini, G. Ingarao, Friction stir extrusion to recycle aluminum alloys scraps: Energy efficiency characterization, Journal of Manufacturing Processes. 43 (2019) 63–69. https://doi.org/10.1016/j.jmapro.2019.03.049.
[173] T. Gutowski, S. Jiang, D. Cooper, G. Corman, M. Hausmann, J.-A. Manson, T. Schudeleit, K. Wegener, M. Sabelle, J. Ramos-Grez, D.P. Sekulic, Note on the Rate and Energy Efficiency Limits for Additive Manufacturing, Journal of Industrial Ecology. 21 (2017) S69–S79.

https://doi.org/10.1111/jiec.12664.